DEVELOPMENT OF A SPATIALLY EXPLICIT STOCHASTIC RAINFALL GENERATOR IN SOUTHEAST ARIZONA

by

Ying Zhao

A Dissertation Submitted to the Faculty of the

SCHOOL OF NATURAL RESOURCES AND THE ENVIRONMENT

In Partial Fulfillment of the Requirements

For the Degree of

DOCTOR OF PHILOSOPHY

WITH A MAJOR IN NATURAL RESOURCES

In the Graduate College

THE UNIVERSITY OF ARIZONA

2019

THE UNIVERSITY OF ARIZONA
GRADUATE COLLEGE

As members of the Dissertation Committee, we certify that we have read the dissertation prepared by ***Ying Zhao***, titled ***Development of a Spatially Explicit Stochastic Rainfall Generator in Southeast Arizona*** and recommend that it be accepted as fulfilling the dissertation requirement for the Degree of Doctor of Philosophy.

D. Phillip Guertin Date: (***04/11/2019***)

Mark A. Nearing Date: (***04/11/2019***)

C. Larry Winter Date: (***04/11/2019***)

Final approval and acceptance of this dissertation is contingent upon the candidate's submission of the final copies of the dissertation to the Graduate College.

We hereby certify that we have read this dissertation prepared under our direction and recommend that it be accepted as fulfilling the dissertation requirement.

D. Phillip Guertin Date: (***04/11/2019***)
Professor
School of Natural Resources and the Environment

Mark A. Nearing Date: (***04/11/2019***)
Research Agricultural Engineer, Adjunct Professor
USDA-ARS Southwest Watershed Research Center

ACKNOWLEDGEMENTS

I would like to thank Dr. Mark Nearing, my research advisor, for providing this opportunity to work at the University of Arizona and USDA-ARS Southwest Watershed Research Center. He gave invaluable research insights and mentoring during my graduate study in the past years. I would like to thank Dr. Phillip Guertin, my academic advisor, for his mentorship and encouragement during this research project, and also for his help with the department paperwork in my graduate program. I would like to thank my dissertation committee and comprehensive exam committee, Drs. Larry Winter, David Goodrich, and Juan Valdes for providing suggestions and knowledge in both this project and classes. I am also grateful to all professors in my coursework for their instruction and help.

Thanks to all the scientists and staff at the USDA-ARS Southwest Watershed Research Center, who always provide the friendship and kindness in the workplace. Special thanks to Mariano Hernandez and Haiyan Wei for their help both in academic and my life in Tucson.

Thanks to my friends, Li Li, Xiaobo Hou, Tao Liu, Lin Ji and others to go through the journey and share the joy with me in Tucson.

Thanks to my beloved husband, Ni Sun, for the happiness and strength you bring me all the time. Thanks to my dear parents for their love and support during all these years.

TABLE OF CONTENTS

ABSTRACT 9

1 INTRODUCTION 11

2 LITERATURE REVIEW 16

2.1 Spatial rainfall generator 16

2.2 Hydrologic response 20

2.3 Hydrologic modeling using rainfall generators 22

3 METHODOLOGY 25

3.1 Study area and data 25

3.2 Spatial rainfall generator development 29

3.2.1 Storm identification 29

3.2.2 Rainfall occurrence 31

3.2.3 Rainfall amount and distribution 33

3.2.4 Multiple events in a day 40

3.2.5 Model evaluation 41

3.3 Hydrologic modeling incorporating two types of rainfall generator 42

3.3.1 Observed rainfall 42

3.3.2 Single-site generator 43

3.3.3 Multi-site generator 44

3.3.4 Watershed modeling 45

3.3.5 Model calibration 46

3.3.6 Model evaluation 48

4 ANALYSIS OF RESULTS 50

4.1 Rainfall characterization 50
4.2 Spatial rainfall generator evaluation 56
4.2.1 Convective storm maximum depth 56
4.2.2 Seasonal and annual rainfall 58
4.3 Comparison of generated precipitation 63
4.4 Hydrologic model calibration results 68
4.5 Comparison of generated runoff 69
5 CONCLUSIONS 74
APPENDIX A: A daily spatially explicit stochastic rainfall generator for a semi-arid climate 77
APPENDIX B: Main generator program 120
APPENDIX C: Subprogram transition 123
APPENDIX D: Subprogram depth 125
APPENDIX E: Subprogram coverage 129
APPENDIX F: Subprogram location 132
REFERENCES 137

LIST OF FIGURES

Figure 1. Rain gage network of USDA-Agricultural Research Service Walnut Gulch Experimental Watershed, Tombstone, Arizona. 28

Figure 2. Map of Flume 1, Flume 2 Flume 6 and main stream networks of Walnut Gulch Experimental Watershed, Tombstone, Arizona. 29

Figure 3. Examples of daily rainfall interpolation results for summer convective storms on Walnut Gulch Experimental Watershed. 30

Figure 4. Flow diagram of the computational processes in the rainfall generator. 33

Figure 5. Conceptual model of convective storms. 36

Figure 6. Rainfall depth spread function of convective storms. 36

Figure 7. Distribution of storms volume during September to November before excluding extreme events. The grey histogram represented the observed counts of storm volume, and the red line represented the theoretical fitting distribution curve. Events on the histogram tail in the black box fitted poorly with the theoretical distribution curve. This subset of large events cannot pass the K-S test at 5% significance level. 39

Figure 8. Lognormal distribution of convective storms maximum depth during July to September, (1) is for the first half month, and (2) is for the second half month. The grey histogram represented the observed counts of storm maximum depth, and the red line represented the theoretical fitting distribution curve. 54

Figure 9. Exponential distribution of frontal storms volume during non-summer months, (1) is for the first half month, and (2) is for the second half month. The grey

histogram represented the observed counts of storm volume, and the red line represented the theoretical fitting distribution curve. 56
Figure 10. CDFs of observed and simulated summer convective storm maximum depths. 58
Figure 11. CDFs of observed and simulated rainfall totals for (a) summer and (b) non-summer periods. 61
Figure 12. CDFs of observed and simulated dry and wet spell length for annual, summer and non-summer periods, (1) first column: dry spell, (2) second column: wet spell. 62
Figure 13. Mean, standard deviation and skewness of daily rainfall. 65
Figure 14. Boxplots of observed, single-site generated, and multi-site generated daily rainfall. 66
Figure 15. Mean, standard deviation and skewness of monthly rainfall. 67
Figure 16. Boxplots of observed, single-site generated, and multi-site generated monthly rainfall. 68
Figure 17. Return periods of generated summer runoff using observed rainfall, single-site rainfall and multi-site rainfall for Flume 1, 2 and 6 in WGEW 73

LIST OF TABLES

Table 1. Parameters calibrated using PEST 47

Table 2. Transition probabilities, probabilities for three types of rainfall, and the probabilities for multiple events in all 24 half month periods 51

Table 3. Characteristics of convective storm area, axis ratio, and orientation. 54

Table 4. Characteristics of observed convective storm maximum depths (mm). 57

Table 5. Characteristics of simulated convective storm maximum depths (mm). 57

Table 6. Observed rainfall totals for summer months of six gages (mm). 60

Table 7. Simulated rainfall totals for summer months of six gages (mm). 60

Table 8. Observed rainfall totals for non-summer months of six gages (mm). 60

Table 9. Simulated rainfall totals for non-summer months of six gages (mm). 61

Table 10. Observed and simulated median length of dry and wet spells (day). 62

Table 11. Statistics of observed and simulated annual rainfall statistics. 64

Table 12 Statistics of flume measured and model simulated summer runoff (unit: mm). 69

Table 13. Statistics of observed and simulated summer runoff (unit: mm). 71

ABSTRACT

Many semi-arid regions of the world experience rainfall patterns characterized by high spatial variability. Accurate spatial representation of different types of rainfall will facilitate the application of distributed hydrological models in these areas. The objective of this study was to develop a daily, spatially distributed, stochastic rainfall generator based on a first-order Markov chain model, calibrated using 50 years of rainfall observations at 88 gages from 1967 through 2016 in the 148-km^2 Walnut Gulch Experimental Watershed, and then apply it in three different sized watersheds to see how spatially varied rainfall inputs will impact the hydrologic responses. Three types of rainfall, including convective, frontal, and tropical depression storms, were simulated separately in the generator using biweekly parameterization. Convective storms were simulated based on an elliptical shape rain cell conceptual model, whereas frontal and tropical depression storms were simulated as uniform rainfall fields over the whole watershed with introduced random variability. The rainfall generator was evaluated by comparing the mean statistics of 30 replicates of 50-year simulated data versus the 50-year rain gage observed data. Most individual storm statistics and aggregated seasonal rainfall statistics were similar to the measured rainfall observations. The long-term mean values of both summer and winter rainfall amount were statistically satisfactory. Afterwards, two rainfall sequence data generated by a single-site rainfall generator (CLIGEN) and the spatial rainfall generator were passed into Soil and Water Assessment Tool (SWAT) for runoff simulation. Statistics showed that single-site and multi-site rainfall generators gave similar results regarding to annual precipitation. However, the

multi-site generator performed much better than the single-site generator in both mean summer flow and different return period flows. Single-site generator derived runoff was significantly overestimated in all three level watersheds, whereas multi-site generator performed satisfactorily in smaller watersheds and only did an overestimation in the largest watershed. It is indicated that in small to medium sized watersheds, the spatial variability of rainfall could still play an important role for hydrologic response, which made the application of multi-site rainfall generator become necessary.

Key Words: spatial rainfall generator; convective storm; hydrologic response; watershed modeling; semi-arid;

1 INTRODUCTION

Precipitation provides input water source for a watershed, which plays an important role in the hydrologic cycle. Understanding the variability of precipitation is essential for hydrologic studies and watershed management. It is a driving force for other hydrologic processes such as infiltration, surface runoff and so on. Globally, rainfall has the most impact on natural environment and human lives among all forms of precipitation. It is also of great interest beyond the hydrological aspect, such as for ecological, biological and environmental concerns. However, current rainfall observations still have problems with either spatial coverage extent, temporal and spatial resolution or accuracy. Traditional methods, like rain gages observation, commonly only provide a sparse representation of spatial rainfall. The density of rain gage networks are inefficient and are heavily biased since most gages are located in wealthier and developed regions (Shuttleworth, 2012). Many countries do not have a thorough plan on rain gage monitoring networks, but rather a localized process (Andiego et al., 2017). Another study pointed out that the actual gage availability for research is highly variable which depends on the latency requirements and time range of study (Kidd et al., 2017). It was noted in several studies that the rain gage network density has an impact on either runoff volumes or peak discharges simulation, and decreasing the network density could lead to information loss when doing rainfall related analysis (Andiego et al., 2017; Hernandez et al., 2000; Shah et al., 1996).

Besides the traditional rain gage data, radar data provides another source of precipitation observation, especially for large spatial coverage. Radar images can

represent the spatial rainfall field since it has a full coverage of the designated area with no gap, which is not achievable by rain gage networks (Bonnifait et al., 2009; Morin et al., 2006; Sidman et al., 2016; Smith et al., 2004). However, the newly developed radar system is not a direct measurement of rainfall but based on rainfall reflection rates. Many factors including drop size and precipitation type can impact the measurement leading to error. The deficiencies are that radar data needs careful calibration with rain gages measured data, or that the pixel size is too large to capture the rainfall variation inside the pixel (Sidman et al., 2016). Another problem with radar data is the lack of continuous long-term records. Long-term, high resolution rainfall data are always needed for hydrologic or agricultural engineering designs and climate change simulations (Wilks and Wilby, 1999). In general, the lack of continuous reliable rainfall records limits the development of hydrologic research and applications. Neither rain gage network or radar system provides adequate precipitation data for those purposes.

Because of the inadequacy of observed precipitation data from rain gages and radar systems, models are used as a complementary way to generate precipitation series. Deterministic weather models utilize numerical algorithms and incorporate a set of equations describing the flow of fluids (Breinl et al., 2017; Wilks and Wilby, 1999). They are extensively used in weather forecasting services. The computational cost is high for this numerical type model since they require large quantities of parameterization and not suitable when running hundreds or thousands of simulations. Another model type is the stochastic models based on statistical characterization and representation of historical precipitation data. Their outputs are not aimed at simulating specific weather sequence at

a given time, but to statistically behave like the long time precipitation data for a certain place (Wilks and Wilby, 1999). Stochastic models can generate a sequence of rainfall events which maintains the key statistical characteristics of the historical records (Mehrotra et al., 2006; Wilks and Wilby, 1999). The results can be seen as a possible realization of the rainfall distribution in time and space, instead of the real events (Ferraris et al., 2003). The advantage is much less computational cost and can easily applied for different scenario simulations (Breinl et al., 2017). Many studies use stochastic rainfall generator as a downscaling method, either temporally or spatially. Theoretically, it can generate the rainfall records as long as needed by any applications. The resolution of generated rainfall records is specifically designated for each type of model. The advantage of simulated rainfall data is that they can provide long series of statistically representative records, which can be used in hydrological models, agricultural models, or climate change impact assessment to produce mathematically stable statistical representations of hydrologic response for a given weather record. As models become more sophisticated, the requirements for higher resolution and continuous rainfall series data become more important (Bonta, 2004a; Breinl et al., 2017; Li et al., 2017; Serinaldi, 2009).

So far, single-site stochastic rainfall generators are still the most commonly used models. They have also be called uni-site generators or point-based generators in some studies. Single-site rainfall generators are based on the statistical characteristics of one single station. It does not consider the correlation between stations, in which case, this kind of model focuses only on the temporal rainfall process. Most widely used single-site

models are based on a daily simulation, including the generation of the rainfall occurrence (wet-dry process) and the rainfall amount (Srikanthan & McMahon, 2001; Wilks & Wilby, 1999). Recently, there has also been work done to model sub-daily rainfall processes (Bonta, 2004a, 2004b; Paschalis, et al., 2013). According to the method of acquiring rainfall occurrence, the models can be classified into two types: Markov chains and alternating renewal processes (Srikanthan and McMahon, 2001). These point generators do not provide an accurate prediction of the variable rainfall fields spatially.

However, hydrologic response is a complex process which is controlled by several factors, such as precipitation, topography, land use and land cover, and soil properties. Precipitation provides the input water source into this process and the link between rainfall variability and runoff generation remains an important issue in hydrology studies. Scholars have done many research studying effect of the spatially variable rainfall on the hydrologic response that is discussed later in the literature review. Recently, research focus has transferred from single-site rainfall generator to more sophisticated multi-site rainfall generators or spatial rainfall generators (Breinl et al., 2017; Hellassa and Souag-Gamane, 2019; Watson et al., 2005; Wilks and Wilby, 1999). In order to accurately model hydrologic response at a watershed scale we need a rainfall generator that can simulate non-uniform rainfall fields in space. Such a spatial generator will provide insight in the application of many watershed hydrological models.

In this study, we will develop a Markov-chain based spatial stochastic rainfall generator to simulate daily rainfall in a semi-arid watershed located in southeastern

Arizona, and further apply the rainfall into hydrological modeling to evaluate the links between spatial rainfall and hydrologic response. The major objectives are:

(1) present a conceptual model to characterize the spatial variation of the summer convective rainfall;

(2) build a stochastic daily rainfall generator capable of simulating three types of rainfall with high spatial resolution that can be used in small to medium sized watersheds;

(3) evaluate the performance of the spatial rainfall generator;

(4) generate and compare precipitation data using both a single-site rainfall generator and the newly developed spatial rainfall generator;

(5) calibrate a hydrological model based on Walnut Gulch Experimental Watershed observed rainfall and runoff data;

(6) replace observed rainfall with both single-site and spatial rainfall generator into the hydrological model and then compare the hydrologic responses of those different rainfall inputs.

2 LITERATURE REVIEW

2.1 Spatial rainfall generator

Rainfall has both temporal and spatial characteristics that need to be accounted for in the generation process. Point-based rainfall generators, which focus on the temporal dimension of rainfall, are the most commonly used models (Arnold and Williams, 1989; Calenda and Napolitano, 1999; Kavvas and Delleur, 1981; Papalexiou et al., 2011; Richardson, 1981; Valdes et al., 1985). These generators are based on single site observations, and therefore not designed to provide spatial resolution. Researchers have studied the effect of spatially variable rainfall on hydrologic response. Some studies argued that the spatial variability of rainfall does not cause significant differences in runoff generation or only causes secondary effects (Beven and Hornberger, 1982; Obled et al., 1994; Schuurmans and Bierkens, 2006). These catchment sizes ranged from 71 to 287 km^2, which were mostly medium sized rural catchments. Obled et al. (1994) noted that their conclusions may not apply for smaller urbanized or larger rural areas. Schuurmans and Bierkens (2006) found that the spatial variability has a major effect on daily simulation of discharge, groundwater level and soil moisture, while for general longer-term behavior of the hydrological system, the areal average rainfall information is adequate. Koren et al. (1999) noted that heterogeneity of rainfall is a major factor for small scale catchments, but the fraction of the watershed covered by rainfall is not as important since rainfall is likely to cover the whole area. However, for larger scales, the fractional area of the watershed covered by rainfall is a major factor for runoff generation. Specific site conditions, in terms of either climate characteristics or size of

the watershed, can lead to quite different conclusions on how spatial rainfall affects hydrological responses. In a semi-arid region, such as is found in much of the southwestern United States, where runoff is dominated by summer convective storms, transmission losses in ephemeral channels are a significant factor in the water budget (Goodrich et al., 1997; Renard et al., 1993). Thus, the spatial distribution of rainfall may matter more in these environments, creating distinctive runoff response for upper and lower streams. Bell and Moore (2000) also pointed out that convective rainfall induces more sensitivity in runoff production than does stratiform rainfall. To facilitate the accurate modeling of hydrologic response in semi-arid regions, such as in southeastern Arizona, a rainfall generator that can simulate non-uniform rainfall fields in space is needed. It will enhance the ability to apply distributed watershed hydrologic models.

Spatial rainfall generators may use multi-site data for a specific region, so they can also be referred to as multi-site rainfall generators. Compared with point-based generators, multi-site rainfall generators take spatial correlation between stations into consideration, since rainfall stations near enough are not totally independent of each other. Storms organize into groups and form linear bands or spiral bands under different weather systems in nature (Shuttleworth, 2012). In recent years there has been extensive research conducted on different types of multi-site rainfall generator models (Asong et al., 2016; Bardossy and Plate, 1992; Breinl et al., 2017; Evin et al., 2018; Ferraris et al., 2003; Leander and Buishand, 2009; Li, 2014; Mehrotra et al., 2006; Peleg and Morin, 2014; Serinaldi, 2009; Wilks, 1999). Most rainfall generators deal with two major components: rainfall occurrence and rainfall amount. There are two basic approaches for

precipitation occurrence generation. One is the Richardson-type (Richardson, 1981) and the other is serial type (Racsko et al., 1991). The Richardson-type generator is based on Markov chain models, which simulates day to day rainfall occurrence using transition probabilities. Serial type generators account for long-term wet or dry trends, usually beginning with the simulation of dry and wet series of years, and then simulate rainfall amount based on dry and wet conditions.

There are also basically two types of methods for representing spatial distribution of rainfall amounts. The first type focuses on the physical structure of small scale rain cells, such as shape and size, either using rain gage data (Cowpertwait et al., 1996; Ferraris et al., 2003; Hsieh, 2002; von Hardenberg et al., 2003) or radar images to acquire the parameters (Morin et al., 2006; Peleg and Morin, 2014, 2012). The other type considers relatively larger scale rainfall fields, usually incorporating mathematical representation of the spatial correlation. Further classification of this type can include several different methods: (1) statistical multi-site models, usually achieved by fitting empirical distributions for rainfall properties and adding spatial correlation matrix to represent inter-sites relation (Brissette et al., 2007; Khalili et al., 2009; Mehrotra and Sharma, 2007; Serinaldi, 2009; Wilks, 1998). (2) resampling/bootstrap models, where rainfall depths were resampled from historical data (Buishand and Brandsma, 2001; Leander and Buishand, 2009). Recent improvements of resampling methods included adding a reshuffle process to maintain the spatial properties (Breinl et al., 2013, 2015). (3) Nonlinearly filtered autoregressive processes (Lanza, 2000; Mejía and Rodríguez-Iturbe, 1974; Rebora et al., 2006). (4) generalized linear models (Asong et al., 2016;

Verdin et al., 2018, 2015). (5) fractal cascade models (Gupta and Waymire, 1993). Of all the above approaches, rain cell models are particularly appropriate to simulate convective storms, since these storms share common features of short duration and limited spatial extent (Osborn et al., 1979). Generalized linear models have failed to capture the summer convective precipitation characteristics (Verdin et al., 2015).

Rain cells can either be simulated using circular (Morin et al., 2005; Morin and Gabella, 2007; Peleg and Morin, 2014) or elliptical shapes (Barnolas et al., 2010; Peleg and Morin, 2012; Syed et al., 2003). The circular shape is easier for modeling since it only has one radius parameter, and the intensity distribution can be simplified as well because the cell is isotropic. The elliptical shape is more complex since it has both a major and minor axis, which also requires an additional orientation parameter. It is also necessary to define the center coordinates of the cell and the coverage area for both kinds of cells. In addition to cell shape parameters, researchers also have studied the representation of rainfall intensity within the cell: (1) rain cells with a constant intensity everywhere; (2) Gaussian decay of intensity from cell center; (3) exponential decay of intensity from cell center; (4) hybrid of Gaussian and exponential decay from cell center. The use of constant intensity makes the model simpler, but not generally realistic, especially when the research focus is on sub-daily rain cell development. Feral et al. (2003) noted that the Gaussian distribution leads to a faster decay of rainfall intensity from the center outwards but to a lower gradient for the outer part. The specific function might differ from region to region, which needs further calibration based on actual data.

Since temporal scale is not the primary consideration in this study, we used a daily step in this rainfall generator. The Richardson-type of generator was used for daily rainfall occurrence. The geographic area we are concerned about is dominated by convective rainfall during the summer, which is suitably represented by a rain-cell based generator. We combined simulations of individual rain cells to acquire the rainfall field over the entire watershed.

2.2 Hydrologic response

There is no consistent conclusion about how rainfall variability affects hydrological response. Some researchers argue that the spatial variability of rainfall does not cause significant difference in runoff generation (Beven and Hornberger, 1982; Obled et al., 1994; Schuurmans and Bierkens, 2006). Notice that these conclusions were drawn under certain conditions. Beven and Hornberger (1982) distinguished spatial rainfall variability into three simple types: upper basin concentrated, lower basin concentrated and relative uniformly distributed. By analyzing the hydrographs, they tested the effect on peak discharge, time to peak and total storm volume. Results showed that only the difference in peak timing was significant, but not the total storm runoff volume. Obled et al. (1994) used two different densities of rain gage network to test the effect of rainfall spatial variability. They claimed that though the spatial representation is important, it only has a secondary effect on explaining the discharge. However, they also pointed out that the conclusion is specifically for this medium-sized catchment (approximately from 100~1000 km^2) in a temperate climate. The mechanism could be different for large and small sized catchments or in arid and semi-arid catchments where downstream

transmission losses into the channels are active and important (Goodrich et al., 1997; Renard et al., 1993). In arid and semi-arid watersheds, transmission losses in ephemeral channels will be a significant part of the water budget. The runoff response in the upper stream and lower stream could have a large difference. The spatial distribution of rainfall matters more in these environments. Schuurmans and Bierkens (2006) found that the spatial variability has a major effect on daily simulation of discharge, groundwater level and soil moisture, while for general, longer-term behavior of the hydrological system the areal average rainfall information is enough. Fu et al. (2011) got similar results that the resolution of rainfall has little effect on annual water balance, and the effect on discharge is relatively low on catchments over 250 km^2.

Despite the above conclusions, which indicate spatial variability of rainfall might not be critical for runoff generation, there are still many studies indicating that the effects are not negligible. Some researchers (Bárdossy and Das, 2006; Caracciolo et al., 2014; Faurès et al., 1995; Hernandez et al., 2000; Lopes, 1996; Segond et al., 2007; Shah et al., 1996; Wilson et al., 1979) explored the impact of different density of rain gage networks as input for hydrological models. The basic idea was to use a full network of rain gages to represent the true rainfall variability field, and then by decreasing the number of gages to compare the different output discharge data, including variables like peak discharge, total runoff volume, time to peak, shape of the hydrographs. Besides gage network density, the location or distribution of the gages also matters (Bell and Moore, 2000; Lopes, 1996). It is easy to imagine that with the same number of gages; a clustered distribution and a dispersed distribution network could capture different rainfall characteristics.

Topography should also be considered in gage distribution, and mountainous areas generally need denser networks than do plain areas to represent the spatial variability. Bell and Moore (2000) pointed out that convective rainfall type induces more sensitivity in runoff production than stratiform rainfall. Thus, we should recognize that high density or resolution does not necessarily mean accurate spatial representation. It also depends on other factors like rainfall types or topography.

2.3 Hydrologic modeling using rainfall generators

Though numerous field experiments provided observed records including rain gage data and flume measured streamflow for research purpose, the uncertainty caused by other watershed factors limits the understanding of how rainfall variability affects hydrologic response. An alternative way instead of using historical rainfall and streamflow data for this research is through hydrological modelling, by varying the input rainfall fields and comparing the runoff generation results based on synthetic data. With the modelling process, all other variables can be kept constant throughout different scenarios.

Simple simulated rainfall data can be generated based on design storms (Sidman et al., 2016; Woolhiser and Goodrich, 1988). A more complicated method would use a rainfall generator to generate different rainfall inputs (Emmanuel et al., 2015; Krajewski et al., 1991; Li et al., 2013; Ogden and Julien, 1993; Xu et al., 2014) and in recent years, study focus has been put into comparison of single-site and multi-site rainfall generator effects on hydrologic modelling (Breinl, 2016; Khalili et al., 2011, 2006; Li et al., 2017;

Watson et al., 2005). The advantage of using rainfall generator is that the input rainfall scenario is no longer limited to historical observed situations, and you can control the statistical characteristics tested. Multi-site or spatial rainfall generators also make the test of rainfall spatial variability on hydrologic responses available. The watershed sizes ranged from 306 to 45421 km^2 in these studies. Watson et al. (2005) compared the single-site generator DMAn (Srikanthan, 2004) versus multi-site generator MS2P (Srikanthan, 2005) using Soil and Water Assessment Tools (SWAT) for runoff simulation in a 306 km^2 watershed in Australia. The results showed that the distinction between single-site and multi-site driven SWAT results was not significant. Li et al. (2017) also applied SWAT simulation in a comparison between single-site generator (Li et al., 2013; Richardson and Nicks, 1990; Wilks and Wilby, 1999) and multi-site generator (Wilks, 1998), but in a much larger river basin of 45421 km^2 in China. He got a contradictory result with Watson that spatial structure of weather generators had a noteworthy effect on hydrological variability prediction, especially for maxima and variances. Since both the watershed scale and climate differed a lot for these two cases, it is not uncommon to draw two different conclusions. Actually, more studies reached similar conclusions with Li et al. (2017). Khalili et al. (2006) did hydrological model simulations in a 9700 km^2 watershed in Canada, using a Richardson type single-site (Richardson, 1981) and a multi-site (Khalili et al., 2006) generated rainfall sequences as inputs. The research indicated that multi-site simulation produced more practical natural flow hydrographs and better extreme events. Another recent research (Breinl, 2016) did comparison in two snow-melt dominated runoff watersheds, with areas of 4637 and 548 km^2 respectively. Conclusions

confirmed that single-site produced rainfall would underestimate extreme stream flows significantly while multi-site generator performed better.

Most studies done above are targeted at medium to large scale watersheds, because at this level, the spatial variability of rainfall is prominent. Our study is focused at a semi-arid region in Arizona of the United States, where convective rainfall dominates the precipitation and summer flow. This type of rain usually covered a limited spatial extent with relatively short duration but high intensity (Goodrich et al., 2008; Nearing et al., 2015; Nichols et al., 2002; Stillman et al., 2013). Thus, our focused area is from small to medium sized watersheds which still receive spatially variable rainfall. The main objective is to run hydrological model simulations with both a single-site and multi-site rainfall generator produced inputs, and then compare whether the rainfall variability still plays an important role in these small to medium level watersheds, under semi-arid climate condition.

3 METHODOLOGY

3.1 Study area and data

The study area is the Walnut Gulch Experimental Watershed, located in southeast Arizona, surrounding the town of Tombstone. It is a sub-watershed of the San Pedro River Basin. The USDA-ARS Southwest Research Center has been operating in the watershed since the 1950s with intensive instrumentation and measurement of precipitation. The drainage area of Walnut Gulch is approximately 148 km^2, and elevation ranging from 1220 m to 1900 m above sea level. Climate is semi-arid type with a mean temperature of 17.7 °C at Tombstone. The average annual precipitation in this semi-arid watershed is approximately 312 mm (Goodrich, Keefer et al., 2008), following a bimodal pattern, with most precipitation occurring in summer and winter seasons (Osborn, 1983). Summer rainfall, during the months of July, August, and September, accounts for approximately 60% of the total annual amount in this region, and results from the North American Monsoon (Nichols et al., 2002; Stillman et al., 2013). The summer rain often forms as convective storms, with relatively short duration but high intensity, and cover a limited spatial extent. The spatial variation of summer convective storms is large. The winter frontal storms are, however, usually of long duration but low intensity, and usually cover the whole watershed more uniformly (Goodrich, Unkrich et al., 2008; Nearing et al., 2015; Nichols et al., 2002; Stillman et al., 2013). Frontal storms during the non-summer months account for approximately 35% of the annual precipitation. Occasionally, snow occurs in winter at the watershed, but it melts quickly and does not accumulate. The remaining 5% of the annual rainfall falls in the form of

tropical depression storms, usually dropping large amounts of water, much of which will be converted into runoff (Gochis et al., 2006; Osborn, 1982).

Walnut Gulch Experiment Watershed has more than sixty years of rainfall monitoring. The earliest rainfall record dates back to 1954. The current rain gage network consists of 88 digital rain gages (Figure 1), which gives an average of approximately 0.6 gage km^2 over the watershed. The dense network provides advantages for spatial rainfall analysis, especially for the summer convective rainfall events with high spatial variation. The full current network of 88 gages was installed by 1967, so this study uses rainfall data from 1967 through 2016 (50 years) to build the generator. From 1967 through 1999, the rainfall data was recorded by analog rain gages, while after 2000, digital gages were used (Goodrich, Keefer et al., 2008). Due to resource considerations, only nine gages operated during the winter months from 1981 through 1991 and in 1999. The reason for this is that winter rainfall in this area is much less spatially variable and the high density of rain gages were not considered necessary (Goodrich, Keefer et al., 2008). All rainfall data used can be acquired on the website of USDA-ARS-SWRC at http://www.tucson.ars.ag.gov/dap/. The rainfall records are stored in an Access database, including both daily rainfall and event rainfall. The daily data recorded the year, month, day and total depth received by a certain gage on that day. The event data recorded the event ID, year, month, day, start time, duration and depth by a certain gage. Each day may have multiple events in the database for a gage. The resolution for depth is 0.254 mm (0.01 inch) and the resolution for duration is 1 minute.

The total drainage area of Walnut Gulch Experimental Watershed is 148 km^2 and monitored by flume 1 at the watershed outlet (Figure 2). The other two flumes selected in this study are flume 2 and flume 6, controlling drainage areas of 112 km^2 and 93 km^2 respectively, accounting for about 75% and 60% of the whole watershed area. The three flumes selected in this study are the same type, which is Walnut Gulch Supercritical Flume. Soils in Walnut Gulch are mainly sandy loam with heavy gravel content. The surface rock coverage can range from very small percent on shallow slopes to over 70% on steep slopes. As for vegetation, there two major type of structure in Walnut Gulch, shrub-dominated and grass-dominated. Shrub-dominated sites have shrub canopy cover from 30% to 40%, whereas on grass-dominated sites, the grass canopy cover ranges between 10 to 80%.

As for streamflow, summer monsoon rainfall induces most runoff events in the watershed between July and September. These summer convective storms possess characteristics of relatively short duration but high intensity, which create preconditions for surface runoff events in Walnut Gulch (Goodrich, Unkrich et al., 2008; Stone et al., 2008). Another source of runoff comes from the tropical depression storms which usually forms in the early fall. They are quite large events but rare in frequency. Winter frontal storms generate little runoff because they are low in intensities (Goodrich Unkrich, et al., 2008; Nearing et al., 2015; Nichols et al., 2002; Stillman et al., 2013). Snow occurs occasionally at the watershed but melts quickly and has little impact on annual runoff. In general, similar to other semi-arid watersheds, runoff in Walnut Gulch follows a seasonal

pattern and most time of the year the channels are dry. Ephemeral streams dominate in this region, and transmission loss process plays an important role in the hydrologic cycle.

Runoff data are also provided on the website of USDA-ARS-SWRC at http://www.tucson.ars.ag.gov/dap/. In this research, daily rainfall data was used for SWAT simulation. As for streamflow, monthly aggregated runoff depth of Flume 1, 2 and 6 were used in the calibration process. The time range is the same with rainfall data, from 1967 through 2016. Other data used in the hydrological modeling process included: USGS 10-meter DEM, National Land Cover Database 2011 (NLCD 2011), and Soil Survey Geographic (SSURGO) database.

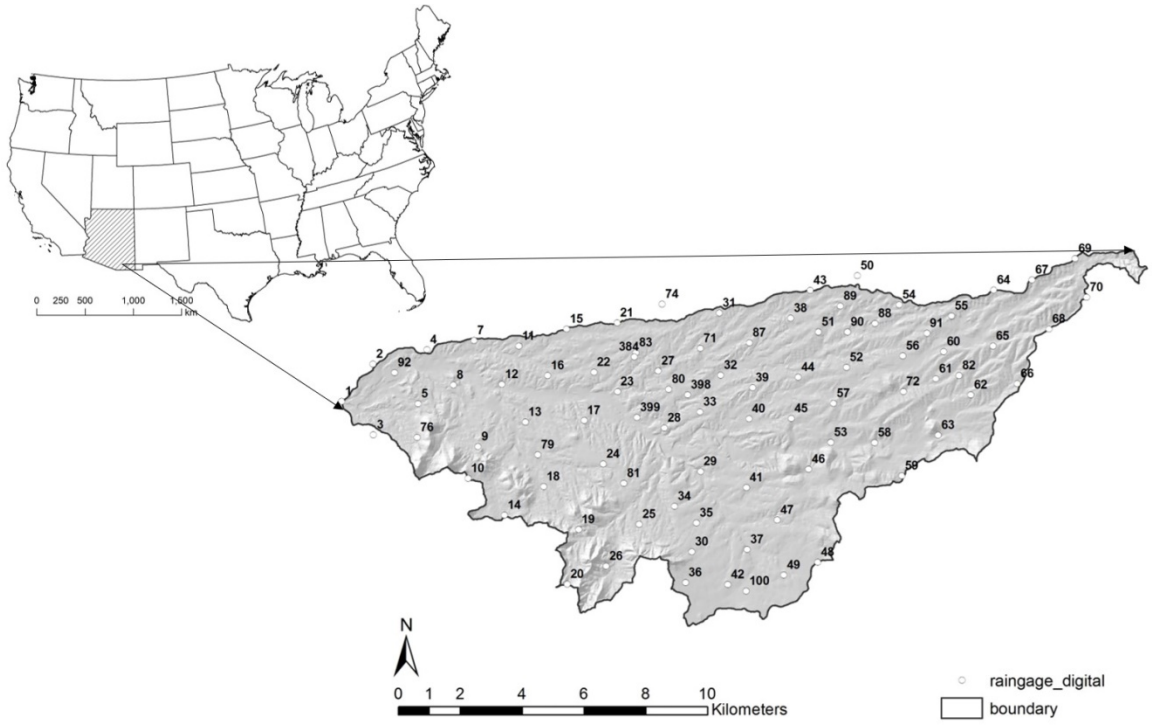

Figure 1. Rain gage network of USDA-Agricultural Research Service Walnut Gulch Experimental Watershed, Tombstone, Arizona.

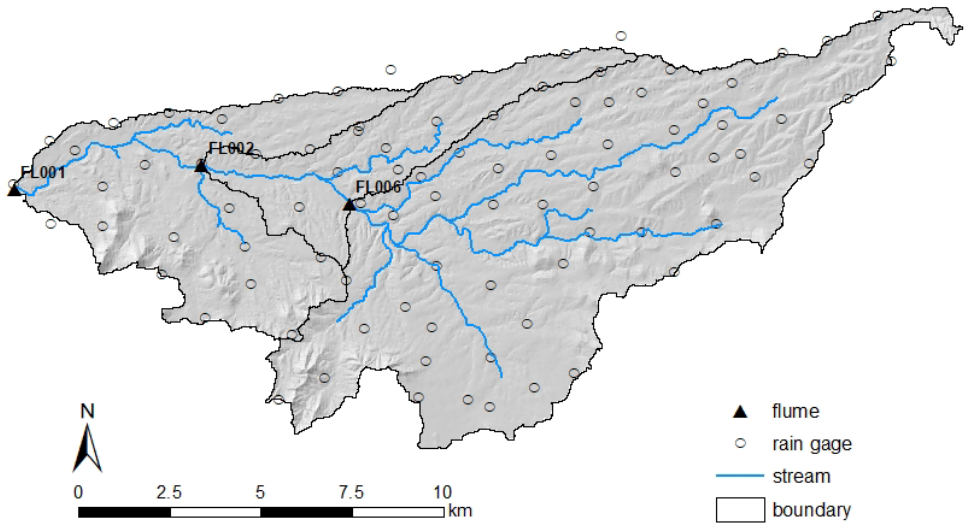

Figure 2. Map of Flume 1, Flume 2 Flume 6 and main stream networks of Walnut Gulch Experimental Watershed, Tombstone, Arizona.

3.2 Spatial rainfall generator development

3.2.1 Storm identification

A continuous rainfall record consists of both wet periods and dry periods. Researchers have explored different methods to distinguish events, usually based on a threshold of the dry period. This threshold can be a fixed time interval for all months, such as 6 hour used in erosive rainfall studies (Wischmeier and Smith, 1978). It can also vary with months, depending on the actual distribution of the inter-arrival time of rainfall in each month. The Walnut Gulch rainfall database has identified events for each gage separately and assigned an event ID to each one. The criteria used for each gage in the database was based on a one hour hiatus (Goodrich, Keefer et al., 2008). However, this separation is only for one rain gage, which means if two gages received rainfall at the

same time, they are still assigned different event IDs in the database. An actual storm occurring in the watershed usually involves more than one gage, so it is necessary to identify the individual storms within the entire gage network. According to visual perusal of daily rainfall interpolation maps (Figure 3), we determined that a reasonable storm cell number within one day was no more than five. Longer thresholds give fewer storms identified for each day, since more gage events will be combined. The 4-hour threshold to separate and identify storms was selected so that the daily storm numbers were equal to or fewer than five. When the event starting times of two gages were within that threshold, they are identified to be the same storm in the watershed. The maximum depth for each storm was also recorded during the storm identification process.

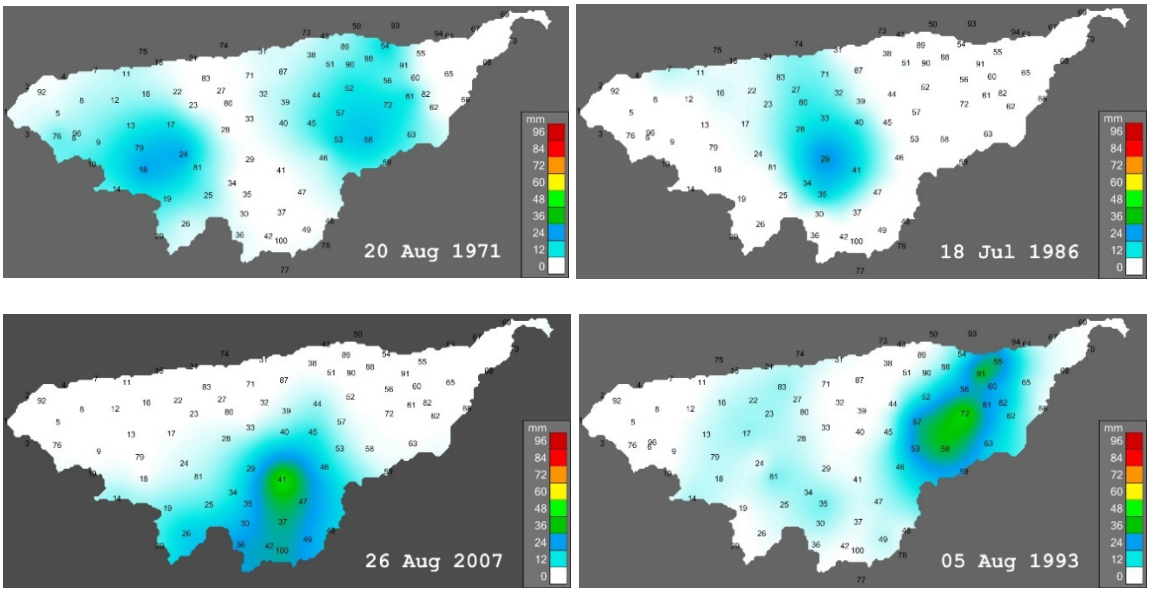

Figure 3. Examples of daily rainfall interpolation results for summer convective storms on Walnut Gulch Experimental Watershed.

3.2.2 Rainfall occurrence

The rainfall generator is built with a Richardson type framework, using a first-order Markov chain model (Richardson, 1981). A flow diagram of the computational processes of rainfall generator was shown in Figure 4. The basic concept of the first-order Markov chain method is that the present state of the system only depends on the previous state, which translated into the rainfall generation process means that the wet or dry state of the current day depends only on the state of the previous day. Using the Markov approach, a wet day is designated if at least one rain gage in the watershed receives rainfall on that day. Once a wet day is generated for the watershed, the model then generates the storm location and coverage, which determines how much simulated rainfall each particular gage receives. In order to generate a sequence of wet and dry days, three transition probabilities need to be calculated. P(W) is the probability of a wet day, P(W|W) is the probability of a wet day following a wet day, and P(W|D) is the probability of a wet day following a dry day. Previous research in Walnut Gulch showed that the transition probabilities for biweekly periods have significant differences from each other (Hsieh, 2002), so all transition probabilities were calculated on a biweekly basis. Modeling of the wet and dry sequence in the rainfall generator is done by first initializing a random number, and then using P(W) to decide the state of first day. After the state of the previous day was decided, then the transition probabilities P(W|W) and P(W|D) were used to calculate the state of the next day in each biweekly period for the entire simulation sequence (Figure 4).

When a wet day is generated, the type of rainfall also needs to be decided for that day. The consensus of most studies on Walnut Gulch is to separate each year into summer months (July-September) and non-summer months (Goodrich, Keefer et al., 2008; Nearing et al., 2015; Nichols et al., 2002; Osborn et al., 1979) in terms of differentiating rainfall types. The dominant type for summer months is convective rainfall, while the dominant type for non-summer months is frontal rainfall. The third type, tropical depression rainfall, occurs primarily in late summer and fall, from September through November (Gochis et al., 2006). Probabilities for these three types of rainfall were calculated for each biweekly period using the daily rainfall. Periods with only one type of rainfall occurrence is straightforward, i.e. the probability of a rainfall to be a frontal type in December and January through June is 1. Similarly, the probability for convective rainfall in July through August is also 1. The complicated period is from September through November, where the probability for tropical depression storms needs to be considered. To do this, the histogram of all maximum depths of the storms in September through November were plotted, and then an exponential distribution was fitted to that histogram. The storms with large maximum depth on the histogram tails, which could not be fitted well by the exponential curve, were identified as tropical storms. Thus, their probabilities were calculated using the number of these storms divided by the total number of storms. All biweekly periods in September through November share the same probability of tropical depression rainfall, and the remainder of the probability for convective and frontal storms in these three months are obtained by

subtracting those from 1. Thus, each day of rainfall as determined by the transition probabilities were categorized as one of the three rainfall types.

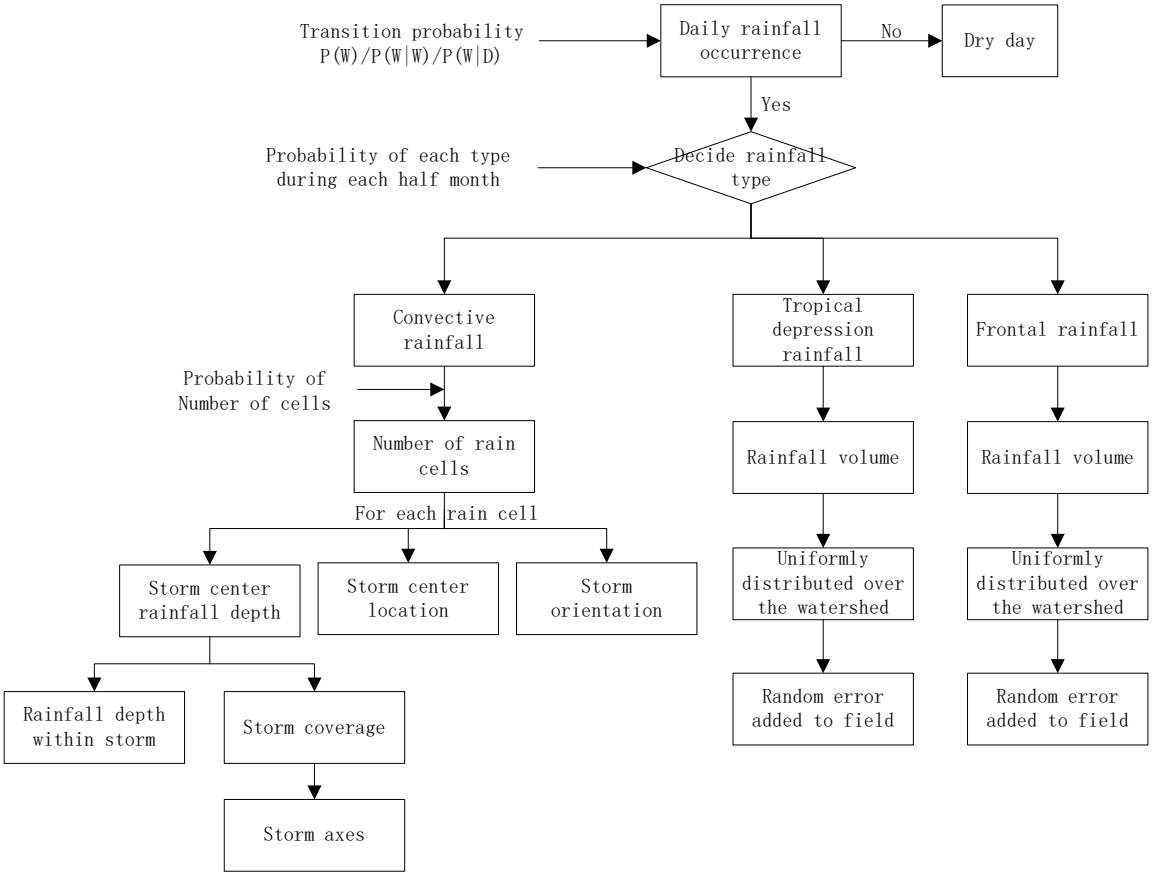

Figure 4. Flow diagram of the computational processes in the rainfall generator.

3.2.3 Rainfall amount and distribution

(1) Convective storms

Convective storms usually show with an approximately elliptical shape in space, as determined either from interpolated daily rainfall maps or radar images (Hsieh, 2002; Karklinsky and Morin, 2006; Peleg and Morin, 2012). Hsieh (2002) analyzed convective storms in Walnut Gulch and proposed a conceptual model to characterize them (Figure

5). This current study followed a similar conceptual model and determined several parameters using rainfall data from July through September collected in 1967 through 2016.

The previous study of Hsieh (2002) showed that the storm centers are distributed randomly in the watershed. Sometimes a storm falls only partly within the watershed boundary, which means the generated storm center can also be outside the boundary. To address this, the generator uses a slightly larger area of 26.5 km by 12.5 km, divided it into 33125 cells, with each cell representing a 100 m by 100 m area and assigned an index from 1 through 33125. The equation to obtain a storm center location Z is:

$$z = \frac{Z}{33125} \tag{1}$$

where Z is the center index ranging from 1 through 33125, and z is the standard uniform deviate ranging from 0 to 1.

Once the storm center is located, a storm center depth is generated from a lognormal distribution and assigned to this storm. Several distributions were tested for the convective storm maximum depth, and the lognormal fit best for the data. It is assumed that the depth at the storm center is the maximum and decays to zero on the storm edge. A modified linear spread function was applied in the generator (Figure 6), which maintains constant intensity amount around the center, and then follows a linear decay function to the edge.

$$depth = \begin{cases} \max dep & 0 \le r \le c \times D \\ \max dep(1 - r / D) / (1 - c) & c \times D < r \le D \end{cases} \quad (2)$$

where *depth* is the rainfall depth at a certain point inside the storm extent, *max dep* is the maximum depth at storm center, *D* is the distance from the center to the edge passing through at a certain point, *r* is the distance from the center to that point, *c* is a constant between 0 and 1. The calibration of *c* was made by matching the simulated total summer rainfall amount to the observed rainfall.

The storm area is related to the maximum depth of the storm. After logarithmic transformation, a linear regression was built between the area and the maximum depth:

$$\ln(area) = a_0 + a_1 \ln(\max dep) + \varepsilon \quad (3)$$

where the units for storm area are km^2, and the units for maximum depth is *mm*, a_0 and a_1 are the coefficients of the linear regression equation, ε is a random error term.

An elliptical shaped storm has two axes, the major axis *a* and the minor axis *b*. The ratio *c* between them is defined as *c = a/b*. The value of *c* follows a normal distribution. Distribution parameters were acquired from Hsieh (2002). The simulated ratio was bounded between one standard deviation around the mean. When both the area and the ratio has been chosen for a storm, the length of major and minor axis can be calculated from the area equation of an ellipse.

The last parameter for a convective storm is the orientation. It is defined as the counter-clockwise angle starting from the east. The orientation for a storm is between 0 and 180 degrees and follows a normal distribution. Distribution parameters were acquired

from Hsieh (2002). The simulated orientation was bounded between one standard deviation around the mean, and extreme values beyond the 0 to 180 degrees range were discarded until a new value within the range was generated.

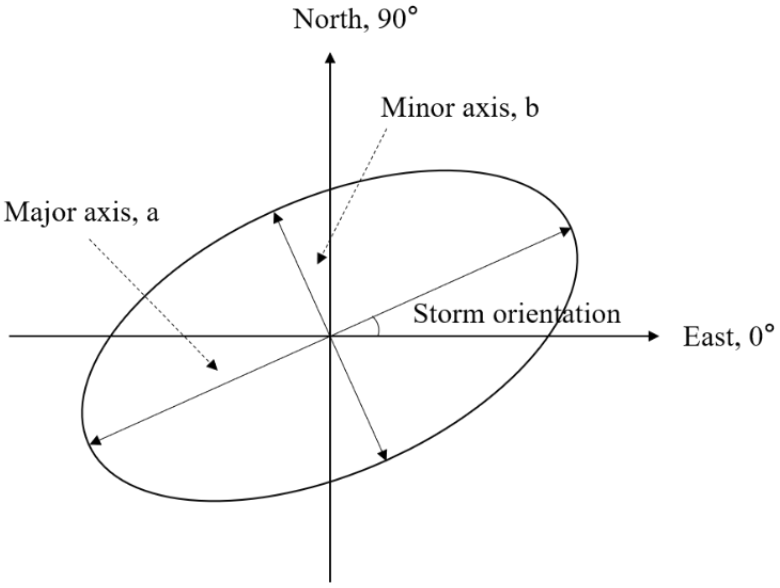

Figure 5. Conceptual model of convective storms.

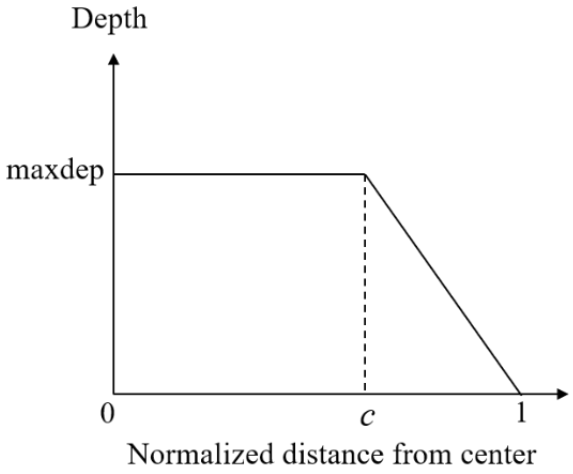

Figure 6. Rainfall depth spread function of convective storms.

(2) Frontal storms

The frontal storms in non-summer months have much less spatial variation than do the convective storms. Osborn et al. (1979) analyzed data from Walnut Gulch in non-monsoon months, suggesting that nine gages are adequate to represent the variability of frontal storms. Rainfall interpolation maps in non-monsoon months also showed this pattern. Since frontal storms usually cover the whole Walnut Gulch, for simplicity, it is assumed that every frontal storm covers the entire watershed in the generation process. The total volume of water of each frontal storm is the important factor for quantifying annual water balance, but from a hydrologic standpoint, winter frontal storms do not usually generate runoff in the channels at Walnut Gulch (Goodrich, Keefer, et al., 2008; Goodrich, Unkrich et al., 2008; Nearing et al., 2015).

The 88 rain gages are nearly uniformly distributed in the watershed, which means the area represented by each gage is approximately the same. The total volume of water that a storm delivers can be calculated by the following equation:

$$Vol = Dep_{avg} \times unit\ area \times N \tag{4}$$

where Vol is the total volume of each frontal storm, Dep_{avg} is the average depth of all gages receiving rainfall, *unit area* is the area of one gage represented, N is the number of gages receiving rainfall. Notice that the *unit area* is not a constant value throughout all the years, because with the deletion or addition of gages over time the number of gages in the full network changed during the recording period. Different *unit area* values needed to be calculated for different years. Data from 1967 through 1980, 1992 through 1998,

and 2000 through 2016 were used to fit a distribution for the total volume of water per storm for each biweekly period. The extremely large values on the tails during September through November fit poorly with the overall distribution curve (Figure 7), which indicates that they follow a different underlying mechanism. Those storms were considered as tropical depression storms and were excluded from the dataset when building the distribution for frontal storms. The model simulation will randomly pick a storm volume from the distribution curve of each biweekly period, first spread it evenly in the whole watershed with each grid having the average depth calculated based on the volume, and then added some randomness for each grid. The random difference added to each grid is based on the standard deviations of the observed rainfall fields, and each standard deviation is corresponded to a certain average storm depth. In order to provide a reasonable variation of the generated rainfall fields, the added randomness is allowed to fluctuate between negative to positive two standard deviations.

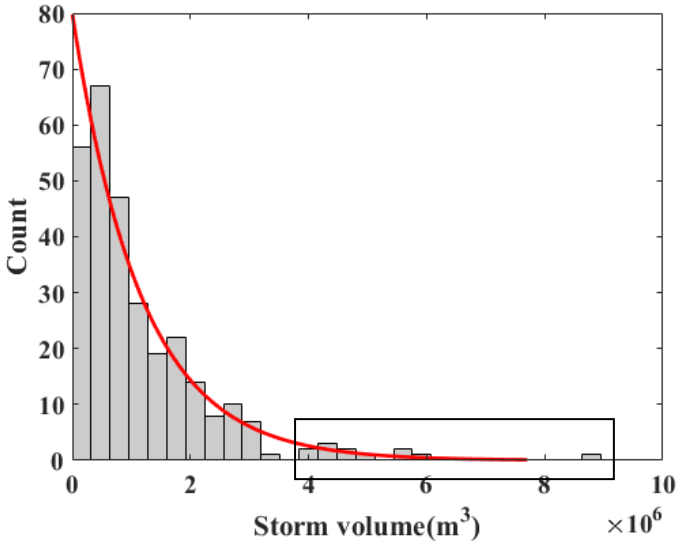

Figure 7. Distribution of storms volume during September to November before excluding extreme events. The grey histogram represented the observed counts of storm volume, and the red line represented the theoretical fitting distribution curve. Events on the histogram tail in the black box fitted poorly with the theoretical distribution curve. This subset of large events cannot pass the K-S test at 5% significance level.

(3) Tropical depression storms

The algorithm to generate tropical depression storms is similar to that of frontal storms. The difference is that these storms are much less frequent and the volume of water dropped by this type is much larger than by frontal storms (Gochis et al., 2006; Osborn, 1982). In the previous steps, the extreme values of storm volumes in September through November were excluded and all these values were fit to a separate distribution, which was used for the tropical depression storms. Unlike the frontal storms, numbers of identified tropical depression storms were limited, so only one distribution was fit for the entire September through November period. The model simulation will randomly pick a

storm volume from the distribution, first spread it evenly in the whole watershed and then add some randomness to each grid. The random difference added to each grid is based on the standard deviations of the observed rainfall fields, and each standard deviation is corresponded to a certain average storm depth. In order to provide a reasonable variation of the generated rainfall fields, the added randomness is allowed to fluctuate between negative to positive two standard deviations.

3.2.4 Multiple events in a day

The results in the Hsieh (2002) model underestimated the total summer rainfall of each gage, partly because the model only simulated one storm per day. Studies from radar analysis have shown that convective rainfall generally consists of several rain cells in one day (Morin et al., 2004; Peleg and Morin, 2014, 2012). Thus, the ability to simulate multiple events per day were enabled in this rainfall generator. Both convective storms and frontal storms can have multiple events per day, whereas the tropical depression storm remained as single event per day because of their sizes and durations. Based on the storm identification process in previous section, probabilities for different numbers of storms occurring in a single day may be calculated. For example, the probability of two events per day is made by counting the number of days with two storms and then dividing it by the number of total rainy days in a biweekly period. Convective rainfall would allow up to five storms per day, while frontal rainfall would allow up to three storms per day in this rainfall generator. Calibration of multiple events probabilities is based on controlling the total number of storms over the fifty-year period. For instance, if the total number of storms is overestimated, then the probability of more than one event was adjusted lower

by multiplying a coefficient between 0 and 1. Consequently, probabilities for one event will be adjusted higher to maintain that the sum of all probabilities adding to one.

3.2.5 Model evaluation

Statistical analyses were performed using MATLAB. The regression equation between convective storm area and maximum depth was based on 4152 convective storms identified in 50 years, with maximum depth ranging from 0.25 mm to 95.12 mm and storm area ranging from 1.59 km^2 to 152.94 km^2. Statistical distribution types were determined for convective storm maximum depths and frontal storm and tropical depression storm volumes by comparing the empirical probability distributions to several theoretical distribution functions, such as lognormal, gamma, and exponential. The Kolmogorov–Smirnov test (K-S test) was used to test the similarity of the empirical distribution to the theoretical ones using a significance level of $p = 0.05$. If more than one theoretical distribution passed the K-S test, then the one with least number of parameters was selected in further modelling processing. After the selection of distribution type, distribution parameters were fit for each type of rainfall as described previously.

The rainfall generator was run for 30 replicates of 50-year simulation (in total 1500 years) to obtain a sequence of simulated daily rainfall, and then compared with the observed 50 years historical rainfall data. Model performance was evaluated in two aspects: individual storm statistics and seasonally aggregated rainfall statistics. Previous research (Goodrich, Keefer et al., 2008; Nearing et al., 2015; Nichols et al., 2002) divided the year into summer months (July-September) and non-summer months (October-

December, January-June), which is adopted in this study as well. The convective storm type was evaluated to determine whether the proposed conceptual model was able capture the major storm characteristics. Seasonally aggregated rainfall amounts were evaluated based on the simulation results of six gages (Gage ID 13, 34, 44, 46, 62, 80). These gages were relatively evenly distributed inside the watershed and were selected as a sample to calculate the seasonal rainfall.

Statistics of both simulated individual storms and aggregated rainfall, including the mean, standard deviation, maximum, minimum, range and skewness, were computed and compared with the 50-year observed data. In addition, simulated and observed cumulative distribution functions (CDFs) were created for both individual storms and aggregated rainfall. K-S tests were performed between simulated and observed CDFs to determine whether they belonged to the same statistical distribution.

Time series properties were evaluated through dry and wet spell lengths of simulated and observed rainfall data. The cumulative distribution function curves of both dry and wet spells were created for summer, non-summer, and annual periods. Seasonal and annual median lengths of dry and wet spells were also calculated for comparison. K-S tests were performed between simulated and observed CDFs to determine whether they belonged to the same statistical distributions.

3.3 Hydrologic modeling incorporating two types of rainfall generator

3.3.1 Observed rainfall

When using the 50 years observed rain gage data as input for watershed simulations, the Thiessen polygon method was employed to create the area-weighted precipitation. Thiessen polygons are zones where any location within the zone is closest to the gage associated with the zone then to any gage. We used Automated Geospatial Watershed Assessment tool (AGWA, Miller et al., 2007) to create the Thiessen polygons, and then intersected it with the sub-watersheds to assign a weight to each polygon representing the percentage of that intersection polygon that comprises the sub-watershed. Then the weighted depth of a certain sub-watershed was calculated by adding all weighted gage depth inside that sub-watershed.

3.3.2 Single-site generator

The single-site rainfall generator used in this study is CLIGEN (Nicks et al., 1995). Many widely used hydrological models, for example WEPP (Flanagan and Nearing, 1995) and SWAT (Arnold et al., 1998; Srinivasan et al., 1998), applied CLIGEN to acquire the rainfall input they needed. It is capable of generating daily precipitation based on the parameter file on a point site. This single-site generator is also under a framework of first-order Markov chain. Rainfall occurrence and amount were simulated in two steps separately. Occurrence is generated based on the transition probabilities P(W|W), and P(W|D), which is the same as the multi-site generator. These probabilities are calculated on a monthly basis. The daily rainfall amount in CLIGEN was generated using a skewed normal distribution of each month. Tombstone station was used to generate a point site rainfall in this study, which is located in the middle of Walnut

Gulch Experimental Watershed. In order to be comparable to the multi-site generator, a same 30 sets of 50-year rainfall dataset was simulated.

3.3.3 Multi-site generator

The multi-site generator we used to compare with CLIGEN was the spatial generator we developed in this study. For better correspondence of name, the spatial generator was referred as multi-site generator hereafter. The detailed generation algorithm was described in the methodology part. This generator can produce a daily gridded rainfall fields with 100 m resolution in space. A brief procedure was described as follows. Rainfall was simulated on a daily basis including two major steps, rainfall occurrence and rainfall amount generation. Occurrence is simply a sequence of wet and dry state, which is acquired by first initializing a random number, and then using the transition probabilities P(W), P(W|W), and P(W|D) to calculate the state of each day, where P(W) is the probability of a wet day, P(W|W) is the probability of a wet day following a wet day, and P(W|D) is the probability of a wet day following a dry day. Different transition probabilities were used for each half month within a year. Once a wet day was generated, the type of rainfall was also designated based on the seasonality, including convective storms, frontal storms and tropical depression storms. The next step is for rainfall amount generation. Convective storms were simulated using a conceptualized elliptical rain cell representing an individual event, where the rainfall depth decreased from cell center to the edge. Several parameters, including the storm center coordinates, area, length of axes, orientation and rainfall depth at the center, were decided based on parameterized statistical distributions of Walnut Gulch rainfall. Frontal

and tropical depression storms were simulated in a similar way, by generating the total volume of water of each storm first, and then distributed it rather uniformly but adding some small variations to the entire rainfall fields. The only difference between these two types was the magnitude of total rainfall volume of each storm, following two distinct exponential distributions parameterized on Walnut Gulch. This multi-site rainfall generator was run for 30 times, each time generating 50-year synthetic daily rainfall sequence on the whole watershed, which were used as rainfall data input for hydrological modeling.

3.3.4 Watershed modeling

Soil and Water Assessment Tool (SWAT) was used in this study for hydrological modeling. SWAT is a watershed model developed by USDA-ARS (Arnold et al., 1998; Srinivasan et al., 1998), aimed at evaluating the impact of land use and management on water, sediment and agriculture chemicals. It is a continuous model designated for long-term simulations on a daily basis, which is suitable to test the effect of daily rainfall generators on runoff responses. All SWAT input parameters except precipitation input were kept the same during simulations, thus to only preserve the relative changes induced by different precipitation input. Climate inputs like temperature and wind speed were simulated by the internal weather generator of SWAT.

SWAT requires the target watershed divided into sub-watersheds and each sub-watershed may include one or more Hydrologic Response Units (HRUs). The three watersheds controlled by flume 1, 2 and 6 of Walnut Gulch were delineated and

discretized using the Automated Geospatial Watershed Assessment tool (AGWA, Miller et al., 2007). Delineation of the controlled watershed was mainly based on the 10-meter DEM data. We first generated flow direction, flow accumulation and stream network step by step, then designated the flume as outlet to delineate the whole drainage area. Discretization into sub-watersheds was based on 2.5% threshold of the total watershed. Initial parameterization was also carried out in AGWA, including inputs of land cover and soil database. After initial parameterization was done, SWAT model input files were created for each flume.

3.3.5 Model calibration

Because SWAT model have several input files for each sub-watershed, including parameter files for watershed configuration, basin, precipitation, temperature, sub-basin, main channel, HRU (hydrologic response unit), management, soil, and groundwater, which in total may have hundreds of parameters to run the model. Thus, it is better to incorporate an automated calibration procedure in this study. We chose the Model-Independent Parameter Estimation (PEST, Doherty, 2015) program to do the calibration based on the monthly runoff in three summer months from July through September. Based on previous research (Van Liew et al., 2007) and knowledge on Walnut Gulch Experimental Watershed, several parameters were selected specifically for PEST optimization in this study (Table 1).

Table 1. Parameters calibrated using PEST

Parameter	Description	Units
CN2	SCS runoff curve number	none
ESCO	Soil evaporation compensation factor	none
SOL_K	Saturated hydraulic conductivity	mm/hr
RCHRG_DP	Deep aquifer percolation fraction	none
CH_K1	Effective hydraulic conductivity in tributary channel alluvium	mm/hr
CH_W1	Average width of tributary channels	meter
SURLAG	Surface runoff lag coefficient	none
SOL_AWC	Available soil water capacity	mm/mm

Calibration was done by comparing between the flume measured monthly runoff versus the SWAT simulated monthly runoff in 50 years (1967-2016), which made a total of 150 observed values with 150 simulated values. In addition to PEST own optimization algorithm, we used another two indices as criteria for evaluation. The first is the Nash-Sutcliffe Efficiency (NSE) (Nash and Sutcliffe, 1970) which measures the observed variance reproduced by the model.

$$NSE = 1 - \left[\frac{\sum_{i=1}^{n} (Q_{iobs} - Q_{isim})^2}{\sum_{i=1}^{n} (Q_{iobs} - Q_{mean})^2} \right] \quad (5)$$

Where Q_{iobs} is the *i*th flume measured runoff value, Q_{isim} is the *i*th model simulated runoff value, and Q_{mean} is the mean of the flume measured runoff values. NSE values range from -∞ to 1 with 1 to represent the best fit of model. Positive values of NSE indicate that the model performed better than the observed mean value.

The second criterion is the percentage bias (PBIAS) (Gupta et al., 1999), which measures the average tendency of simulated runoff to be overestimated or underestimated comparing to the observed values. The optimal value for PBIAS is 0.0, and a positive

value indicating the model underestimation while a negative value indicating the model overestimation.

$$PBIAS = \sum_{i=1}^{n}(Q_{iobs} - Q_{isim}) \times 100 / \sum_{i=1}^{n} Q_{iobs} \quad (6)$$

3.3.6 Model evaluation

Once calibrated, SWAT was run first with the observed 50-year rainfall data to get a sequence of streamflow as a comparison reference for later analysis. The reason to use this synthetic streamflow for comparison, instead of the real observed streamflow, was to eliminate the uncertainty caused by the hydrological model itself. Finally, both the 30 sets of 50-year synthetic rainfall sequences generated from multi-site and single-site were fed into SWAT, producing two sets of simulated runoff responses respectively.

Two parts of evaluation procedures regarding both the precipitation and streamflow were performed in this study. Basic statistics such as daily, monthly and annual mean, standard deviation, and skewness were compared between the multi-site and single-site rainfall simulation results, using corresponding observed rainfall statistics as a reference. As for streamflow, the magnitude of runoff depth is quite small in this area, so statistics of summer total runoff were compared instead of the daily or monthly values during the evaluation of models. In addition to basic statistical characteristics, return periods of total summer runoff were calculated based on a 95% confidence interval for both multi-site and single-site generated results, and then compared with the simulated runoff return periods using observed rainfall sequence. The return frequency plot created here was the empirical frequency plot. We ranked the runoff values in

ascending order and each value was assigned an order number, then estimated the probability that the magnitude of an item will not be exceeded.

4 ANALYSIS OF RESULTS

4.1 Rainfall characterization

The transition probabilities for rainfall occurrence somewhere on the watershed for the 24 half-month periods are shown in Table 2. The probability of wet P(W) clearly showed that rainfall frequency reaches its peak in summer, exceeding 0.5, from the first half of July to the first half of September. The second wettest period is in winter from December through February, where P(W) ranges from 0.2 to 0.3. P(W|W) is always greater than P(W|D), which means that wet days tend to be clustered together.

Table 2. Transition probabilities, probabilities for three types of rainfall, and the probabilities for multiple events in all 24 half month periods

Half month		1	2	3	4	5	6	7	8	9	10	11	12
Transition probabilities	P(W)	0.2053	0.2225	0.2547	0.1914	0.1880	0.1338	0.1147	0.0960	0.0960	0.1175	0.1240	0.2640
	P(W|W)	0.4740	0.5000	0.5602	0.4776	0.4752	0.3738	0.4186	0.4167	0.3750	0.5106	0.4624	0.6111
	P(W|D)	0.1359	0.1431	0.1503	0.1237	0.1215	0.0952	0.0753	0.0619	0.0664	0.0652	0.0761	0.1377
Probabilities for types of rainfall	Convective	0	0	0	0	0	0	0	0	0	0	0	0
	Frontal	1	1	1	1	1	1	1	1	1	1	1	1
	Tropical	0	0	0	0	0	0	0	0	0	0	0	0
Probabilities for multiple events	1	0.7309	0.7155	0.6589	0.7629	0.6751	0.7312	0.6690	0.8808	0.8217	0.7066	0.7868	0.8031
	2	0.1651	0.1626	0.2321	0.1626	0.2188	0.1680	0.2242	0.1022	0.1426	0.1726	0.1745	0.1663
	3	0.1040	0.1219	0.1089	0.0745	0.1061	0.1008	0.1068	0.0170	0.0357	0.1208	0.0388	0.0306
	4												
	5												
Parameter of distributions*	μ (mm or 10^5 m^3)	2.6923	2.8794	2.1721	1.8628	2.6981	2.0318	1.5667	1.6052	1.4837	1.6541	2.3326	2.1434
	σ (mm)												

Half month		13	14	15	16	17	18	19	20	21	22	23	24
Transition probabilities	P(W)	0.6213	0.7738	0.7547	0.6438	0.5320	0.2733	0.2160	0.1950	0.1440	0.1613	0.2173	0.2288
	P(W|W)	0.7854	0.8336	0.8269	0.7592	0.7118	0.5561	0.5185	0.4615	0.4444	0.3884	0.5215	0.5191
	P(W|D)	0.3521	0.5635	0.5326	0.4316	0.3276	0.1651	0.1327	0.1304	0.0935	0.1176	0.1329	0.1410
Probabilities for types of rainfall	Convective	1	1	1	1	0.9876	0.9876	0	0	0	0	0	0
	Frontal	0	0	0	0	0	0	0.9876	0.9876	0.9876	0.9876	1	1
	Tropical	0	0	0	0	0.0124	0.0124	0.0124	0.0124	0.0124	0.0124	0	0
Probabilities for multiple events	1	0.6449	0.6499	0.6450	0.6842	0.7133	0.6966	0.7409	0.7515	0.7496	0.7596	0.7801	0.6929
	2	0.2187	0.2227	0.2171	0.2178	0.1633	0.1678	0.1766	0.1792	0.2019	0.1492	0.1367	0.1906
	3	0.0961	0.0911	0.0953	0.0713	0.0867	0.0807	0.0824	0.0694	0.0485	0.0912	0.0832	0.1165
	4	0.0362	0.0300	0.0310	0.0255	0.0250	0.0323						
	5	0.0042	0.0062	0.0115	0.0013	0.0117	0.0226						
Parameter of distributions*	μ (mm or 10^5 m^3)	1.5314	1.7461	1.6551	1.6105	1.6272	1.3189	2.4079	2.4877	2.5405	2.0375	3.2548	2.3647
	σ (mm)	1.4235	1.4680	1.4851	1.4827	1.4576	1.5344						

*** (1) July-September (13-18): lognormal distribution for convective rainfall maximum depth, unit: mm. (2) Other months (1-12,19-24): exponential distribution for frontal rainfall volume, unit: 10^5 m^3. (3) September-November (17-22): μ of exponential distribution for tropical depression rainfall is $4.2643*10^6$ m^3.**

Axis ratio and orientation statistics were acquired from Hsieh (2002). Those parameters are measured directly from interpolated rainfall surfaces and shown in Table 3. The mean value of axis ratio was 1.54, which is slightly greater than that found in previous work on Walnut Gulch, which showed a major to minor axis ratio of between 1.0 and 1.5 (Fogel and Duckstein, 1969). The mean value of orientation found in Hsieh (2002) was 91.40, which points generally north as defined in the previous section. The area statistics acquired in this study showed a mean of 58.01 km^2, which is approximately one-third of the watershed area. The regression equation of area and maximum depth (see Eq. 3) was determined as:

$$\ln(area) = 2.1784 + 0.6851\ln(\max\ dep) + \varepsilon \quad (R^2 = 0.57, n = 4152) \qquad (7)$$

Hsieh (2002), using data also from Walnut Gulch, developed a similar regression equation (Equation 6) between area and maximum depth from 48 interpolated storm surfaces, with the maximum depth ranging from 4.83 mm to 47.75mm, and storm areas ranging from 3.6 km^2 to 181.26 km^2.

$$\ln(area) = 1.1569 + 0.93\ln(\max\ \ dep) + \varepsilon \quad (R^2 = 0.46, n = 48) \qquad (8)$$

The number of storms used in this study was much greater than used by Hsieh (2002). The slope of Equation 5 is less than Equation 6, because the 48 storm samples Hsieh chose were mostly larger storms with clear elliptical shapes in space, which may be biased in terms of area representation.

The decay function to distribute rainfall from the convective storm center to the edge was determined as (see Figure 6):

$$depth = \begin{cases} \max\ dep & 0 \le r \le 0.59D \\ \text{maxdep}(1 - r / D) / 0.41 & 0.59D < r \le D \end{cases} \quad (9)$$

Previous work on Walnut Gulch has used either an exponential type decay function (Fogel and Duckstein, 1969) or simple linear decay function (Hsieh, 2002) to distribute the rainfall from the storm center to the edge. However, in this study, we found that these two methods both underestimate the rainfall total. Observed from radar images and interpolated rain gage isohyets, the convective rain cell tends to have a flat distribution around the center. The rationale behind it is that as the storm moves in space it creates a region with relatively uniform maximum depth in the storm center (Fogel and Duckstein, 1969).

Other model parameters, including the probabilities for different types of rainfall, probabilities for multiple events occurring in a day, and the distribution parameters for rainfall amount are shown in Table 2. The distribution for convective storm maximum depth was determined to be lognormal with two parameters, mean (μ) and variance (σ), the fitting plots were shown in Figure 8. Whereas, the best-fit distribution for frontal and tropical depression storms was determined to be exponential, with only one parameter μ, and fitting plots were shown in Figure 9. Notice that the units for convective storms and the other two types are different in Table 2, because one is for depth and the other two are for volume.

Table 3. Characteristics of convective storm area, axis ratio, and orientation.

	Mean	Std.dev	Skewness	Max	Min
Area (km^2)	58.01	50.50	0.56	152.94	1.59
Axis ratio (a/b) *	1.54	0.37	0.96	2.50	1.08
Orientation (degree) *	91.40	38.27	0.06	170.00	0.00

***From Hsieh (2002)**

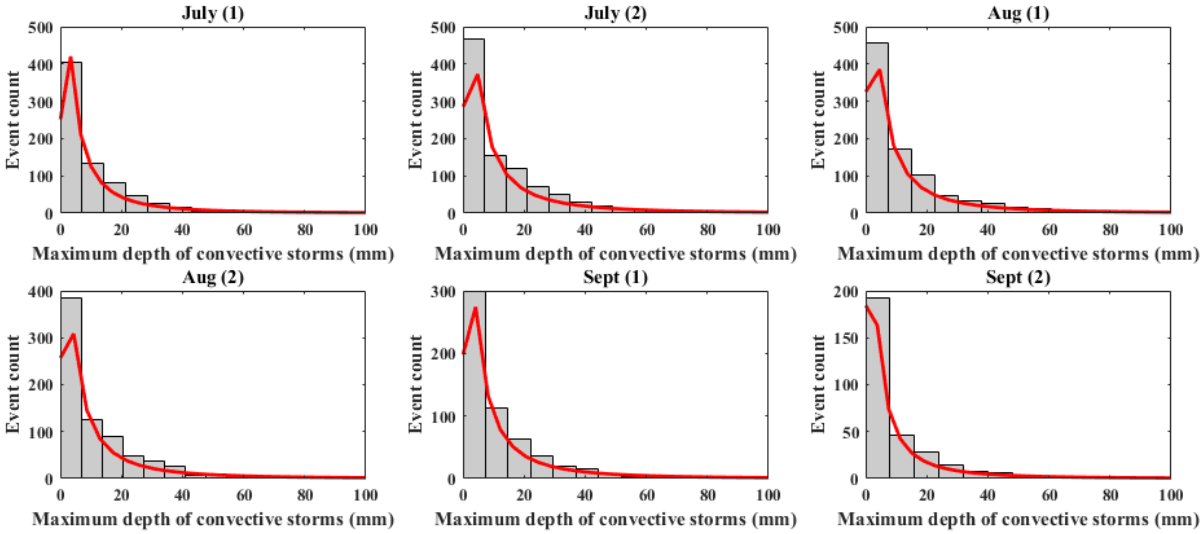

Figure 8. Lognormal distribution of convective storms maximum depth during July to September, (1) is for the first half month, and (2) is for the second half month. The grey histogram represented the observed counts of storm maximum depth, and the red line represented the theoretical fitting distribution curve.

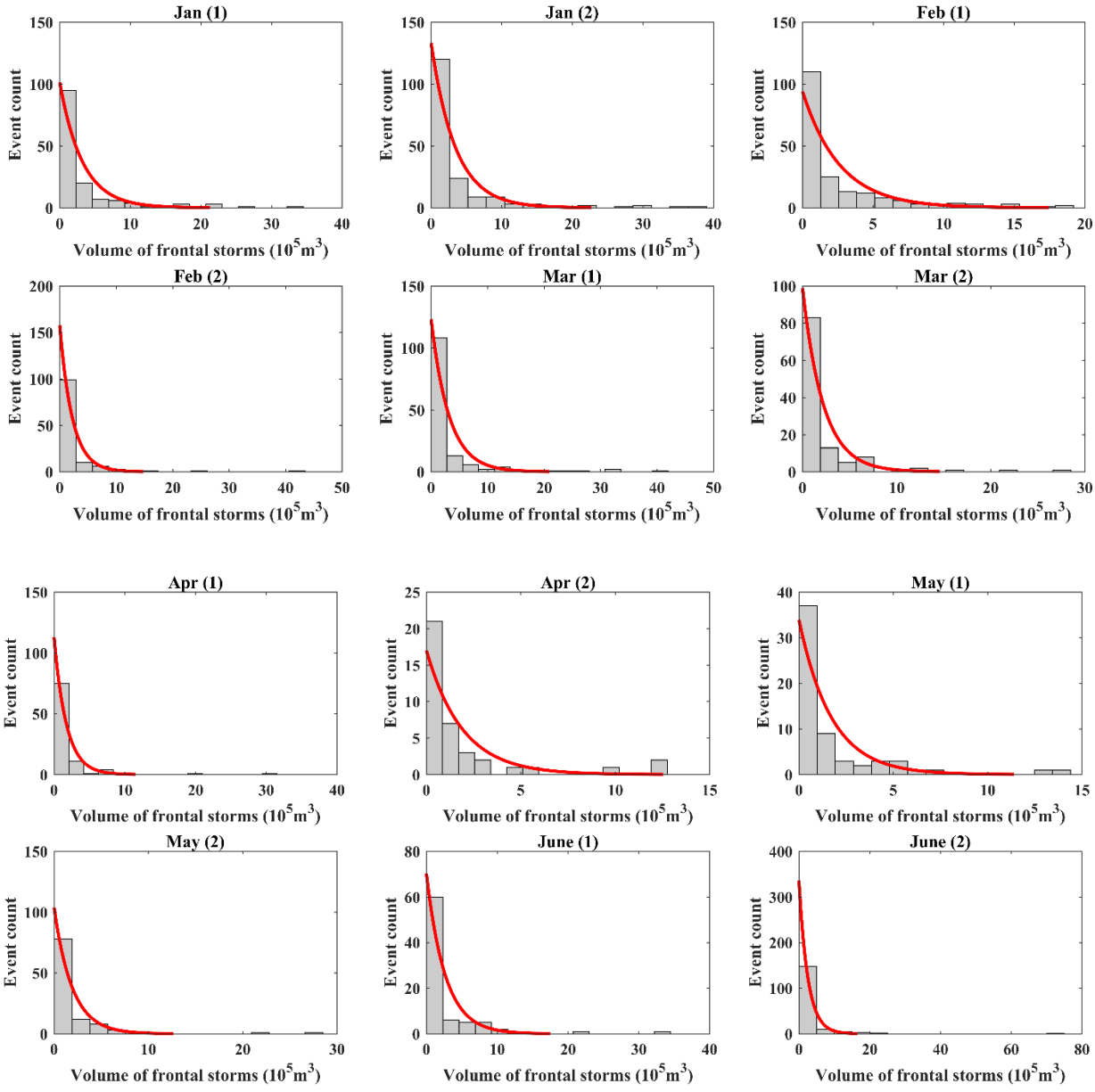
Jan (1)
Jan (2)
Feb (1)
Feb (2)
Mar (1)
Mar (2)
Apr (1)
Apr (2)
May (1)
May (2)
June (1)
June (2)
Event count
Volume of frontal storms (10^5m^3)

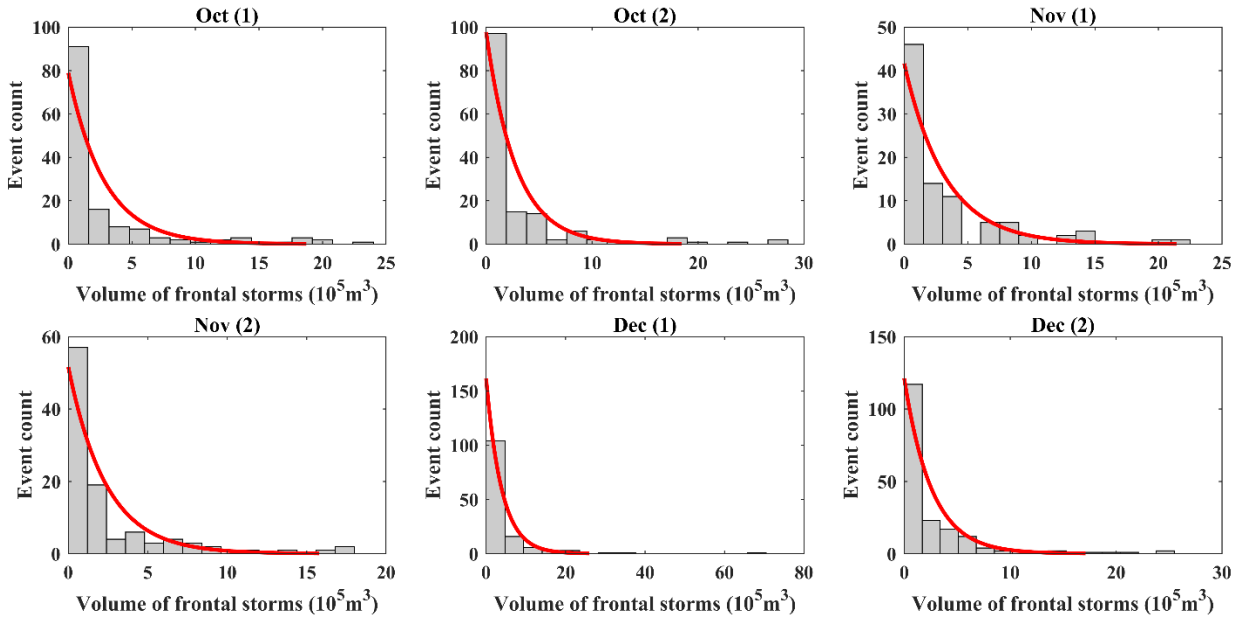

Figure 9. Exponential distribution of frontal storms volume during non-summer months, (1) is for the first half month, and (2) is for the second half month. The grey histogram represented the observed counts of storm volume, and the red line represented the theoretical fitting distribution curve.

4.2 Spatial rainfall generator evaluation

4.2.1 Convective storm maximum depth

The statistics of observed and simulated convective storm maximum depth from July through September are presented in Table 4 and Table 5. The mean value simulated in all six half months with convective storms had less than 6% difference. The fact that the simulated storm depths had a broader range of maximum depths is expected since the model was run for 30 replicates of 50-year time range (in total 1500 years) and should include extreme values that were not captured in the historical data. The shape of

simulated and observed CDF curves for all six periods were similar (Figure 10). The K-S test showed that there were no significant ($p = 0.05$) differences between the observed and simulated CDFs in all half month periods.

Table 4. Characteristics of observed convective storm maximum depths (mm).

	July 1-15	July 16-31	Aug 1-15	Aug 16-31	Sept 1-15	Sept 16-30
Mean	10.32	12.85	12.05	11.52	11.38	9.45
Std.dev	12.62	14.78	14.30	13.58	13.41	12.99
Max	85.60	83.31	91.19	81.03	87.63	95.12
Min	0.25	0.25	0.25	0.25	0.25	0.25
Range	85.34	83.06	90.93	80.77	87.38	94.87
Skewness	2.25	1.79	1.91	1.86	2.03	2.85

Table 5. Characteristics of simulated convective storm maximum depths (mm).

	July 1-15	July 16-31	Aug 1-15	Aug 16-31	Sept 1-15	Sept 16-30
Mean	10.26	13.23	12.73	11.73	11.93	9.46
Std.dev	14.86	20.08	19.36	17.53	17.85	14.94
Max	104.28	143.36	136.68	129.45	125.26	108.26
Min	0.25	0.25	0.25	0.25	0.25	0.25
Range	104.03	143.11	136.43	129.20	125.01	108.01
Skewness	2.97	3.07	3.05	3.01	3.05	3.25

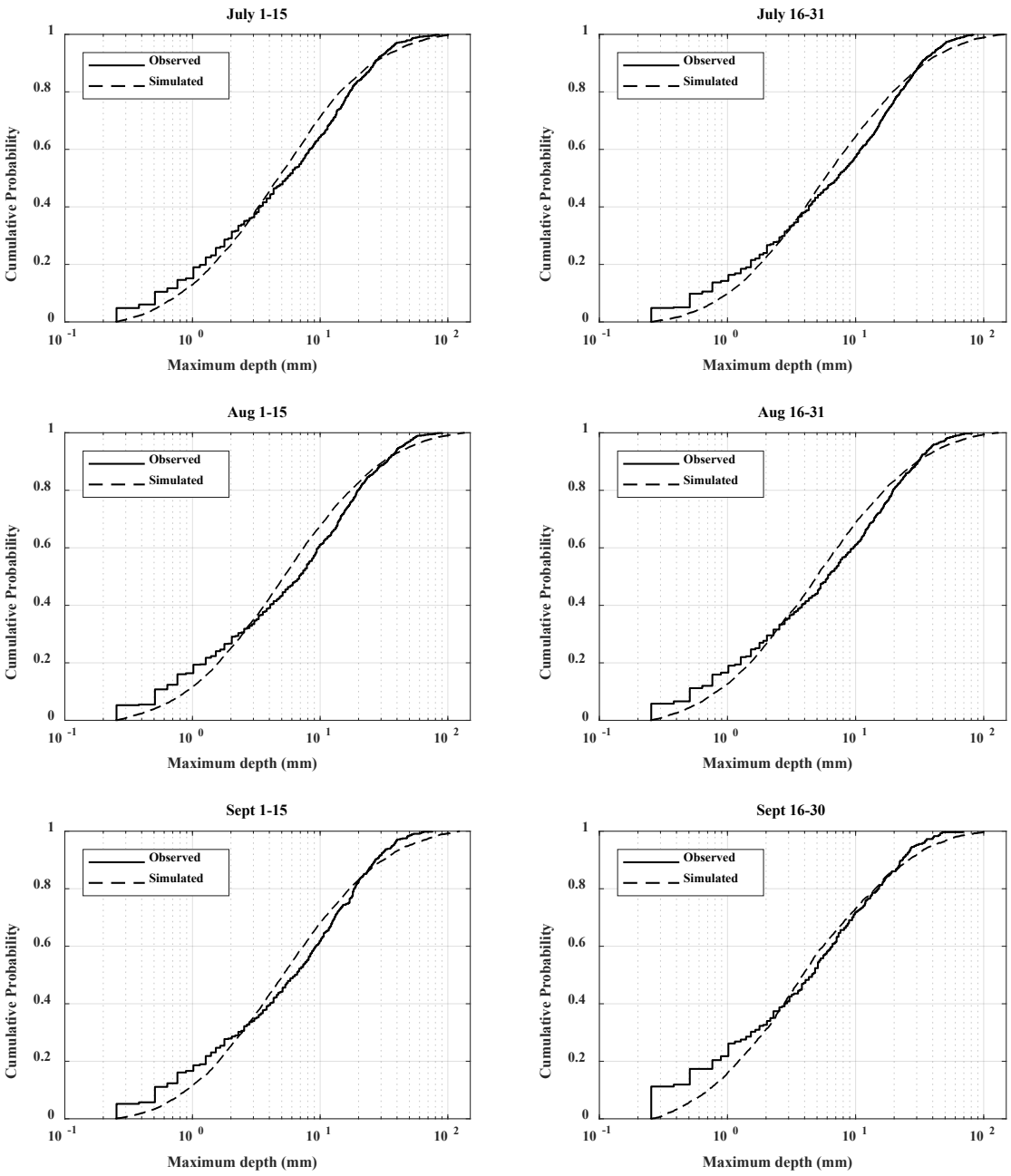

Figure 10. CDFs of observed and simulated summer convective storm maximum depths.

4.2.2 Seasonal and annual rainfall

The average summer rainfall total of the selected six gages was 192.9 mm, whereas the simulated summer rainfall total was 190.4 mm, with 1.3% difference (Table 6 and Table 7). The simulated range of summer rainfall total was almost twice that of the observed values, with lesser minimum and greater maximum values. Consequently, the simulated standard deviation was approximately 100 mm, which was greater than the observed values which were approximately 60 mm. K-S test results showed that there was no significant difference between the two curves in summer (Figure 11a), under p = 0.05 significance level. The simulated data variability was greater than the historical data, could have resulted from more extreme values being simulated in the long synthetic time series. This is consistent with the individual convective storms evaluation, where some extreme values exceeding the historical records were simulated.

As for non-summer rainfall, observed mean of six gages was 122.6 mm, and the simulated mean was 122.2 mm (Table 8 and Table 9). The range of winter rainfall had 15.6% difference between the observed and simulated, which is mostly caused by the overestimation of the minimum values. The simulated maximum winter rainfall was slightly less than the observed. Thus, the standard deviation was also underestimated by the model compared to historical records. The reason for this is related to the method used to distribute the generated the rainfall volume over the watershed. Since winter frontal storms have less variability than summer convective rainfall, for simplicity in this rainfall generator, every storm volume was distributed uniformly to all gages, only adding a small random variance. As a result, the variation in both space and time has been lost to some degree. The two CDF curves of non-summer rainfall total amounts

failed the K-S test (Figure 11b), which means that there was some difference between the simulated and observed data. However, the winter storms in Walnut Gulch rarely cause runoff and erosion due to their low intensity (Goodrich, Keefer, et al., 2008; Goodrich, Unkrich et al., 2008; Nearing et al., 2015), so it was considered acceptable to miss some variation in the generated storm depth totals as long as the total amount is similar and annual water balance was maintained.

Table 6. Observed rainfall totals for summer months of six gages (mm).

Gage ID	13	34	44	46	62	80
Mean	186.7	192.2	194.6	199.5	194.5	189.7
Std.dev	60.4	63.7	58.6	61.4	52.2	66.8
Max	336.6	345.7	345.9	410.5	327.3	380.0
Min	89.8	70.2	81.0	77.7	88.8	75.4
Range	246.8	275.5	264.9	332.7	238.5	304.5
Skewness	0.5	0.4	0.4	0.5	-0.2	0.6

Table 7. Simulated rainfall totals for summer months of six gages (mm).

Gage ID	13	34	44	46	62	80
Mean	196.3	187.1	185.8	191.8	186.5	195.0
Std.dev	100.4	99.7	101.6	102.6	96.3	100.7
Max	508.3	561.7	623.5	617.3	534.2	511.9
Min	3.6	1.5	7.2	8.2	10.4	9.1
Range	504.8	560.2	616.3	609.1	523.9	502.8
Skewness	0.5	0.6	1.0	0.9	0.6	0.6

Table 8. Observed rainfall totals for non-summer months of six gages (mm).

Gage ID	13	34	44	46	62	80
Mean	122.7	120.7	121.6	132.8	116.9	120.9
Std.dev	59.7	65.8	61.1	65.1	64.3	59.8
Max	266.4	308.9	295.0	318.8	300.4	282.8
Min	19.8	18.0	13.2	16.3	10.7	12.2
Range	246.6	290.8	281.8	302.5	289.7	270.6
Skewness	0.6	0.9	0.9	0.8	1.2	0.7

Table 9. Simulated rainfall totals for non-summer months of six gages (mm).

Gage ID	13	34	44	46	62	80
Mean	122.6	122.0	122.0	122.7	121.6	122.1
Std.dev	34.2	34.1	33.7	34.7	34.0	34.3
Max	265.0	305.8	282.0	280.8	264.7	256.8
Min	42.3	41.9	42.3	33.2	44.7	30.3
Range	222.7	263.9	239.8	247.6	219.9	226.5
Skewness	0.5	0.6	0.4	0.5	0.6	0.4

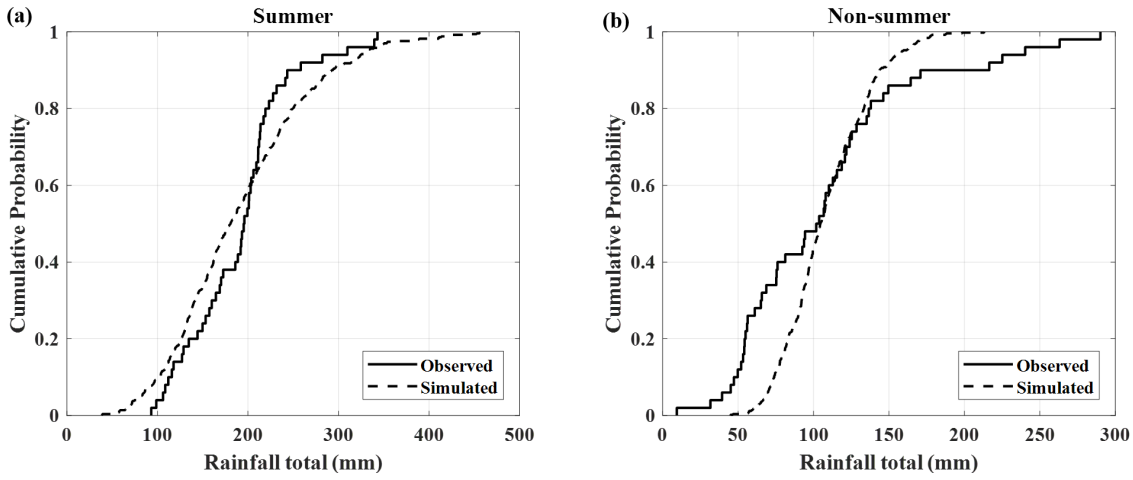

Figure 11. CDFs of observed and simulated rainfall totals for (a) summer and (b) non-summer periods.

Simulated and observed median lengths of dry and wet spell were shown in Table 10, which represents the central tendency of spell length distribution. The median of simulated dry spell length was slightly shorter than observed throughout the year, whereas the median of simulated wet spell length was longer than observed for summer, but the same for non-summer months. The overestimated wet spell length also caused an overestimation for annual wet spell length. The cumulative distribution function curves for seasonal and annual were shown in Figure 12. Five of the six pairs of observed and simulated curves passed the K-S test under p = 0.05 significance level. The significant

difference for the summer wet spell curves indicated that the rainfall generator tends to simulate slightly longer wet periods during summer season.

Table 10. Observed and simulated median length of dry and wet spells (day).

	Annual	Summer	Non-summer		Annual	Summer	Non-summer
Dry_obs	4.2	2.2	7.2	Wet_obs	1.0	1.0	1.0
Dry_sim	4.0	2.0	6.0	Wet_sim	2.0	3.0	1.0

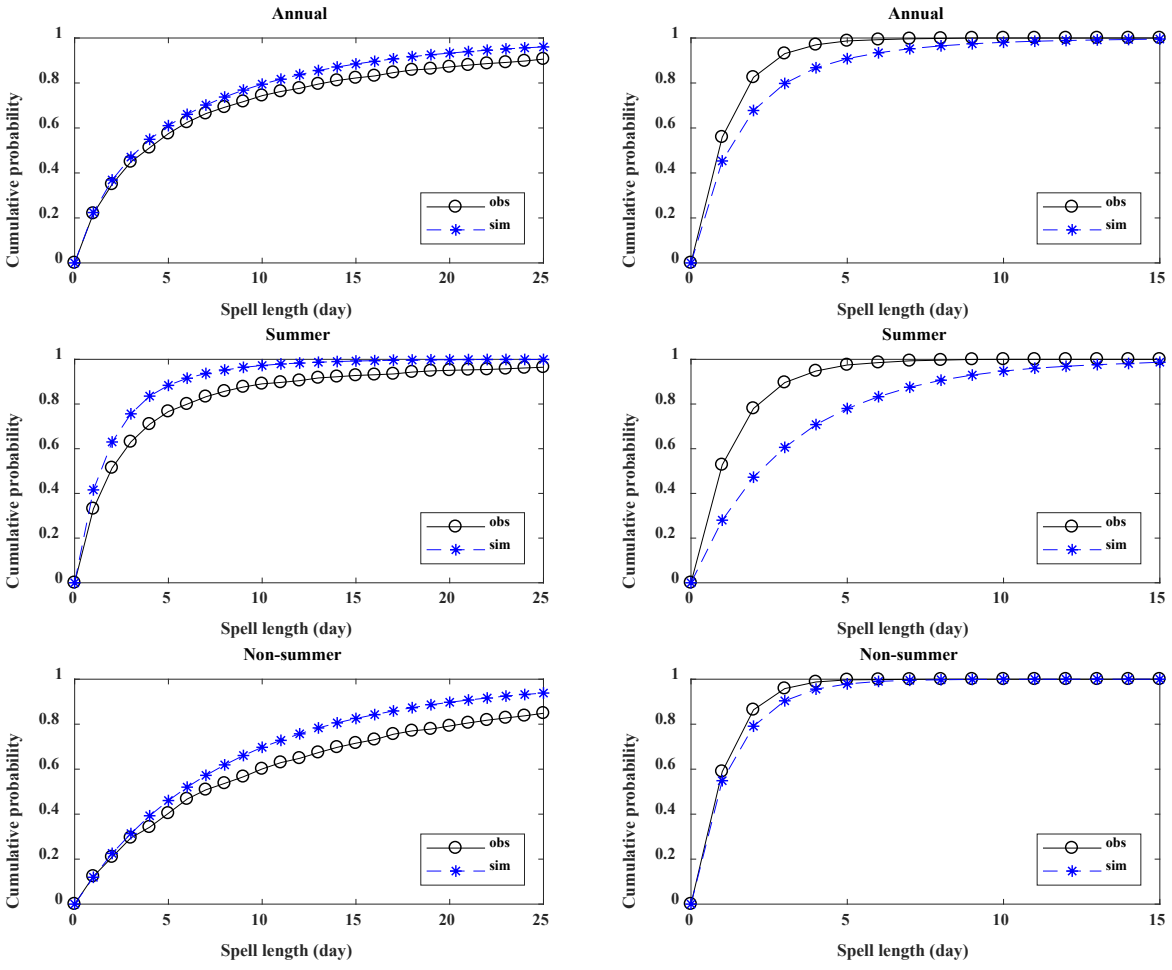

Figure 12. CDFs of observed and simulated dry and wet spell length for annual, summer and non-summer periods, (1) first column: dry spell, (2) second column: wet spell.

4.3 Comparison of generated precipitation

The overall annual rainfall amount was preserved well by the multi-site rainfall generator, with only a 1% difference, which is better than the single-site model with a 7% difference (Table 11). Total number of wet days are satisfactorily reproduced by both type of models. As for standard deviation, both single-site and multi-site made an overestimation, could be due to inclusion of broader range of rainfall data, since both generators were run for 30 replicates of 50-years. The multi-site simulated standard deviation was slightly better compared to the single-site model. Skewness was neither reproduced well by the single-site or multi-site model, both having an overestimation.

Daily and monthly rainfall statistics and boxplots were shown from Figure 13 to Figure 16. The mean daily and monthly rainfall amounts were generally simulated well by both models. Multi-site rainfall generator outperforms single-site generator in most non-summer months, while in summer months, both models have a slight offset from the historical data. The multi-site generator tended to underestimate summer rainfall amount and the single-site generator would overestimate it. K-S test results showed that there was no significant difference either between the daily and monthly rainfall of observed versus the multi-site or the observed versus the single-site (Figure 13 and 14), at $p = 0.05$ significance level. The daily and monthly standard deviation were generally reproduced satisfactorily in non-summer months by both the single-site and multi-site rainfall generators. However, discrepancies occurred during the summer months especially in July and August, which was also the main reason for an overestimation of the overall annual standard deviation. As we stated above, it could be due to a broader range of

simulated dataset inducing more variations, and maybe also because Walnut Gulch is dominated by the summer monsoon precipitation which has large variation from day to day and year to year, this variation is hard to be captured very precisely with both single-site and multi-site models in this study. The boxplot which showed the 25th and 75th percentiles, indicated similar results that both sets of simulated rainfall had a wider range than the historical rainfall data. Skewness was not represented adequately by both models, though the single-site output is slightly better than the multi-site model.

Table 11. Statistics of observed and simulated annual rainfall statistics.

Statistic	Observed	Single-site	Multi-site
Mean (mm)	315.5	338.3	312.6
Std.dev (mm)	66.08	83.73	75.22
Skewness	0.16	0.44	0.57
Number of wet days	49	49	50

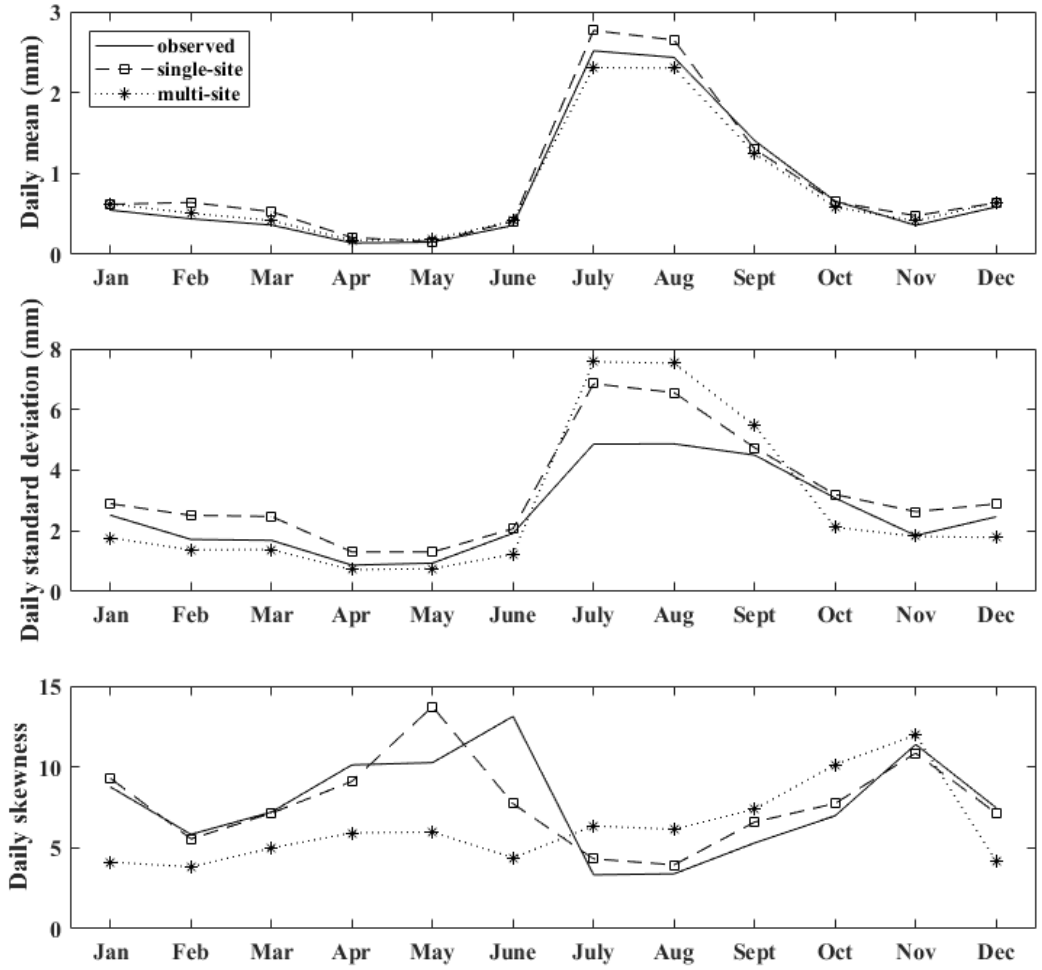

Figure 13. Mean, standard deviation and skewness of daily rainfall.

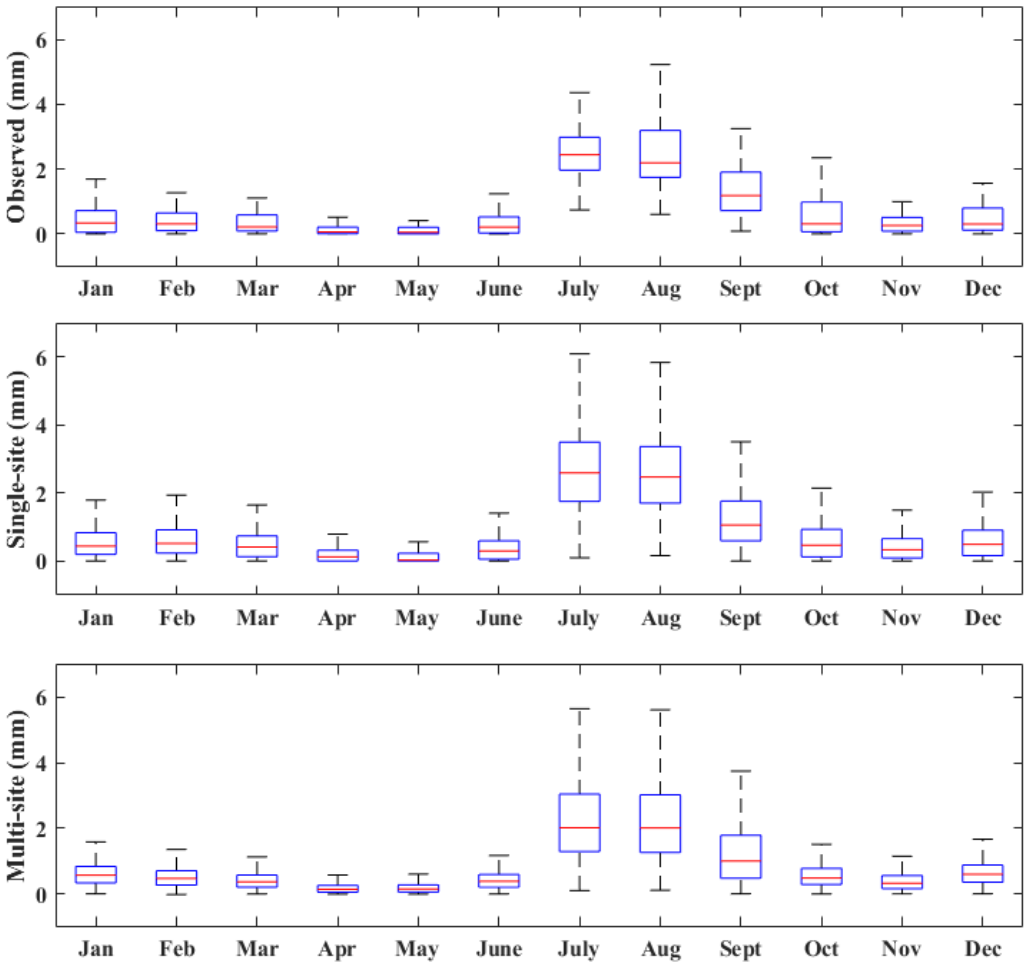

Figure 14. Boxplots of observed, single-site generated, and multi-site generated daily rainfall.

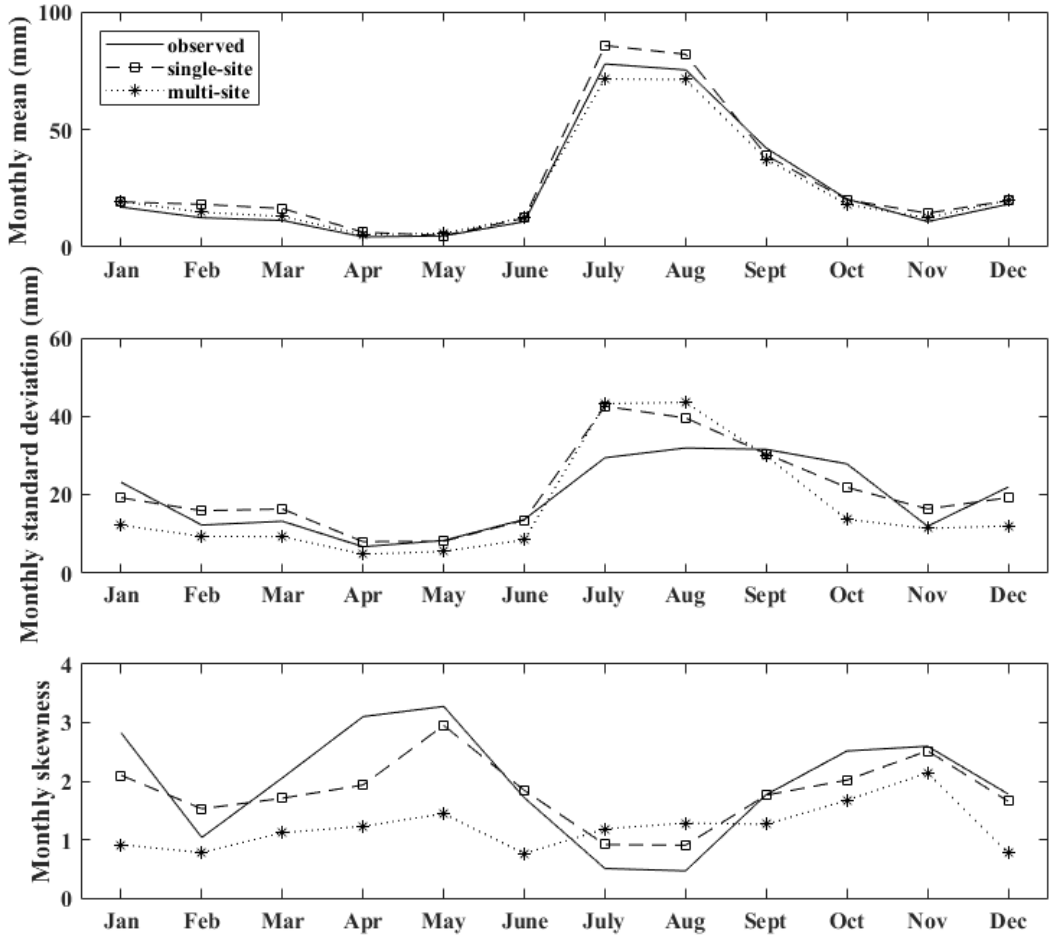

Figure 15. Mean, standard deviation and skewness of monthly rainfall.

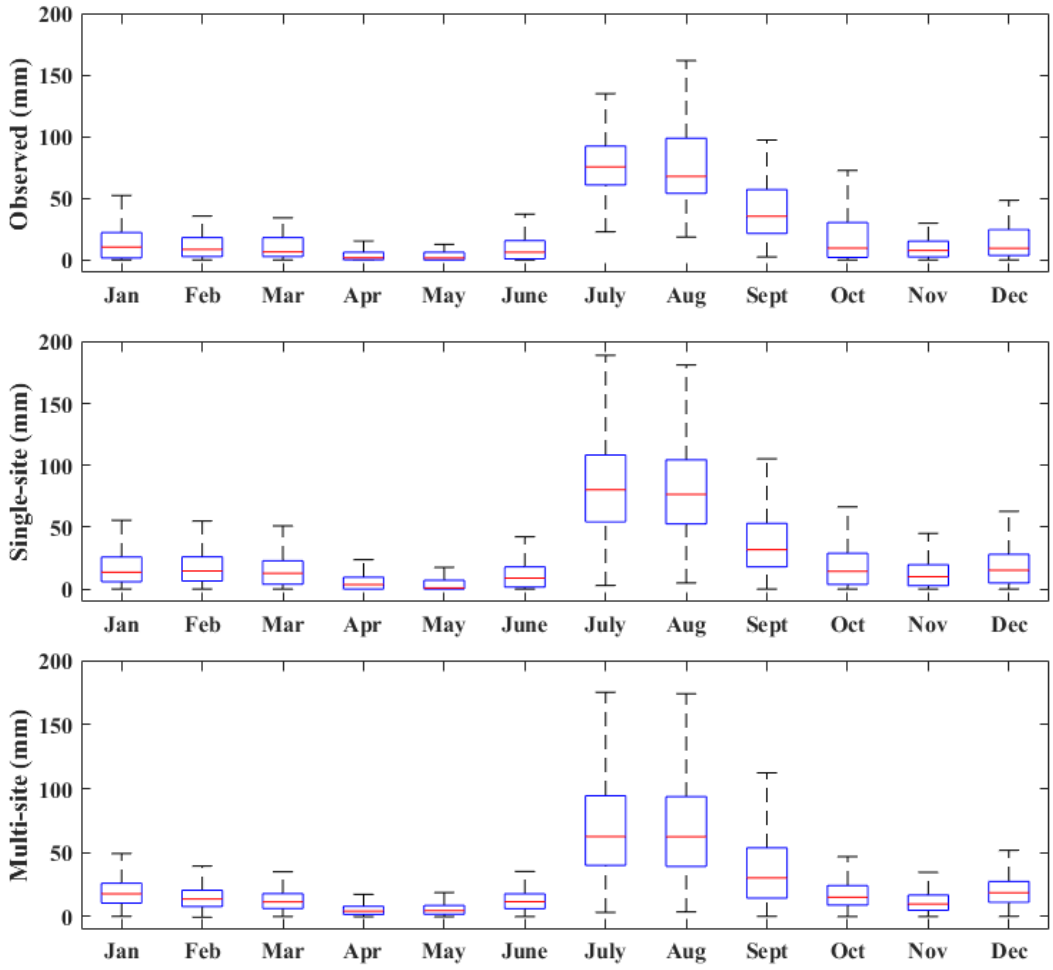

Figure 16. Boxplots of observed, single-site generated, and multi-site generated monthly rainfall.

4.4 Hydrologic model calibration results

During the calibration process, we found that the monthly runoff magnitude in Walnut Gulch was quite small, usually below 1.0 mm, which made the calibration process difficult because the magnitude of model uncertainty was close to the magnitude of the simulated runoff itself. The statistics of flume measured summer runoff and model simulated summer runoff were shown in Table 12, as well as the two calibration criteria.

Through several trials of combination of parameters, the final PBIAS values for all three flumes ranged between -5% (underestimation) to 5% (overestimation). The other index NSE was negative for Flume 1, which indicated that the mean of measured runoff value was a better predictor than the model. The NSE for Flume 2 and Flume 6 were both positive and indicated better model performance in these two smaller watersheds compared to Flume 1.

Table 12 Statistics of flume measured and model simulated summer runoff (unit: mm)

	Measured with flumes			Simulated after calibration		
Flume	**1**	**2**	**6**	**1**	**2**	**6**
Mean	2.30	3.01	3.75	2.20	3.10	3.81
Std.dev	2.24	3.12	4.08	2.24	2.10	2.48
Skewness	1.90	1.86	2.23	5.06	4.29	4.28
Max	11.84	15.38	21.51	16.08	15.49	18.33
Min	0.00	0.00	0.00	0.26	0.69	1.01
NSE				-0.3	0.1	0.1
PBIAS (%)				4.18	-3.03	-1.56

4.5 Comparison of generated runoff

The observed and simulated summer runoff statistics were shown in Table 13. It should be noted here the observed summer runoff is not directly from flume measurements, but generated runoff based on measured rainfall data. This is the way to eliminate the uncertainty of hydrological model itself, since all three runoff data series were reproduced through the same procedures inside the model. As shown in Figure 2, the area controlled by Flume 1 was the largest, Flume 2 smaller and Flume 6 being the smallest. Most precipitation on Walnut Gulch will be infiltrated into the surface and then being evaporated or transpired by vegetation. Only a little portion of precipitation forms runoff, and due to transmission losses in the channels, the amount of runoff actually reaches the

watershed outlet will be even less. According to SWAT simulation results (Table 13), the observed runoff was the largest at Flume 6, then Flume 2 and least at the whole watershed outlet Flume 1. Stone et al. (2008) found the same pattern using stream flow measurements at WGEW. Magnitude of summer runoff ranges from 2 to 4 mm.

Though from the rainfall simulation results, we know that the single-site and multi-site generators can both well reproduced the mean daily, monthly and annual rainfall amount. The situation was different in runoff generating. Both multi-site and single-site generated rainfall tended to induce an overestimation in runoff. However, the multi-site generator still performed better than the single-site generator. The percentage errors of multi-site generated runoff for Flume 2 and Flume 6 were less than 5%, while for Flume 1 was 23%. Whereas, the single-site generated runoff had an over 25% percentage errors for all three flumes, and error for Flume 1 reached 43%. The simulated standard deviations were also larger than the observed runoff, still the multi-site generator performed better than the single-site generator. An overestimation of standard deviation could be attributed to the simulated rainfall having a larger standard deviation. Skewness of both models were underestimated compared to observed runoff. Simulated maximum and minimum values induced a broader range of runoff data for both generators.

Table 13. Statistics of observed and simulated summer runoff (unit: mm).

	Observed			Multi-site			Single-site		
Flume	**1**	**2**	**6**	**1**	**2**	**6**	**1**	**2**	**6**
Mean	2.20	3.10	3.81	2.70	3.17	3.97	3.14	4.25	4.76
Std.dev	2.24	2.10	2.48	3.81	3.69	4.14	4.61	5.07	4.87
Skewness	5.06	4.29	4.28	2.69	2.67	2.42	3.11	3.02	2.87
Max	16.08	15.49	18.33	19.77	19.76	21.87	24.90	28.46	27.50
Min	0.26	0.69	1.01	0.06	0.22	0.36	0.16	0.48	0.69

Another important aspect for runoff simulation is to reproduce the runoff return periods adequately, for designing and planning purposes. The three different levels of watershed controlled by Flume 1, 2 and 6 showed distinguishable results in comparing the simulated return frequency of total summer runoff (Figure 17). For the smallest watersheds controlled by 6, the short return period flows (1-2 year) tended to be overestimated a little, but the prediction got better as the return period became longer, especially for those simulated using the multi-site generated rainfall. The observed return frequency curve completely fell into the 95% confidence interval of multi-site generated results. While the single-site generated flows tended to be overestimated for longer return periods. As the watershed size got larger, the prediction for longer return period became not so satisfactorily. A discrepancy occurred between the observed flow curve and simulated runoff, especially for return periods longer than ten-year. The larger the watershed size, the more significant of the discrepancy between observed and simulated runoff. Flume 1 was the least satisfactorily predicted. These results indicated that the SWAT model might not work well for large-sized watersheds in this semi-arid climate region, due to a poor characterization of the transmission loss in the channel systems.

Smaller watershed such as which controlled by Flume 6, with a size of 93 km^2, can be simulated accurately with the multi-site model generated rainfall.

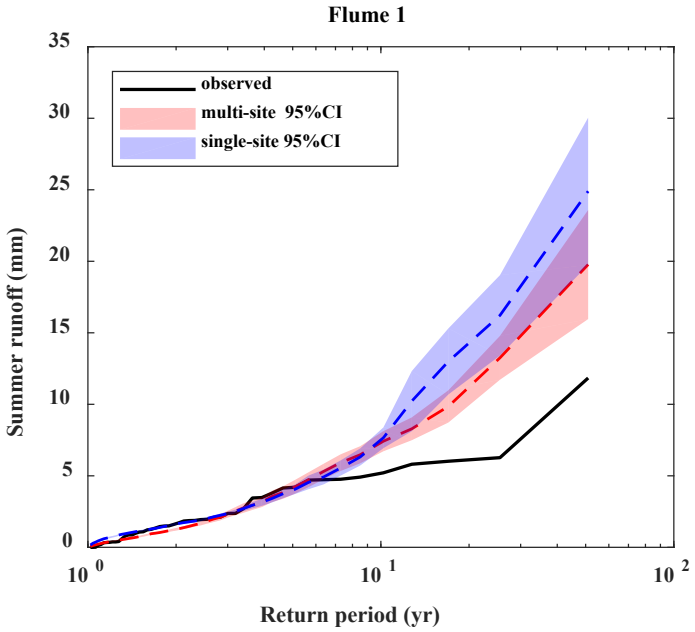

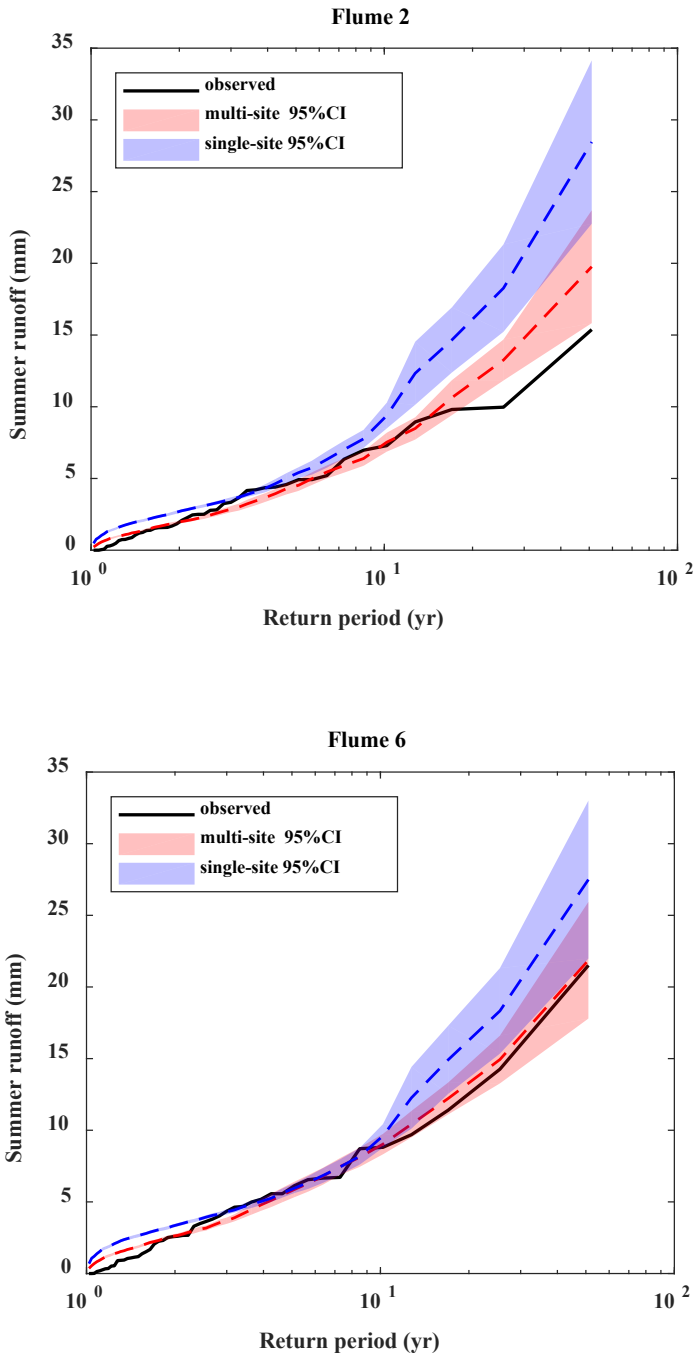

Figure 17. Return periods of generated summer runoff using observed rainfall, single-site rainfall and multi-site rainfall for Flume 1, 2 and 6 in WGEW.

5 CONCLUSIONS

This study presented modeling concepts and processes of a daily, spatial, stochastic rainfall generator in a semi-arid watershed in southeastern Arizona. Unlike most daily rainfall generators which give only the daily rainfall amount, this model is capable of simulating individual storms within a day. Simulation of four elements, including daily rainfall occurrence, the number of storms per day, the maximum depth or total volume of a storm, and spatial distribution of the rainfall was illustrated using 50-years of rain gage observations in Walnut Gulch Experimental Watershed, Arizona. The separation process of generating three types of rainfall (convective, frontal and tropical depression) is appropriate in this region, since they all have quite different physical features. The concept of elliptical shape of convective storms works well in this study and has been tested in other research. The simulated individual convective storm statistics were similar to the observed. The simulated seasonal rainfall performed differently for summer and non-summer periods, with a slight overestimation of variation of annual summer rainfall and an underestimation of variation in non-summer period, but the long-term mean values of both summer and non-summer periods are satisfactory.

Single-site and multi-site rainfall generators gave similar simulations regarding to annual precipitation statistics, with multi-site generator slightly outperformed single-site in reproduction of annual mean and standard deviation. As for daily and monthly statistics, both types of generator would slightly overestimate the summer months precipitation with a larger standard deviation and broader range between minima and

maxima. However, the overall performances of precipitation simulation were still acceptable for both generators.

For stream flow simulation, the multi-site generator performed much better than the single-site generator in both mean summer flow and different return period flows. Single-site generator derived runoff was significantly overestimated in all three level watersheds, whereas multi-site generator performed satisfactorily in smaller watersheds and only did an overestimation in larger watersheds. This overestimation for larger watersheds could be due to the nature of the SWAT model, where transmission loss was not well represented. A previous research (Van Liew et al., 2007) also noted that SWAT performance in desert or semidesert climates were not as good as in humid climates. The results of runoff generation were consistent with most previous research (Breinl, 2016; Khalili et al., 2011, 2006; Li et al., 2017) to some degree. This study confirmed that even in small to medium sized watersheds, the spatial variability of rainfall could still play an important role for hydrologic response, which made the application of multi-site rainfall generator become necessary. Smaller watershed area does not guarantee the homogeneity of rainfall distribution and using single-site generated rainfall sequence might lead to some bias in both prediction of long-term mean flow and extreme events. Semi-arid watersheds like WGEW are dominated by summer convective rainfall generated flow, where the rainfall spatial variability is quite high and cannot be ignored.

There are limitations for this generator. It is a well calibrated model based on the dense rain gage network of Walnut Gulch Experimental Watershed, and expanding it to larger area application will require additional analysis linking the point statistics with

area statistics. Possible solutions for obtaining larger area statistics, such as convective storm area, may need incorporation of radar rainfall images. This rainfall generator is initially targeted at semi-arid watersheds where convective rainfall dominated, thus it may not be immediately applicable in regions with significantly different rainfall types.

Possible uses of the rainfall generator include application into hydrological models, erosion models as rainfall input, where spatial rainfall information could have an impact on runoff response or sediment yield. It may also be applied in climate change studies by manipulating model parameters to account for future trends and testing the outcomes. Developing the rainfall generator into a high-resolution temporal model is a future research need, which will require further studies of storm movement in space and time.

APPENDIX A: A daily spatially explicit stochastic rainfall generator for a semi-arid climate

This appendix has been published by a peer reviewed journal:

Zhao, Y., Nearing, M. A., Guertin, D. P., 2019. A daily spatially explicit stochastic rainfall generator for a semi-arid climate. J. Hydrol. 574, 181–192. https://doi.org/10.1016/j.jhydrol.2019.04.006

Abstract

Many semi-arid regions of the world experience rainfall patterns characterized by high spatial variability. Accurate spatial representation of different types of rainfall will facilitate the application of distributed hydrological models in these areas. This study presents a daily, spatially distributed, stochastic rainfall generator based on a first-order Markov chain model, calibrated using 50 years of rainfall observations at 88 gages from 1967 through 2016 in the 148-km^2 Walnut Gulch Experimental Watershed. Three types of rainfall, including convective, frontal, and tropical depression storms, were simulated separately in the generator using biweekly parameterization. Convective storms were simulated based on an elliptical shape rain cell conceptual model, whereas frontal and tropical depression storms were simulated as uniform rainfall fields over the whole watershed with introduced random variability. The rainfall generator was evaluated by comparing the mean statistics of 30 sets of 50-year simulated data versus the 50-year rain gage observed data. Most individual storm statistics and aggregated seasonal rainfall statistics were similar to the measured rainfall observations. The long-term mean values of both summer and winter rainfall amount were statistically satisfactory. This model can

serve as a guide for application in areas with convective, frontal, and tropical depression storms.

Key Words: rainfall generator; spatial; semi-arid; convective storm; Markov chain

1 Introduction

Precipitation is a driving force of many hydrologic processes, especially for regions with semi-arid and arid climates. However, the lack of reliable rainfall records limits the development of hydrologic research and applications. Stochastic rainfall generators can simulate the key characteristics of natural rainfall records (Wilks and Wilby, 1999). The advantage of simulated rainfall data is that they can provide long series of statistically representative records, which can be used in hydrological models, agricultural models, or climate change impact assessment to produce mathematically stable statistical representations of hydrologic response for a given weather record. As models become more sophisticated, the requirements for higher resolution and continuous rainfall series data become more important (Bonta, 2004; Breinl et al., 2017; Li et al., 2017; Serinaldi, 2009).

Rainfall has both temporal and spatial characteristics that need to be accounted for in the generation process. Point-based rainfall generators, which focus on the temporal dimension of rainfall, are the most commonly used models (Arnold and Williams, 1989; Calenda and Napolitano, 1999; Kavvas and Delleur, 1981; Papalexiou et al., 2011; Richardson, 1981; Valdes et al., 1985). These generators are based on single site observations, and therefore not designed to provide spatial resolution. Researchers have

studied the effect of spatially variable rainfall on hydrologic response. Some studies argued that the spatial variability of rainfall does not cause significant differences in runoff generation or only causes secondary effects (Beven and Hornberger, 1982; Obled et al., 1994; Schuurmans and Bierkens, 2006). These catchment sizes ranged from 71 to 287 km^2, which were mostly medium sized rural catchments. Obled et al. (1994) noted that their conclusions may not apply for smaller urbanized or larger rural areas. Schuurmans and Bierkens (2006) found that the spatial variability has a major effect on daily simulation of discharge, groundwater level and soil moisture, while for general longer-term behavior of the hydrological system, the areal average rainfall information is adequate. Koren et al. (1999) noted that heterogeneity of rainfall is a major factor for small scale catchments, but the fraction of the watershed covered by rainfall is not as important since rainfall is likely to cover the whole area. However, for larger scales, the fractional area of the watershed covered by rainfall is a major factor for runoff generation. Specific site conditions, in terms of either climate characteristics or size of the watershed, can lead to quite different conclusions on how spatial rainfall affects hydrological responses. In a semi-arid region, such as is found in much of the southwestern United States, where runoff is dominated by summer convective storms, transmission losses in ephemeral channels are a significant factor in the water budget (Goodrich et al., 1997; Renard et al., 1993). Thus, the spatial distribution of rainfall may matter more in these environments, creating distinctive runoff response for upper and lower streams. Bell and Moore (2000) also pointed out that convective rainfall induces more sensitivity in runoff production than does stratiform rainfall. To facilitate the

accurate modeling of hydrologic response in semi-arid regions, such as in southeastern Arizona, a rainfall generator that can simulate non-uniform rainfall fields in space is needed. It will enhance the ability to apply distributed watershed hydrologic models.

Spatial rainfall generators may use multi-site data for a specific region, so they can also be referred to as multi-site rainfall generators. Compared with point-based generators, multi-site rainfall generators take spatial correlation between stations into consideration, since rainfall stations near enough are not totally independent of each other. Storms organize into groups and form linear bands or spiral bands under different weather systems in nature (Shuttleworth, 2012). In recent years there has been extensive research conducted on different types of multi-site rainfall generator models (Asong et al., 2016; Bardossy and Plate, 1992; Breinl et al., 2017; Evin et al., 2018; Ferraris et al., 2003; Leander and Buishand, 2009; Li, 2014; Mehrotra et al., 2006; Peleg and Morin, 2014; Serinaldi, 2009; Wilks, 1999). Most rainfall generators deal with two major components: rainfall occurrence and rainfall amount. There are two basic approaches for precipitation occurrence generation. One is the Richardson-type (Richardson, 1981) and the other is serial type (Racsko et al., 1991). The Richardson-type generator is based on Markov chain models, which simulates day to day rainfall occurrence using transition probabilities. Serial type generators account for long-term wet or dry trends, usually beginning with the simulation of dry and wet series of years, and then simulate rainfall amount based on dry and wet conditions.

There are also basically two types of methods for representing spatial distribution of rainfall amounts. The first type focuses on the physical structure of small scale rain

cells, such as shape and size, either using rain gage data (Cowpertwait et al., 1996; Ferraris et al., 2003; Hsieh, 2002; von Hardenberg et al., 2003) or radar images to acquire the parameters (Morin et al., 2006; Peleg and Morin, 2014, 2012). The other type considers relatively larger scale rainfall fields, usually incorporating mathematical representation of the spatial correlation. Further classification of this type can include several different methods: (1) statistical multi-site models, usually achieved by fitting empirical distributions for rainfall properties and adding spatial correlation matrix to represent inter-sites relation (Brissette et al., 2007; Khalili et al., 2009; Mehrotra and Sharma, 2007; Serinaldi, 2009; Wilks, 1998). (2) resampling/bootstrap models, where rainfall depths were resampled from historical data (Buishand and Brandsma, 2001; Leander and Buishand, 2009). Recent improvements of resampling methods included adding a reshuffle process to maintain the spatial properties (Breinl et al., 2013, 2015). (3) Nonlinearly filtered autoregressive processes (Lanza, 2000; Mejía and Rodríguez-Iturbe, 1974; Rebora et al., 2006). (4) generalized linear models (Asong et al., 2016; Verdin et al., 2018, 2015). (5) fractal cascade models (Gupta and Waymire, 1993). Of all the above approaches, rain cell models are particularly appropriate to simulate convective storms, since these storms share common features of short duration and limited spatial extent (Osborn et al., 1979). Generalized linear models have failed to capture the summer convective precipitation characteristics (Verdin et al., 2015).

Rain cells can either be simulated using circular (Morin et al., 2005; Morin and Gabella, 2007; Peleg and Morin, 2014) or elliptical shapes (Barnolas et al., 2010; Peleg and Morin, 2012; Syed et al., 2003). The circular shape is easier for modeling since it

only has one radius parameter, and the intensity distribution can be simplified as well because the cell is isotropic. The elliptical shape is more complex since it has both a major and minor axis, which also requires an additional orientation parameter. It is also necessary to define the center coordinates of the cell and the coverage area for both kinds of cells. In addition to cell shape parameters, researchers also have studied the representation of rainfall intensity within the cell: (1) rain cells with a constant intensity everywhere; (2) Gaussian decay of intensity from cell center; (3) exponential decay of intensity from cell center; (4) hybrid of Gaussian and exponential decay from cell center. The use of constant intensity makes the model simpler, but not generally realistic, especially when the research focus is on sub-daily rain cell development. Feral et al. (2003) noted that the Gaussian distribution leads to a faster decay of rainfall intensity from the center outwards but to a lower gradient for the outer part. The specific function might differ from region to region, which needs further calibration based on actual data.

In this study, we will employ a Markov-chain based rain cell model to simulate daily spatial rainfall in a semi-arid watershed located in southeastern Arizona. The major objectives are: (1) present a conceptual model to characterize the spatial variation of the summer convective rainfall, (2) build a stochastic daily rainfall generator capable of simulating three types of rainfall with high spatial resolution that can be used in small to medium sized watersheds, and (3) evaluate the performance of the rainfall generator. Since temporal scale is not the primary consideration in this study, we used a daily step in this rainfall generator. The Richardson-type of generator was used for daily rainfall occurrence. The geographic area we are concerned about is dominated by convective

rainfall during the summer, which is suitably represented by a rain-cell based generator. We combined simulations of individual rain cells to acquire the rainfall field over the entire watershed.

2 Methods

2.1 Study area and data

The study area is the Walnut Gulch Experimental Watershed, located in southeast Arizona, surrounding the town of Tombstone. It is a sub-watershed of the San Pedro River Basin. The USDA-ARS Southwest Research Center has been operating the watershed since the 1950s with intensive instrumentation and measurement of precipitation. The drainage area of Walnut Gulch is approximately 148 km^2, and elevation ranging from 1220 m to 1900 m above sea level. The average annual precipitation in this semi-arid watershed is approximately 312 mm (Goodrich and Keefer et al., 2008), following a bimodal pattern, with most precipitation occurring in summer and winter seasons (Osborn, 1983). Summer rainfall, during the months of July, August, and September, accounts for approximately 60% of the total annual amount in this region, and results from the North American Monsoon (Nichols et al., 2002; Stillman et al., 2013). The summer rain often forms as convective storms, with relatively short duration but high intensity, and cover a limited spatial extent. The spatial variation of summer convective storms is large. The winter frontal storms are, however, usually of long duration but low intensity, and usually cover the whole watershed more uniformly (Goodrich and Unkrich et al., 2008; Nearing et al., 2015; Nichols et al., 2002; Stillman et

al., 2013). Frontal storms during the non-summer months account for approximately 35% of the annual precipitation. Occasionally, snow occurs in winter at the watershed, but it melts quickly and does not accumulate. The remaining 5% of the annual rainfall falls in the form of tropical depression storms, usually dropping large amounts of water, much of which will be converted into runoff (Gochis et al., 2006; Osborn, 1982).

Walnut Gulch Experiment Watershed has more than sixty years of rainfall monitoring. The earliest rainfall record dates back to 1954. The current rain gage network consists of 88 digital rain gages (Figure 1), which gives an average of approximately 0.6 gage km^{-2} over the watershed. The dense network provides advantages for spatial rainfall analysis, especially for the summer convective rainfall events with high spatial variation. The full current network of 88 gages was installed by 1967, so this study uses rainfall data from 1967 through 2016 (50 years) to build the generator. From 1967 through 1999, the rainfall data was recorded by analog rain gages, while after 2000, digital gages were used (Goodrich and Keefer et al., 2008). Due to resource considerations, only nine gages operated out of the monsoon season, during the winter months from 1981 through 1991 and in 1999. The reason for this is that winter rainfall in this area is much less spatially variable and the high density of rain gages were not considered necessary (Goodrich et al., 2008). All rainfall data used can be acquired on the website of USDA-ARS-SWRC. The rainfall records are stored in an Access database, including both daily rainfall and event rainfall. The daily data recorded the year, month, day and total depth received by a certain gage on that day. The event data recorded the event ID, year, month, day, start time, duration and depth by a certain gage. Each day may have multiple events in the

database for a gage. The resolution for depth is 0.254 mm (0.01 inch) and the resolution for duration is 1 minute.

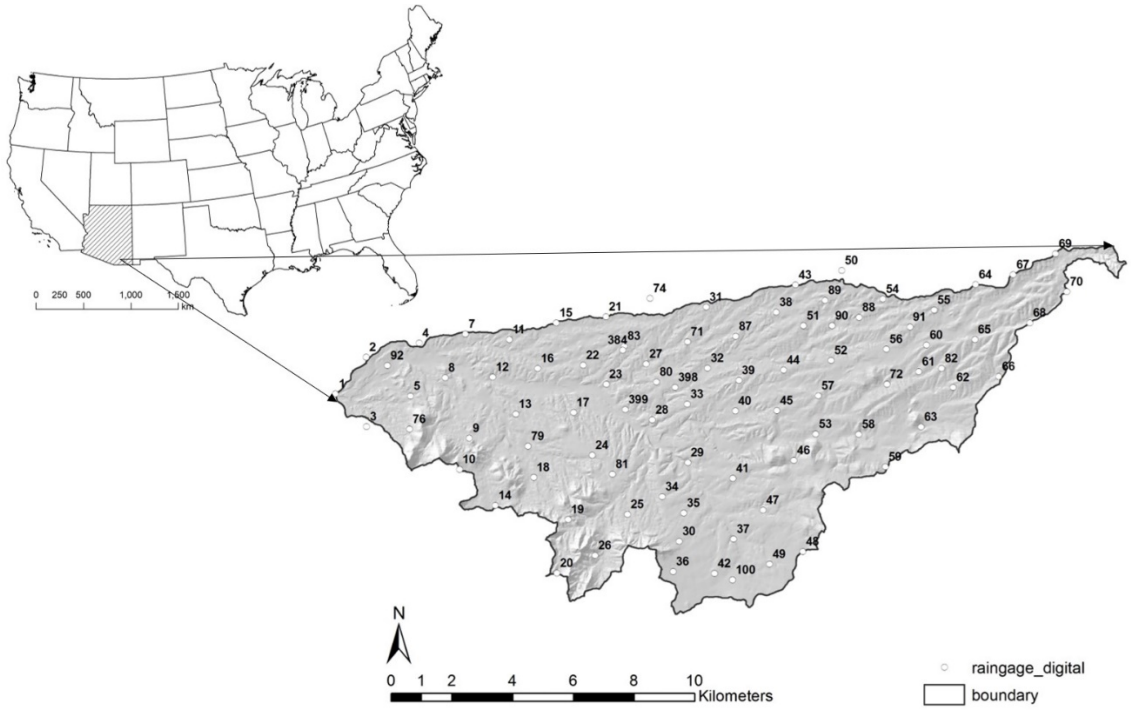

Figure 1. Rain gage network of USDA-Agricultural Research Service Walnut Gulch Experimental Watershed, Tombstone, Arizona.

2.2 Storm identification

A continuous rainfall record consists of both wet periods and dry periods. Researchers have explored different methods to distinguish events, usually based on a threshold of the dry period. This threshold can be a fixed time interval for all months, such as 6 hour used in erosive rainfall studies (Wischmeier and Smith, 1978). It can also vary with months, depending on the actual distribution of the inter-arrival time of rainfall in each month. The Walnut Gulch rainfall database has identified events for each gage separately and assigned an event ID to each one. The criteria used for each gage in the

database was based on a one hour hiatus (Goodrich and Keefer et al., 2008). However, this separation is only for one rain gage, which means if two gages received rainfall at the same time, they are still assigned different event IDs in the database. An actual storm occurring in the watershed usually involves more than one gage, so it is necessary to identify the individual storms within the entire gage network. According to visual perusal of daily rainfall interpolation maps (Figure S1 in supplemental material), we determined that a reasonable storm cell number within one day was no more than five. Longer thresholds give fewer storms identified for each day, since more gage events will be combined. The 4-hour threshold to separate and identify storms was selected so that the daily storm numbers were equal to or fewer than five. When the event starting times of two gages were within that threshold, they are identified to be the same storm in the watershed. The maximum depth for each storm was also recorded during the storm identification process.

2.3 Rainfall occurrence

The rainfall generator is built with a Richardson type framework, using a first-order Markov chain model (Richardson, 1981). A flow diagram of the computational processes of rainfall generator was shown in Figure 2. The basic concept of the first-order Markov chain method is that the present state of the system only depends on the previous state, which translated into the rainfall generation process means that the wet or dry state of the current day depends only on the state of the previous day. Using the Markov approach, a wet day is designated if at least one rain gage in the watershed receives rainfall on that day. Once a wet day is generated for the watershed, the model then

generates the storm location and coverage, which determines how much simulated rainfall each particular gage receives. In order to generate a sequence of wet and dry days, three transition probabilities need to be calculated. P(W) is the probability of a wet day, P(W|W) is the probability of a wet day following a wet day, and P(W|D) is the probability of a wet day following a dry day. Previous research in Walnut Gulch showed that the transition probabilities for biweekly periods have significant differences from each other (Hsieh, 2002), so all transition probabilities were calculated on a biweekly basis. Modeling of the wet and dry sequence in the rainfall generator is done by first initializing a random number, and then using P(W) to decide the state of first day. After the state of the previous day was decided, then the transition probabilities P(W|W) and P(W|D) were used to calculate the state of the next day in each biweekly period for the entire simulation sequence (Figure 2).

When a wet day is generated, the type of rainfall also needs to be decided for that day. The consensus of most studies on Walnut Gulch is to separate each year into summer months (July-September) and non-summer months (Goodrich and Keefer et al., 2008; Nearing et al., 2015; Nichols et al., 2002; Osborn et al., 1979) in terms of differentiating rainfall types. The dominant type for summer months is convective rainfall, while the dominant type for non-summer months is frontal rainfall. The third type, tropical depression rainfall, occurs primarily in late summer and fall, from September through November (Gochis et al., 2006). Probabilities for these three types of rainfall were calculated for each biweekly period using the daily rainfall. Periods with only one type of rainfall occurrence is straightforward, i.e. the probability of a rainfall to

be a frontal type in December and January through June is 1. Similarly, the probability for convective rainfall in July through August is also 1. The complicated period is from September through November, where the probability for tropical depression storms needs to be considered. To do this, the histogram of all maximum depths of the storms in September through November were plotted, and then an exponential distribution was fitted to that histogram. The storms with large maximum depth on the histogram tails, which could not be fitted well by the exponential curve, were identified as tropical storms. Thus, their probabilities were calculated using the number of these storms divided by the total number of storms. All biweekly periods in September through November share the same probability of tropical depression rainfall, and the remainder of the probability for convective and frontal storms in these three months are obtained by subtracting those from 1. Thus, each day of rainfall as determined by the transition probabilities were categorized as one of the three rainfall types.

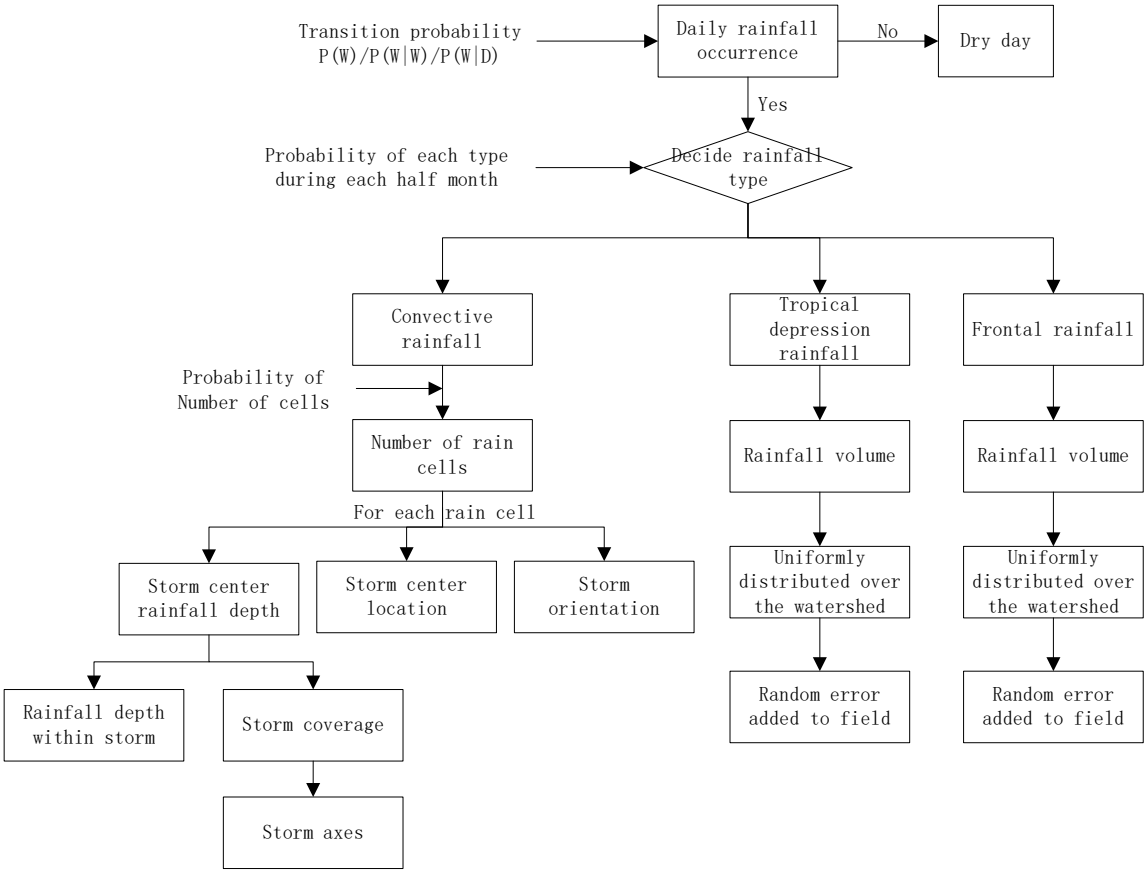

Figure 2. Flow diagram of the computational processes in the rainfall generator.

2.4 Rainfall amount and distribution

2.4.1 Convective storms

Convective storms usually show with an approximately elliptical shape in space, as determined either from interpolated daily rainfall maps or radar images (Hsieh, 2002; Karklinsky and Morin, 2006; Peleg and Morin, 2012). Hsieh (2002) analyzed convective storms in Walnut Gulch and proposed a conceptual model to characterize them (Figure 3). This current study followed a similar conceptual model and determined several

parameters using rainfall data from July through September collected in 1967 through 2016.

The previous study of Hsieh (2002) showed that the storm centers are distributed randomly in the watershed. Sometimes a storm falls only partly within the watershed boundary, which means the generated storm center can also be outside the boundary. To address this, the generator uses a slightly larger area of 26.5 km by 12.5 km, divided it into 33125 cells, with each cell representing a 100 m by 100 m area and assigned an index from 1 through 33125. The equation to obtain a storm center location Z is:

$$z = \frac{Z}{33125} \tag{1}$$

where Z is the center index ranging from 1 through 33125, and z is the standard uniform deviate ranging from 0 to 1.

Once the storm center is located, a storm center depth is generated from a lognormal distribution and assigned to this storm. Several distributions were tested for the convective storm maximum depth, and the lognormal fit best for the data. It is assumed that the depth at the storm center is the maximum and decays to zero on the storm edge. A modified linear spread function was applied in the generator (Figure 4), which maintains constant intensity amount around the center, and then follows a linear decay function to the edge.

$$depth = \begin{cases} \max dep & 0 \le r \le c \times D \\ \max dep(1 - r / D) / (1 - c) & c \times D < r \le D \end{cases} \tag{2}$$

where *depth* is the rainfall depth at a certain point inside the storm extent, *max dep* is the maximum depth at storm center, *D* is the distance from the center to the edge passing through at a certain point, *r* is the distance from the center to that point, *c* is a constant between 0 and 1. The calibration of *c* was made by matching the simulated total summer rainfall amount to the observed rainfall.

The storm area is related to the maximum depth of the storm. After logarithmic transformation, a linear regression was built between the area and the maximum depth:

$$\ln(area) = a_0 + a_1 \ln(\max dep) + \varepsilon \qquad (3)$$

where the units for storm area are km^2, and the units for maximum depth is *mm*, a_0 and a_1 are the coefficients of the linear regression equation, ε is a random error term.

An elliptical shaped storm has two axes, the major axis *a* and the minor axis *b*. The ratio *c* between them is defined as $c = a/b$. The value of *c* follows a normal distribution. Distribution parameters were acquired from Hsieh (2002). The simulated ratio was bounded between one standard deviation around the mean. When both the area and the ratio has been chosen for a storm, the length of major and minor axis can be calculated from the area equation of an ellipse.

The last parameter for a convective storm is the orientation. It is defined as the counter-clockwise angle starting from the east. The orientation for a storm is between 0 and 180 degrees and follows a normal distribution. Distribution parameters were acquired from Hsieh (2002). The simulated orientation was bounded between one standard

deviation around the mean, and extreme values beyond the 0 to 180 degrees range were discarded until a new value within the range was generated.

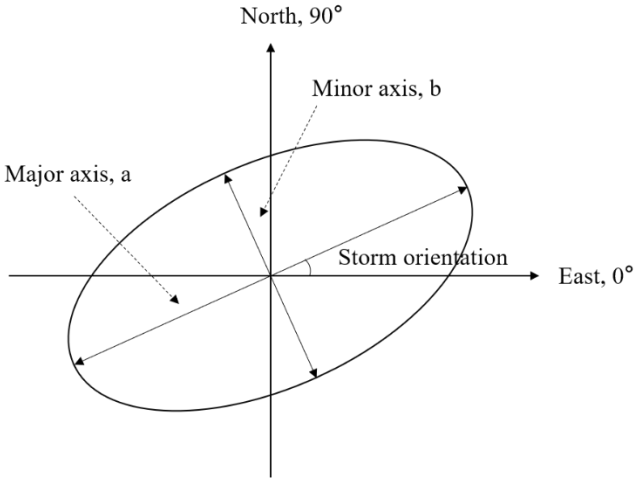

Figure 3. Conceptual model of convective storms of convective storms

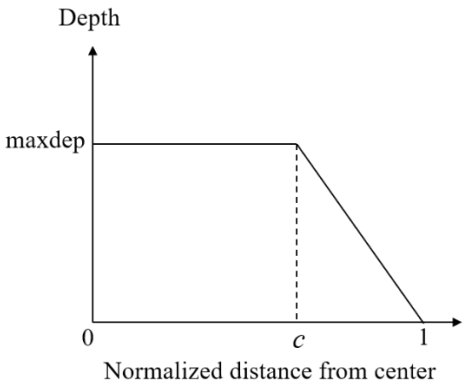

Figure 4. Rainfall depth spread function

2.4.2 Frontal storms

The frontal storms in non-summer months have much less spatial variation than do the convective storms. Osborn et al. (1979) analyzed data from Walnut Gulch in non-monsoon months, suggesting that nine gages are adequate to represent the variability of frontal storms. Rainfall interpolation maps in non-monsoon months also showed this pattern. Since frontal storms usually cover the whole Walnut Gulch, for simplicity, it is assumed that every frontal storm covers the entire watershed in the generation process. The total volume of water of each frontal storm is the important factor for quantifying annual water balance, but from a hydrologic standpoint, winter frontal storms do not

generate runoff in the channels at Walnut Gulch (Goodrich, Keefer, et al., 2008; Goodrich, Unkrich et al., 2008; Nearing et al., 2015).

The 88 rain gages are nearly uniformly distributed in the watershed, which means the area represented by each gage is approximately the same. The total volume of water that a storm delivers can be calculated by the following equation:

$$Vol = Dep_{avg} \times unit\ area \times N \qquad (4)$$

where Vol is the total volume of each frontal storm, Dep_{avg} is the average depth of all gages receiving rainfall, *unit area* is the area of one gage represented, N is the number of gages receiving rainfall. Notice that the *unit area* is not a constant value throughout all the years, because with the deletion or addition of gages over time the number of gages in the full network changed during the recording period. Different *unit area* values needed to be calculated for different years. Data from 1967 through 1980, 1992 through 1998, and 2000 through 2016 were used to fit a distribution for the total volume of water per storm for each biweekly period. The extremely large values on the tails during September through November fit poorly with the overall distribution curve (Figure S2), which indicates that they follow a different underlying mechanism. Those storms were considered as tropical depression storms and were excluded from the dataset when building the distribution for frontal storms. The model simulation will randomly pick a storm volume from the distribution curve of each biweekly period, first spread it evenly in the whole watershed with each grid having the average depth calculated based on the volume, and then added some randomness for each grid. The random difference added to

each grid is based on the standard deviations of the observed rainfall fields, and each standard deviation is corresponded to a certain average storm depth. In order to provide a reasonable variation of the generated rainfall fields, the added randomness is allowed to fluctuate between negative to positive two standard deviations.

2.4.3 Tropical depression storms

The algorithm to generate tropical depression storms is similar to that of frontal storms. The difference is that these storms are much less frequent and the volume of water dropped by this type is much larger than by frontal storms (Gochis et al., 2006; Osborn, 1982). In the previous steps, the extreme values of storm volumes in September through November were excluded and all these values were fit to a separate distribution, which was used for the tropical depression storms. Unlike the frontal storms, numbers of identified tropical depression storms were limited, so only one distribution was fit for the entire September through November period. The model simulation will randomly pick a storm volume from the distribution, first spread it evenly in the whole watershed and then add some randomness to each grid. The random difference added to each grid is based on the standard deviations of the observed rainfall fields, and each standard deviation is corresponded to a certain average storm depth. In order to provide a reasonable variation of the generated rainfall fields, the added randomness is allowed to fluctuate between negative to positive two standard deviations.

2.5 Multiple events in a day

The results in the Hsieh (2002) model underestimated the total summer rainfall of each gage, partly because the model only simulated one storm per day. Studies from radar analysis have shown that convective rainfall generally consists of several rain cells in one day (Morin et al., 2004; Peleg and Morin, 2014, 2012). Thus, the ability to simulate multiple events per day were enabled in this rainfall generator. Both convective storms and frontal storms can have multiple events per day, whereas the tropical depression storm remained as single event per day because of their sizes and durations. Based on the storm identification process in previous section, probabilities for different numbers of storms occurring in a single day may be calculated. For example, the probability of two events per day is made by counting the number of days with two storms and then dividing it by the number of total rainy days in a biweekly period. Convective rainfall would allow up to five storms per day, while frontal rainfall would allow up to three storms per day in this rainfall generator. Calibration of multiple events probabilities is based on controlling the total number of storms over the fifty-year period. For instance, if the total number of storms is overestimated, then the probability of more than one event was adjusted lower by multiplying a coefficient between 0 and 1. Consequently, probabilities for one event will be adjusted higher to maintain that the sum of all probabilities adding to one.

2.6 Statistics

Statistical analyses were performed using MATLAB. The regression equation between convective storm area and maximum depth was based on 4152 convective storms identified in 50 years, with maximum depth ranging from 0.25 mm to 95.12 mm and storm area ranging from 1.59 km^2 to 152.94 km^2. Statistical distribution types were

determined for convective storm maximum depths and frontal storm and tropical depression storm volumes by comparing the empirical probability distributions to several theoretical distribution functions, such as lognormal, gamma, and exponential. The Kolmogorov–Smirnov test (K-S test) was used to test the similarity of the empirical distribution to the theoretical ones using a significance level of $p = 0.05$. If more than one theoretical distribution passed the K-S test, then the one with least number of parameters was selected in further modelling processing. After the selection of distribution type, distribution parameters were fit for each type of rainfall as described previously.

2.7 Model evaluation

The rainfall generator was run for 30 replicates of 50-year simulation (in total 1500 years) to obtain a sequence of simulated daily rainfall, and then compared with the observed 50 years historical rainfall data. Model performance was evaluated in two aspects: individual storm statistics and seasonally aggregated rainfall statistics. Previous research (Goodrich and Keefer et al., 2008; Nearing et al., 2015; Nichols et al., 2002) divided the year into summer months (July-September) and non-summer months (October-December, January-June), which is adopted in this study as well. The convective storm type was evaluated to determine whether the proposed conceptual model was able capture the major storm characteristics. Seasonally aggregated rainfall amounts were evaluated based on the simulation results of six gages (Gage ID 13, 34, 44, 46, 62, 80). These gages were relatively evenly distributed inside the watershed and were selected as a sample to calculate the seasonal rainfall.

Statistics of both simulated individual storms and aggregated rainfall, including the mean, standard deviation, maximum, minimum, range and skewness, were computed and compared with the 50-year observed data. In addition, simulated and observed cumulative distribution functions (CDFs) were created for both individual storms and aggregated rainfall. K-S tests were performed between simulated and observed CDFs to determine whether they belonged to the same statistical distribution.

Time series properties were evaluated through dry and wet spell lengths of simulated and observed rainfall data. The cumulative distribution function curves of both dry and wet spells were created for summer, non-summer, and annual periods. Seasonal and annual median lengths of dry and wet spells were also calculated for comparison. K-S tests were performed between simulated and observed CDFs to determine whether they belonged to the same statistical distributions.

3 Results and discussion

3.1 Rainfall characterization

The transition probabilities for rainfall occurrence somewhere on the watershed for the 24 half-month periods are shown in Table 1. The probability of wet P(W) clearly showed that rainfall frequency reaches its peak in summer, exceeding 0.5, from the first half of July to the first half of September. The second wettest period is in winter from December through February, where P(W) ranges from 0.2 to 0.3. P(W|W) is always greater than P(W|D), which means that wet days tend to be clustered together.

Table 1. Transition probabilities, probabilities for three types of rainfall, and the probabilities for multiple events in all 24 half month periods

Half month		1	2	3	4	5	6	7	8	9	10	11	12
Transition probabilities	P(W)	0.2053	0.2225	0.2547	0.1914	0.1880	0.1338	0.1147	0.0960	0.0960	0.1175	0.1240	0.2640
	P(W|W)	0.4740	0.5000	0.5602	0.4776	0.4752	0.3738	0.4186	0.4167	0.3750	0.5106	0.4624	0.6111
	P(W|D)	0.1359	0.1431	0.1503	0.1237	0.1215	0.0952	0.0753	0.0619	0.0664	0.0652	0.0761	0.1377
Probabilities for types of rainfall	Convective	0	0	0	0	0	0	0	0	0	0	0	0
	Frontal	1	1	1	1	1	1	1	1	1	1	1	1
	Tropical	0	0	0	0	0	0	0	0	0	0	0	0
Probabilities for multiple events	1	0.7309	0.7155	0.6589	0.7629	0.6751	0.7312	0.6690	0.8808	0.8217	0.7066	0.7868	0.8031
	2	0.1651	0.1626	0.2321	0.1626	0.2188	0.1680	0.2242	0.1022	0.1426	0.1726	0.1745	0.1663
	3	0.1040	0.1219	0.1089	0.0745	0.1061	0.1008	0.1068	0.0170	0.0357	0.1208	0.0388	0.0306
	4												
	5												
Parameter of distributions*	μ (mm or 10^5 m^3)	2.6923	2.8794	2.1721	1.8628	2.6981	2.0318	1.5667	1.6052	1.4837	1.6541	2.3326	2.1434
	σ (mm)												

Table 1. (continued)

Half month		13	14	15	16	17	18	19	20	21	22	23	24
Transition probabilities	P(W)	0.6213	0.7738	0.7547	0.6438	0.5320	0.2733	0.2160	0.1950	0.1440	0.1613	0.2173	0.2288
	P(W|W)	0.7854	0.8336	0.8269	0.7592	0.7118	0.5561	0.5185	0.4615	0.4444	0.3884	0.5215	0.5191
	P(W|D)	0.3521	0.5635	0.5326	0.4316	0.3276	0.1651	0.1327	0.1304	0.0935	0.1176	0.1329	0.1410
Probabilities for types of rainfall	Convective	1	1	1	1	0.9876	0.9876	0	0	0	0	0	0
	Frontal	0	0	0	0	0	0	0.9876	0.9876	0.9876	0.9876	1	1
	Tropical	0	0	0	0	0.0124	0.0124	0.0124	0.0124	0.0124	0.0124	0	0
Probabilities for multiple events	1	0.6449	0.6499	0.6450	0.6842	0.7133	0.6966	0.7409	0.7515	0.7496	0.7596	0.7801	0.6929
	2	0.2187	0.2227	0.2171	0.2178	0.1633	0.1678	0.1766	0.1792	0.2019	0.1492	0.1367	0.1906
	3	0.0961	0.0911	0.0953	0.0713	0.0867	0.0807	0.0824	0.0694	0.0485	0.0912	0.0832	0.1165
	4	0.0362	0.0300	0.0310	0.0255	0.0250	0.0323						
	5	0.0042	0.0062	0.0115	0.0013	0.0117	0.0226						
Parameter of distributions*	μ (mm or 10^5 m^3)	1.5314	1.7461	1.6551	1.6105	1.6272	1.3189	2.4079	2.4877	2.5405	2.0375	3.2548	2.3647
	σ (mm)	1.4235	1.4680	1.4851	1.4827	1.4576	1.5344						

*** (1) July-September (13-18): lognormal distribution for convective rainfall maximum depth, unit: mm. (2) Other months (1-12,19-24): exponential distribution for frontal rainfall volume, unit: 10^5 m^3. (3) September-November (17-22): μ of exponential distribution for tropical depression rainfall is $4.2643*10^6$ m^3.**

Axis ratio and orientation statistics were acquired from Hsieh (2002). Those parameters are measured directly from interpolated rainfall surfaces and shown in Table 2. The mean value of axis ratio was 1.54, which is slightly greater than that found in previous work on Walnut Gulch, which showed a major to minor axis ratio of between 1.0 and 1.5 (Fogel and Duckstein, 1969). The mean value of orientation found in Hsieh (2002) was 91.40, which points generally north as defined in the previous section. The area statistics acquired in this study showed a mean of 58.01 km^2, which is approximately one-third of the watershed area. The regression equation of area and maximum depth (see Eq. 3) was determined as:

$$\ln(area) = 2.1784 + 0.6851\ln(\max\ dep) + \varepsilon \quad (R^2 = 0.57, n = 4152) \tag{5}$$

Hsieh (2002), using data also from Walnut Gulch, developed a similar regression equation (Equation 6) between area and maximum depth from 48 interpolated storm surfaces, with the maximum depth ranging from 4.83 mm to 47.75mm, and storm areas ranging from 3.6 km^2 to 181.26 km^2.

$$\ln(area) = 1.1569 + 0.93\ln(\max\ dep) + \varepsilon \quad (R^2 = 0.46, n = 48) \tag{6}$$

The number of storms used in this study was much greater than used by Hsieh (2002). The slope of Equation 5 is less than Equation 6, because the 48 storm samples Hsieh chose were mostly larger storms with clear elliptical shapes in space, which may be biased in terms of area representation.

The decay function to distribute rainfall from the convective storm center to the edge was determined as (see Figure 4):

$$depth = \begin{cases} \max\ dep & 0 \le r \le 0.59D \\ \text{maxdep}(1 - r / D) / 0.41 & 0.59D < r \le D \end{cases} \quad (7)$$

Previous work on Walnut Gulch has used either an exponential type decay function (Fogel and Duckstein, 1969) or simple linear decay function (Hsieh, 2002) to distribute the rainfall from the storm center to the edge. However, in this study, we found that these two methods both underestimate the rainfall total. Observed from radar images and interpolated rain gage isohyets, the convective rain cell tends to have a flat distribution around the center. The rationale behind it is that as the storm moves in space it creates a region with relatively uniform maximum depth in the storm center (Fogel and Duckstein, 1969).

Other model parameters, including the probabilities for different types of rainfall, probabilities for multiple events occurring in a day, and the distribution parameters for rainfall amount are shown in Table 1. The distribution for convective storm maximum depth was determined to be lognormal with two parameters, mean (μ) and variance (σ), the fitting plots were shown in supplemental material Figure S3. Whereas, the best-fit distribution for frontal and tropical depression storms was determined to be exponential, with only one parameter μ, and fitting plots were shown in supplemental material Figure S4. Notice that the units for convective storms and the other two types are different in Table 1, because one is for depth and the other two are for volume.

Table 2. Characteristics of convective storm area, axis ratio, and orientation

	Mean	Std.dev	Skewness	Max	Min
Area (km^2)	58.01	50.50	0.56	152.94	1.59
Axis ratio (a/b)*	1.54	0.37	0.96	2.50	1.08
Orientation (degree)*	91.40	38.27	0.06	170.00	0.00

***From Hsieh (2002)**

3.2 Model evaluation

The statistics of observed and simulated convective storm maximum depth from July through September are presented in Table 3. The mean value simulated in all six half months with convective storms had less than 6% difference. The fact that the simulated storm depths had a broader range of maximum depths is expected since the model was run for 30 replicates of 50-year time range (in total 1500 years) and should include extreme values that were not captured in the historical data. The shape of simulated and observed CDF curves for all six periods were similar (Figure 5). The K-S test showed that there were no significant ($p = 0.05$) differences between the observed and simulated CDFs in all half month periods.

Table 3. Characteristics of convective storm maximum depths (mm)

	Observed						Simulated					
	July 1-15	July 16-31	Aug 1-15	Aug 16-31	Sept 1-15	Sept 16-30	July 1-15	July 16-31	Aug 1-15	Aug 16-31	Sept 1-15	Sept 16-30
Mean	10.32	12.85	12.05	11.52	11.38	9.45	10.26	13.23	12.73	11.73	11.93	9.46
Std.dev	12.62	14.78	14.30	13.58	13.41	12.99	14.86	20.08	19.36	17.53	17.85	14.94
Max	85.60	83.31	91.19	81.03	87.63	95.12	104.28	143.36	136.68	129.45	125.26	108.26
Min	0.25	0.25	0.25	0.25	0.25	0.25	0.25	0.25	0.25	0.25	0.25	0.25
Range	85.34	83.06	90.93	80.77	87.38	94.87	104.03	143.11	136.43	129.20	125.01	108.01
Skewness	2.25	1.79	1.91	1.86	2.03	2.85	2.97	3.07	3.05	3.01	3.05	3.25

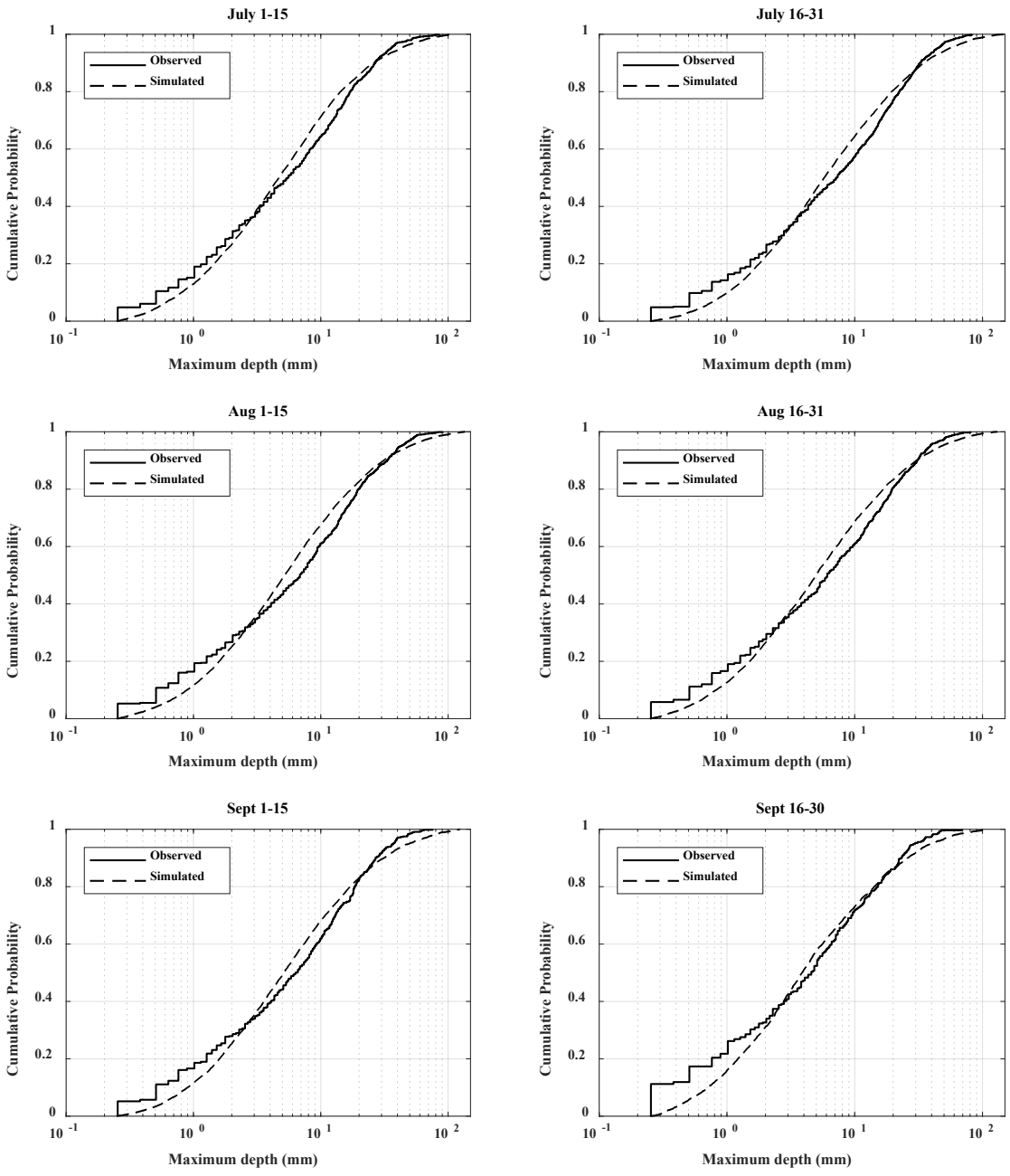

Figure 5. CDFs of observed and simulated summer convective storm maximum depths.

The average summer rainfall total of the selected six gages was 192.9 mm, whereas the simulated summer rainfall total was 190.4 mm, with 1.3% difference (Table

4). The simulated range of summer rainfall total was almost twice that of the observed values, with lesser minimum and greater maximum values. Consequently, the simulated standard deviation was approximately 100 mm, which was greater than the observed values which were approximately 60 mm. K-S test results showed that there was no significant difference between the two curves in summer (Figure 6a), under $p = 0.05$ significance level. The simulated data variability was greater than the historical data, could have resulted from more extreme values being simulated in the long synthetic time series. This is consistent with the individual convective storms evaluation, where some extreme values exceeding the historical records were simulated.

As for non-summer rainfall, observed mean of six gages was 122.6 mm, and the simulated mean was 122.2 mm. The range of winter rainfall had 15.6% difference between the observed and simulated, which is mostly caused by the overestimation of the minimum values. The simulated maximum winter rainfall was slightly less than the observed. Thus, the standard deviation was also underestimated by the model compared to historical records. The reason for this is related to the method used to distribute the generated the rainfall volume over the watershed. Since winter frontal storms have less variability than summer convective rainfall, for simplicity in this rainfall generator, every storm volume was distributed uniformly to all gages, only adding a small random variance. As a result, the variation in both space and time has been lost to some degree. The two CDF curves of non-summer rainfall total amounts failed the K-S test (Figure 6b), which means that there was some difference between the simulated and observed data. However, the winter storms in Walnut Gulch rarely cause runoff and erosion due to

their low intensity (Goodrich, Keefer, et al., 2008; Goodrich, Unkrich et al., 2008; Nearing et al., 2015), so it was considered acceptable to miss some variation in the generated storm depth totals as long as the total amount is similar and annual water balance was maintained.

Table 4. Observed and simulated rainfall totals for summer months of six gages (mm)

	Observed						Simulated					
Gage ID	**13**	**34**	**44**	**46**	**62**	**80**	**13**	**34**	**44**	**46**	**62**	**80**
Mean	186.7	192.2	194.6	199.5	194.5	189.7	196.3	187.1	185.8	191.8	186.5	195.0
Std.dev	60.4	63.7	58.6	61.4	52.2	66.8	100.4	99.7	101.6	102.6	96.3	100.7
Max	336.6	345.7	345.9	410.5	327.3	380.0	508.3	561.7	623.5	617.3	534.2	511.9
Min	89.8	70.2	81.0	77.7	88.8	75.4	3.6	1.5	7.2	8.2	10.4	9.1
Range	246.8	275.5	264.9	332.7	238.5	304.5	504.8	560.2	616.3	609.1	523.9	502.8
Skewness	0.5	0.4	0.4	0.5	-0.2	0.6	0.5	0.6	1.0	0.9	0.6	0.6

Table 5. Observed and simulated rainfall totals for non-summer months of six gages (mm)

	Observed						Simulated					
Gage ID	**13**	**34**	**44**	**46**	**62**	**80**	**13**	**34**	**44**	**46**	**62**	**80**
Mean	122.7	120.7	121.6	132.8	116.9	120.9	122.6	122.0	122.0	122.7	121.6	122.1
Std.dev	59.7	65.8	61.1	65.1	64.3	59.8	34.2	34.1	33.7	34.7	34.0	34.3
Max	266.4	308.9	295.0	318.8	300.4	282.8	265.0	305.8	282.0	280.8	264.7	256.8
Min	19.8	18.0	13.2	16.3	10.7	12.2	42.3	41.9	42.3	33.2	44.7	30.3
Range	246.6	290.8	281.8	302.5	289.7	270.6	222.7	263.9	239.8	247.6	219.9	226.5
Skewness	0.6	0.9	0.9	0.8	1.2	0.7	0.5	0.6	0.4	0.5	0.6	0.4

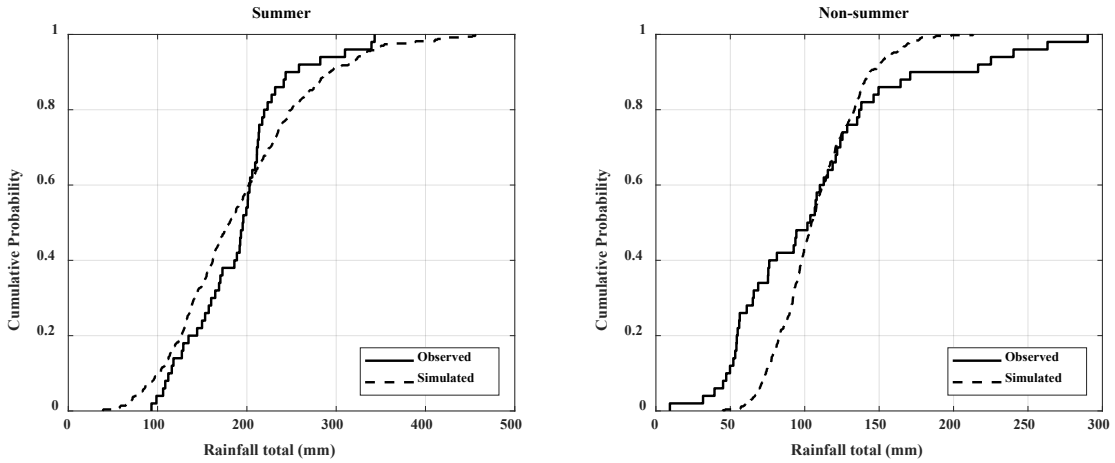

Figure 6. CDFs of observed and simulated rainfall totals for (a) summer and (b) non-summer periods.

Simulated and observed median lengths of dry and wet spell were shown in Table 6, which represents the central tendency of spell length distribution. The median of simulated dry spell length was slightly shorter than observed throughout the year, whereas the median of simulated wet spell length was longer than observed for summer, but the same for non-summer months. The overestimated wet spell length also caused an overestimation for annual wet spell length. The cumulative distribution function curves for seasonal and annual were shown in Figure 7. Five of the six pairs of observed and simulated curves passed the K-S test under $p = 0.05$ significance level. The significant difference for the summer wet spell curves indicated that the rainfall generator tends to simulate slightly longer wet periods during summer season.

Table 6. Observed and simulated median length of dry and wet spells (day)

	Annual	Summer	Non-summer		Annual	Summer	Non-summer
Dry_observed	4.2	2.2	7.2	Wet_observed	1.0	1.0	1.0
Dry_simulated	4.0	2.0	6.0	Wet_simulated	2.0	3.0	1.0

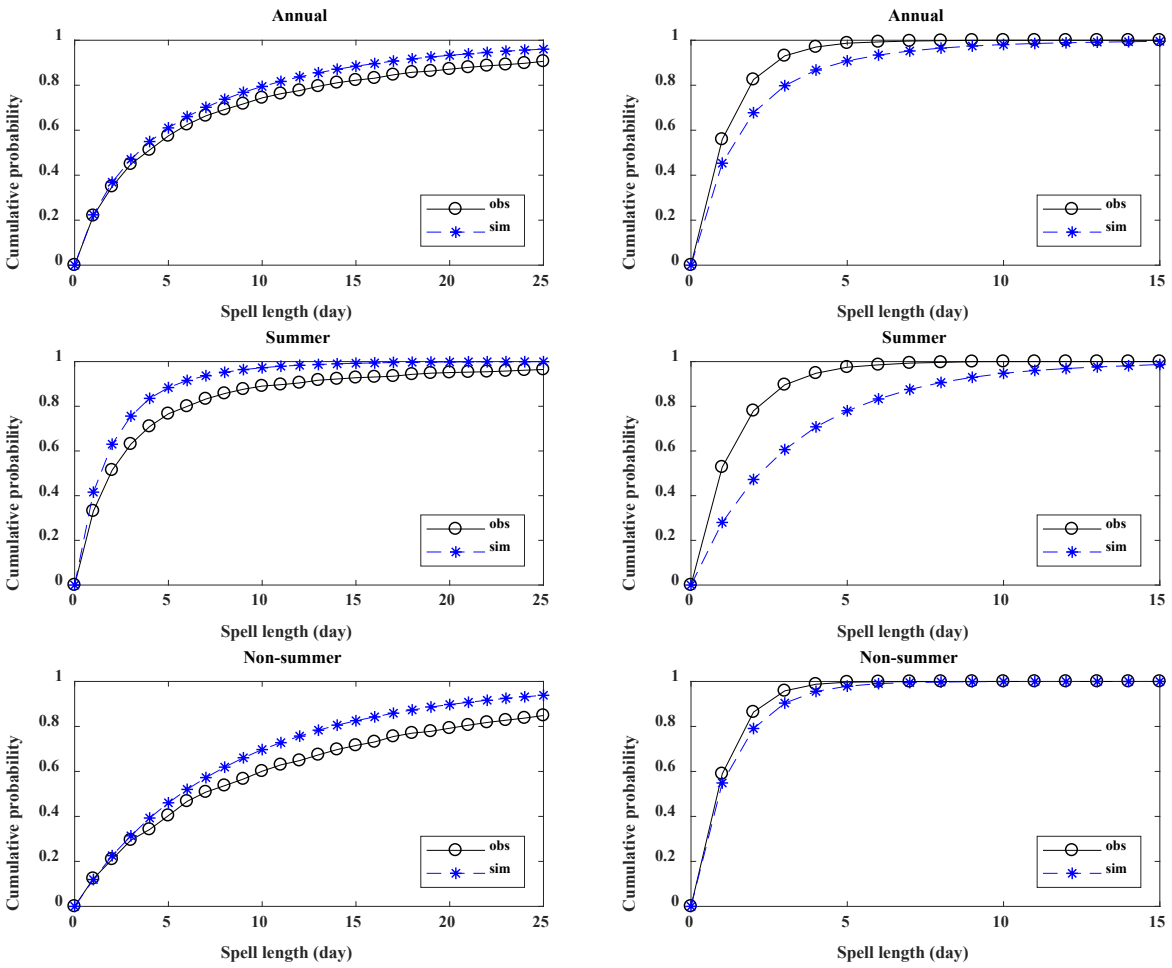

Figure 7. CDFs of observed and simulated dry and wet spell length for annual, summer and non-summer periods, (1) first column: dry spell, (2) second column: wet spell.

4 Conclusion

This study presented modeling concepts and processes of a daily, spatial, stochastic rainfall generator in a semi-arid watershed in southeastern Arizona. Unlike most daily rainfall generators which give only the daily rainfall amount, this model is capable of simulating individual storms within a day. Simulation of four elements, including daily rainfall occurrence, the number of storms per day, the maximum depth or

total volume of a storm, and spatial distribution of the rainfall was illustrated using 50-years of rain gage observations in Walnut Gulch Experimental Watershed, Arizona. The separation process of generating three types of rainfall (convective, frontal and tropical depression) is appropriate in this region, since they all have quite different physical features. The concept of elliptical shape of convective storms works well in this study and has been tested in other research. The simulated individual convective storm statistics were similar to the observed. The simulated seasonal rainfall performed differently for summer and non-summer periods, with a slight overestimation of variation of annual summer rainfall and an underestimation of variation in non-summer period, but the long-term mean values of both summer and non-summer periods are satisfactory.

There are limitations for this generator. It is a well calibrated model based on the dense rain gage network of Walnut Gulch Experimental Watershed, and expanding it to larger area application will require additional analysis linking the point statistics with area statistics. Possible solutions for obtaining larger area statistics, such as convective storm area, may need incorporation of radar rainfall images. This rainfall generator is initially targeted at semi-arid watersheds where convective rainfall dominated, thus it may not be immediately applicable in regions with significantly different rainfall types.

Possible uses of the rainfall generator include application into hydrological models, erosion models as rainfall input, where spatial rainfall information could have an impact on runoff response or sediment yield. It may also be applied in climate change studies by manipulating model parameters to account for future trends and testing the outcomes. Developing the rainfall generator into a high-resolution temporal model is a

future research need, which will require further studies of storm movement in space and time.

Acknowledgements

Acknowledgement goes to the field staff of the Walnut Gulch Experimental Watershed and all of the previous scientists and staff of the USDA-ARS Southwest Watershed Research Center for the dedication and effort that made the collection and use of these data possible. Rainfall data used in this study can be acquired at http://www.tucson.ars.ag.gov/dap/.

This work was funded by a Specific Cooperative Agreement between the USDA Agricultural Research Service (Agreement number 58-53424-018) and the University of Arizona (Agreement number 2022-13610-012-22S).

Declarations of interest: none.

Reference

Arnold, J.G., Williams, J.R., 1989. Stochastic Generation of Internal Storm Structure at a Point. Trans. ASAE 32, 161–167.

Asong, Z.E., Khaliq, M.N., Wheater, H.S., 2016. Multisite multivariate modeling of daily precipitation and temperature in the Canadian Prairie Provinces using generalized linear models. Clim. Dyn. 47, 1–21. https://doi.org/10.1007/s00382-016-3004-z

Bardossy, A., Plate, E.J., 1992. Space-time model for daily rainfall using atmospheric circula.pdf.

Barnolas, M., Rigo, T., Llasat, M.C., 2010. Characteristics of 2-D convective structures in Catalonia (NE Spain): an analysis using radar data and GIS. Hydrol. Earth Syst. Sci. 14, 129–139. https://doi.org/10.1016/j.atmosres.2005.08.014

Bell, V.A., Moore, R.J., 2000. The sensitivity of catchment runoff models to rainfall data at different spatial scales. Hydrol. Earth Syst. Sci. https://doi.org/10.5194/hess-4-653-2000

Beven, K., Hornberger, G., 1982. Assesing the effect of spatial pattern of precipitation in modeling stream flow hydrographs. Water Resour. Bullettin 18, 823–829. https://doi.org/10.1111/j.1752-1688.1982.tb00078.x

Bonta, J. V, 2004. Stochastic simulation of storm occurrence,depth,duration and within-storm intensities. Trans. ASAE 47, 1573–1584.

Breinl, K., Di Baldassarre, G., Girons Lopez, M., Hagenlocher, M., Vico, G., Rutgersson, A., 2017. Can weather generation capture precipitation patterns across different climates, spatial scales and under data scarcity? Sci. Rep. 7, 3–7.

https://doi.org/10.1038/s41598-017-05822-y

Breinl, K., Turkington, T., Stowasser, M., 2015. Simulating daily precipitation and temperature: A weather generation framework for assessing hydrometeorological hazards. Meteorol. Appl. 22, 334–347. https://doi.org/10.1002/met.1459

Breinl, K., Turkington, T., Stowasser, M., 2013. Stochastic generation of multi-site daily precipitation for applications in risk management. J. Hydrol. 498, 23–35. https://doi.org/10.1016/j.jhydrol.2013.06.015

Brissette, F.P., Khalili, M., Leconte, R., 2007. Efficient stochastic generation of multi-site synthetic precipitation data. J. Hydrol. 345, 121–133. https://doi.org/10.1016/j.jhydrol.2007.06.035

Buishand, T. a., Brandsma, T., 2001. Multisite simulation of daily precipitation and temperature in the Rhine basin by nearest-neighbor resampling. Water Resour. Res. 37, 2761–2776. https://doi.org/10.1029/2001WR000291

Calenda, G., Napolitano, F., 1999. Parameter estimation of Neyman-Scott processes for temporal point rainfall simulation. J. Hydrol. 225, 45–66. https://doi.org/10.1016/S0022-1694(99)00133-X

Cowpertwait, P.S.P., O'Connell, P.E., Metcalfe, A.V., Mawdsley, J.A., 1996. Stochastic point process modelling of rainfall. II. Regionalisation and disaggregation. J. Hydrol. 175, 47–65. https://doi.org/10.1016/S0022-1694(96)80005-9

Evin, G., Favre, A.C., Hingray, B., 2018. Stochastic generation of multi-site daily precipitation focusing on extreme events. Hydrol. Earth Syst. Sci. 22, 655–672. https://doi.org/10.5194/hess-22-655-2018

Féral, L., Sauvageot, H., Castanet, L., Lemorton, J., 2003. HYCELL - A new hybrid model of the rain horizontal distribution for propagation studies: 1. Modeling of the rain cell. Radio Sci. 38, 1–20. https://doi.org/10.1029/2002RS002802

Ferraris, L., Gabellani, S., Rebora, N., Provenzale, A., 2003. A comparison of stochastic models for spatial rainfall downscaling. Water Resour. Res. 39, 1–8. https://doi.org/10.1029/2003WR002504

Fogel, M.M., Duckstein, L., 1969. Point Rainfall Frequencies in Convective Storms. Water Resour. Res. 5, 1229–1237. https://doi.org/10.1029/WR005i006p01229

Gochis, D.J., Brito-Castillo, L., Shuttleworth, W.J., 2006. Hydroclimatology of the North American Monsoon region in northwest Mexico. J. Hydrol. 316, 53–70. https://doi.org/10.1016/j.jhydrol.2005.04.021

Goodrich, D.C., Keefer, T.O., Unkrich, C.L., Nichols, M.H., Osborn, H.B., Stone, J.J., Smith, J.R., 2008. Long-term precipitation database, Walnut Gulch Experimental Watershed, Arizona, United States. Water Resour. Res. 44, W05S04. https://doi.org/10.1029/2006WR005782

Goodrich, D.C., Lane, L.J., Shillito, R.M., Miller, S.N., Syed, K.H., Woolhiser, A., 1997. Linearity of basin response as a function of scale in a semiarid watershed. Water Resour. Res. 33, 2951–2965.

Goodrich, D.C., Unkrich, C.L., Keefer, T.O., Nichols, M.H., Stone, J.J., Levick, L.R., Scott, R.L., 2008. Event to multidecadal persistence in rainfall and runoff in southeast Arizona. Water Resour. Res. 44, W05S14. https://doi.org/10.1029/2007WR006222

Gupta, V.K., Waymire, E.C., 1993. A Statistical Analysis of Mesoscale Rainfall as a Random Cascade. J. Appl. Meteorol. 32, 251–267. https://doi.org/10.1175/1520-0450(1993)032<0251:ASAOMR>2.0.CO;2

Hsieh, H.-H., 2002. Stochastic daily thunderstorm generation in southeast Arizona. Univ. Arizona. https://doi.org/10.16953/deusbed.74839

Karklinsky, M., Morin, E., 2006. Spatial characteristics of radar-derived convective rain cells over southern Israel. Meteorol. Zeitschrift 15, 513–520. https://doi.org/10.1127/0941-2948/2006/0153

Kavvas, L., Delleur, J.W., 1981. Cluster Model of Daily Rainfall Sequences. Water Resour. Res. 17, 1151–1160. https://doi.org/10.1029/WR017i004p01151

Khalili, M., Brissette, F., Leconte, R., 2009. Stochastic multi-site generation of daily weather data. Stoch. Environ. Res. Risk Assess. 23, 837–849. https://doi.org/10.1007/s00477-008-0275-x

Koren, V.I., Finnerty, B.D., Schaake, J.C., Smith, M.B., Seo, D.J., Duan, Q.Y., 1999. Scale dependencies of hydrologic models to spatial variability of precipitation. J. Hydrol. 217, 285–302. https://doi.org/10.1016/S0022-1694(98)00231-5

Lanza, L.G., 2000. A conditional simulation model of intermittent rain fields. Hydrol. Earth Syst. Sci. https://doi.org/10.5194/hess-4-173-2000

Leander, R., Buishand, T.A., 2009. A daily weather generator based on a two-stage resampling algorithm. J. Hydrol. 374, 185–195. https://doi.org/10.1016/j.jhydrol.2009.06.010

Li, Z., 2014. A new framework for multi-site weather generator: A two-stage model

combining a parametric method with a distribution-free shuffle procedure. Clim. Dyn. 43, 657–669. https://doi.org/10.1007/s00382-013-1979-2

Li, Z., Lü, Z., Li, J., Shi, X., 2017. Links between the spatial structure of weather generator and hydrological modeling. Theor. Appl. Climatol. 128, 103–111. https://doi.org/10.1007/s00704-015-1691-8

Mehrotra, R., Sharma, A., 2007. A semi-parametric model for stochastic generation of multi-site daily rainfall exhibiting low-frequency variability. J. Hydrol. 335, 180–193. https://doi.org/10.1016/j.jhydrol.2006.11.011

Mehrotra, R., Srikanthan, R., Sharma, A., 2006. A comparison of three stochastic multi-site precipitation occurrence generators. J. Hydrol. 331, 280–292. https://doi.org/10.1016/j.jhydrol.2006.05.016

Mejía, J.M., Rodríguez-Iturbe, I., 1974. On the synthesis of random field sampling from the spectrum: An application to the generation of hydrologic spatial processes. Water Resour. Res. https://doi.org/10.1029/WR010i004p00705

Morin, E., Gabella, M., 2007. Radar-based quantitative precipitation estimation over Mediterranean and dry climate regimes. J. Geophys. Res. Atmos. 112, 1–13. https://doi.org/10.1029/2006JD008206

Morin, E., Goodrich, D., Maddox, R., Gao, X., Gupta, H., 2004. Spatial patterns in thunderstorm rainfall events : conceptual modeling and hydrological insights, in: Sixth International Symposium on Hydrological Applications of Weather Radar.

Morin, E., Goodrich, D.C., Maddox, R. a., Gao, X., Gupta, H. V., Sorooshian, S., 2006. Spatial patterns in thunderstorm rainfall events and their coupling with watershed

hydrological response. Adv. Water Resour. 29, 843–860. https://doi.org/10.1016/j.advwatres.2005.07.014

Morin, E., Goodrich, D.C., Maddox, R. a., Gao, X., Gupta, H. V., Sorooshian, S., 2005. Rainfall modeling for integrating radar information into hydrological model. Atmos. Sci. Lett. 6, 23–30. https://doi.org/10.1002/asl.86

Nearing, M.A., Unkrich, C.L., Goodrich, D.C., Nichols, M.H., Keefer, T.O., 2015. Temporal and elevation trends in rainfall erosivity on a 149 km2 watershed in a semi-arid region of the American Southwest. Int. Soil Water Conserv. Res. 3, 77–85. https://doi.org/10.1016/j.iswcr.2015.06.008

Nichols, M.H., Renard, K.G., Osborn, H.B., 2002. Precipitation changes from 1956 to 1996 on the Walnut Gulch Experimental Watershed. J. Am. Water Resour. Assoc. 38, 161–172. https://doi.org/10.1111/j.1752-1688.2002.tb01543.x

Obled, C., Wendling, J., Beven, K., 1994. The sensitivity of hydrological models to spatial rainfall patterns: an evaluation using observed data. J. Hydrol. 159, 305–333. https://doi.org/10.1016/0022-1694(94)90263-1

Osborn, H.B., 1983. Precipitation characteristics affecting hydrologic response of southwestern rangelands. Agricultural Research Service, Agricultural Reviews and Manuals, Western Series, No.34.

Osborn, H.B., 1982. Quantifiable differences between airmass and frontal-convective thunderstorm rainfall in the southwestern united states, in: Statistical Analysis of Rainfall and Runoff. pp. 21–32.

Osborn, H.B., Renard, K.G., Simanton, J.R., 1979. Dense networks to measure

convective rainfall in the southwestern United States. Water Resour. Res. 15, 1701–1711. https://doi.org/10.1029/WR015i006p01701

Papalexiou, S.M., Koutsoyiannis, D., Montanari, A., 2011. Can a simple stochastic model generate rich patterns of rainfall events? J. Hydrol. 411, 279–289. https://doi.org/10.1016/j.jhydrol.2011.10.008

Peleg, N., Morin, E., 2014. Stochastic convective rain-field simulation using a high-resolution synoptically conditioned weather generator (HiReS-WG). Water Resour. Res. 50, 1–16. https://doi.org/10.1002/2013WR014836

Peleg, N., Morin, E., 2012. Convective rain cells: Radar-derived spatiotemporal characteristics and synoptic patterns over the eastern Mediterranean. J. Geophys. Res. Atmos. 117, 1–17. https://doi.org/10.1029/2011JD017353

Racsko, P., Szeidl, L., Semenov, M., 1991. A serial approach to local stochastic weather models. Ecol. Modell. 57, 27–41. https://doi.org/10.1016/0304-3800(91)90053-4

Rebora, N., Ferraris, L., von Hardenberg, J., Provenzale, A., 2006. RainFARM: Rainfall Downscaling by a Filtered Autoregressive Model. J. Hydrometeorol. 7, 724–738. https://doi.org/10.1175/JHM517.1

Renard, K.G., Lane, L.J., Simanton, J.R., Emmerich, W.E., Stone, J.J., Weltz, M. a, Goodrich, D.C., Yakowitz, D.S., 1993. Agricultural impacts in an arid environment: Walnut Gulch studies. Hydrol. Sci. Technol. 9, 145–190.

Richardson, C.W., 1981. Stochastic simulation of daily precipitation, temperature, and solar radiation. Water Resour. Res. 17, 182–190. https://doi.org/10.1029/WR017i001p00182

Schuurmans, J.M., Bierkens, M.F.P., 2006. Effect of spatial distribution of daily rainfall on interior catchment response of a distributed hydrological model. Hydrol. Earth Syst. Sci. Discuss. 3, 2175–2208. https://doi.org/10.5194/hessd-3-2175-2006

Serinaldi, F., 2009. A multisite daily rainfall generator driven by bivariate copula-based mixed distributions. J. Geophys. Res. Atmos. 114, 1–13. https://doi.org/10.1029/2008JD011258

Stillman, S., Zeng, X., Shuttleworth, W.J., Goodrich, D.C., Unkrich, C.L., Zreda, M., 2013. Spatiotemporal Variability of Summer Precipitation in Southeastern Arizona. J. Hydrometeorol. 14, 1944–1951. https://doi.org/10.1175/JHM-D-13-017.1

Syed, K.H., Goodrich, D.C., Myers, D.E., Sorooshian, S., 2003. Spatial characteristics of thunderstorm rainfall fields and their relation to runoff. J. Hydrol. 271, 1–21. https://doi.org/10.1016/S0022-1694(02)00311-6

Valdes, J.B., Rodriguez-Iturbe, I., Gupta, V.K., 1985. Approximations of Temporal Rainfall From a Multidimensional Model. Water Resour. Res. 21, 1259–1270. https://doi.org/10.1029/WR021i008p01259

Verdin, A., Rajagopalan, B., Kleiber, W., Katz, R.W., 2015. Coupled stochastic weather generation using spatial and generalized linear models. Stoch. Environ. Res. Risk Assess. 29, 347–356. https://doi.org/10.1007/s00477-014-0911-6

Verdin, A., Rajagopalan, B., Kleiber, W., Podestá, G., Bert, F., 2018. A conditional stochastic weather generator for seasonal to multi-decadal simulations. J. Hydrol. 556, 835–846. https://doi.org/10.1016/j.jhydrol.2015.12.036

von Hardenberg, J., Ferraris, L., Provenzale, A., 2003. The shape of convective rain cells.

Geophys. Res. Lett. 30, 1–4. https://doi.org/10.1029/2003GL018539

Wilks, D.S., 1999. Simultaneous stochastic simulation of daily precipitation, temperature and solar radiation at multiple sites in complex terrain. Agric. For. Meteorol. 96, 85–101. https://doi.org/10.1016/S0168-1923(99)00037-4

Wilks, D.S., 1998. Multisite generalization of a daily stochastic precipitation generation model. J. Hydrol. 210, 178–191. https://doi.org/10.1016/S0022-1694(98)00186-3

Wilks, D.S., Wilby, R.L., 1999. The weather generation game: a review of stochastic weather models. Prog. Phys. Geogr. 23, 329–357. https://doi.org/10.1191/030913399666525256

Wischmeier, W.H., Smith, D.D., 1978. Predicting Rainfall Erosion Losses: A Guide to Conservation Planning. Dept. of Agriculture, Science and Education Administration. Agriculture handbook, No.537.

APPENDIX B: Main generator program

```
%% program main
% This program is used to generate the summer daily rainfall depths in the
% southeast Arizona

% The program generates biweekly daily rainfall starting on Jan 1, loop
% through the end of Dec for the first year and then start over the
% first Jan for the second year summer daily rainfall in the same routine,
% then loops until the desired generation period

% The program contains one main program and 4 subroutines
% The following lines explain the function of each subroutine
% transition.m: generates a sequence of storm occurrences
% depth.m: generates the maximum rainfall depth within a storm cell
% coverage.m: calculates the related storm coverage and generates storm
%   orientations and the ratios of the major to the minor axes (elliptical
%   storm shape) and calculated the lengths of the major and minor axes
% location.m: generates the locations of storm centers and computes rainfall
%   depths at user specified locations by using spread functions to spread
%   the storm outwardly from the storm center



% The following lines describe the variables used in the main program
% nyear: years of generations
% nperiods: number of generation period
% occurrence: an array of precipitation occurrences
% maxdep: an array of maximum rainfall depths within storm centers

% area: an array of the calculated storm coverage
% orient: an array of generated storm orientations
% ratio: an array of generated ratios of the major to the minor axes
% a,b: arrays of calculated lengths of the major and minor axes
% idum: a random number
% n: number of days within each biweekly period
% nset: the index of parameter sets for each simulation period

load('grids.mat');
load('center.mat');
```

```
nyear = 50; % number of years in simulation
days = 16; % the maximum days in a period is 16

% parameters for 12 months
nperiod = 24; % 24 half months
nset = 1:24;
% n is the number of days during each half month
n = [15,16,15,14,15,16 ...
    15,15,15,16,15,15 ...
    15,16,15,16,15,15 ...
    15,16,15,15,15,16];

% matrix to store cell and gage values
occu_final = zeros(16,nperiod,nyear,'single');
gage_final = zeros(88,4,days,nperiod,nyear,'single');

% matrix is too large, may consider aggregate days for one period
% cell_final = zeros(265,125,3,days,nperiod,nyear,'single');

% store the grid rainfall of nyears in two seasons
cell_year = zeros(265,125,nyear,2); % 4th dimension: (1)summer (2)winter

% multiple events/day, up to 5 storms/day
% max store space = 5 storms/day * 16 days = 80
maxdep_final = zeros(80,nperiod,nyear,'single');
area_final = zeros(80,nperiod,nyear,'single');
ratio_final = zeros(80,nperiod,nyear,'single');
orient_final = zeros(80,nperiod,nyear,'single');
center_final = zeros(2,80,nperiod,nyear,'single'); % x,y coordinates of storm
center

% matrix to store pcp data for SWAT
pcp1 = zeros(366,32,nyear); % 32 subwatersheds
pcp2 = zeros(366,20,nyear); % 20 subwatersheds
pcp6 = zeros(366,35,nyear); % 35 subwatersheds
pcp11 = zeros(366,17,nyear); % 17 subwatersheds

tic;
% loop for years
for i1 = 1:nyear
```

```
    date = 0; % record which day is it in current year

    % start generation for different periods
    for i2 = 1:24

        % call each subroutines to generate storms
        occurrence = transition(nset(i2),n(i2));
        [maxdep,num] = depth(nset(i2),n(i2),occurrence);
        [area,orient,c,a,b] = coverage(n(i2),maxdep,occurrence);
        [center,cell_biweekly,gage_biweekly] =
location(n(i2),occurrence,maxdep,orient,c,a,b,num);

        % store the results for validation
        L = length(occurrence); % get the length of current period data
        occu_final(1:L,i2,i1) = occurrence;
        maxdep_final(1:L*5,i2,i1) = maxdep;
        area_final(1:L*5,i2,i1) = area;
        ratio_final(1:L*5,i2,i1) = c;
        orient_final(1:L*5,i2,i1) = orient;
        center_final(:,1:L*5,i2,i1) = center;
        gage_final(:,:,:,i2,i1) = gage_biweekly;



    end

end


toc;
```

APPENDIX C: Subprogram transition

```
%% subroutine transition (nset,n,occurrence)
% generate a sequence of 0,1,2,3 for different period to obtain a sequence
% of rainfall occurrence

function [occurrence] = transition(nset,n)

% load biweekly transition probabilities for the whole watershed
dt = load('TP.mat');
Pw = dt.TP(1,:);
Pww = dt.TP(2,:);
Pdd = 1-dt.TP(3,:); % 3rd row in TP is P(w|d)
stabilize = zeros(1,1500);
occurrence = zeros(1,n);

% initialize the first day(wet/dry)
% nset indicates which half month Pw to be used, provided from main.m
p = rand(1);
if p > Pw(nset)
    stabilize(1) = 0;
else
    stabilize(1) = 1;
end

% produce a sequence of 1 or 0 for occurrence
for i = 2:1000 + n % n is the number of days in that simulation period
    p = rand(1);
    if stabilize(i-1) == 0
        if p <= Pdd(nset)
            stabilize(i) = 0;
        else
            stabilize(i) = 1;
        end
    else
        if p <= Pww(nset)
            stabilize(i) = 1;
        else
            stabilize(i) = 0;
        end
```

```
    end
end

% drop the first 1000 random numbers to stabilize
occu = stabilize(1001:(1000+n));

% load the probability for three types of rainfall
% row 1: convective
% row 2: frontal
% row 3: tropical depression
load('Ptype.mat');

% periods for different types of rainfall, 4 groups
% Jan-Jun,Dec: only frontal
% Jul,Aug: convective, frontal
% Oct,Nov: tropical, frontal
% Sep: convective, tropical, frontal
% g1 = [1:12,23:24];
% g2 = 13:16;
% g3 = 19:22;
% g4 = 17:18;

% decide which type of rainfall on each day

for d = 1:n
    if occu(1,d) == 1

        rndtype = rand(1);
        if rndtype <= Ptype(1,nset)
            occurrence(d) = 1; % convective
        elseif rndtype > Ptype(1,nset) && rndtype <= Ptype(2,nset)
            occurrence(d) = 2; % frontal
        elseif rndtype > Ptype(2,nset) && rndtype <= Ptype(3,nset)
            occurrence(d) = 3; % tropical depression
        end

    end
end

end
```

APPENDIX D: Subprogram depth

```
%% subroutine depth (nset,n,occurrence,maxdep)
% generate three types of rainfall
% (1) convective: max depth within a storm cell using lognormal
% distribution
% (2) frontal: average volume
% (3) tropical depression: average volume

function [maxdep,num] = depth(nset,n,occurrence)
% matrix to store maxdepth/avg_depth of generated storms
% maxmimum number of storms is (n days * 5 storms/day)

% though the name is maxdep, but actually for frontal and tropical
% depression it generates the volume of an event
maxdep = zeros(1,n*5); % initialize maxdep
num = zeros(1,n); % keep record of how many storms each day

% probabilities for multiple storms/day
% values are accumulated probabilities
% convective: 5*10 matrix, 1/2/3/4/5 storms/day, 6 columns for 6 periods Jul-
Sep
load('probac.mat');
% frontal: 3*24 matrix, 1/2/3 storms/day, 24 columns for 24 half months
% column 13-18 is zero, since Jul-Sep do not generate frontal rainfall
load('probaf.mat');

%% (1) parameters for convective rainfall
% lognormal distribution for max depth (unit:mm)
% ubpor: the portion of the standard deviation of the upper bound of the
% maximum depth, if the generated normal deviate is greater than the upper
% bound, then discard it and get another normal deviate

% initialize paramters for lognormal-distributed maximum depth
% 6 paramter sets for 6 simulation periods from Jul-Sep (ln base)
summer = 13:18;
if ismember(nset,summer)
    % parameters for all events
    mean = [ 1.5314 1.7461  1.6551  1.6105  1.6272  1.3189];
```

```
    std = [1.4235   1.4680  1.4851  1.4827  1.4576  1.5344];
    ubpor = ones(1,6)*2.2;
    % ubpor = [2.2,2.15,2.15,2.15,2.2,2.15];

    % parameters when all summer put together
    % mean = ones(1,6)*1.6112;
    % std = ones(1,6)*1.4694;
    % ubpor = [2.5,2.5,2.5,2.5,2.5,2.5];

    lb = 0.25; % lower bound of max depth 0.5mm
    ub = exp(mean(nset-12) + ubpor(nset-12)*std(nset-12)); % upper bound of the
standard normal deviate
end

%% (2) parameters for frontal rainfall
% exponential distribution for average volume (unit:in*km2)
% 1st row: mu; 2nd row: lower bound;  3rd row: upper bound
load('fpar.mat');

%% (3) parameters for tropical depression
% exponential distribution (unit:in*km2)

mu = 53.8870;
const = 114; % constant value add back to random variable
trop_lb = 100;
trop_ub = 500;

%% simulate each day
for i = 1:n

    % if convective rainfall,generate max depth
    if occurrence(i) == 1
        % decide how many storms on that day
        q = rand(1);
        if q <= probac(1,nset-12)
            num(i) = 1;
        elseif q > probac(1,nset-12) && q <= probac(2,nset-12)
            num(i) = 2;
        elseif q > probac(2,nset-12) && q <= probac(3,nset-12)
            num(i) = 3;
```

```
        elseif q > probac(3,nset-12) && q <= probac(4,nset-12)
            num(i) = 4;
        elseif q > probac(4,nset-12) && q <= probac(5,nset-12)
            num(i) = 5;
        end

        % generate max depth for each storm
        for j = 1:num(i)
            while maxdep(5*(i-1)+j) <= lb || maxdep(5*(i-1)+j) > ub
                p = normrnd(0,1);
                maxdep(5*(i-1)+j) = exp(std(nset-12)*p + mean(nset-12));
            end
        end

    % if frontal rainfall,generate event volume
    elseif occurrence(i) == 2
        % decide how many events on that day
        q = rand(1);
        if q <= probaf(1,nset)
            num(i) = 1;
        elseif q > probaf(1,nset) && q <= probaf(2,nset)
            num(i) = 2;
        elseif q > probaf(2,nset) && q <= probaf(3,nset)
            num(i) = 3;
        end

        % generate the rainfall volume for each storm
        for j = 1:num(i)
            while maxdep(5*(i-1)+j) <= fpar(2,nset) || maxdep(5*(i-1)+j) >
fpar(3,nset)
                maxdep(5*(i-1)+j) = exprnd(fpar(1,nset));
            end
        end

    % if tropical depression, generate event volume
    elseif occurrence(i) == 3
        num(i) = 1;
        while maxdep(5*(i-1)+1) <= trop_lb || maxdep(5*(i-1)+1) > trop_ub
            maxdep(5*(i-1)+1) = exprnd(mu) + const;
        end
```

```
    end
end

end
```

APPENDIX E: Subprogram coverage

```
%% subroutine coverage (n,depth,area,orientation,gratio,a,b)
% compute the storm areal coverage from generated max storm depth and
% compute the values of major axis and minor axis.

function [area,orientation,gratio,a,b] = coverage(n,depth,occurrence)
% The areal coverage ban be expressed as:
% area = exp(2.1784)*depth^0.68507+/-20std(random error)

% The subroutine also generate a uniform sequence 0~1 to decide to add 20%
% std to the area or minus 20% std to the calculated area
% The subroutine also generate an orientation for the storm
% The storm orientation in WGEW has a normal distribution with a mean of
% 91.4 and a std 38.272. The orientation is 0 degree from the West and 180
% degree in the East.

% variables:
% depth: maximum storm depth
% area: areal coverage
% a: major axis, b: minor axis, c: a/b ratio deviate
% ratio: ratio of major/minor axis
% ratio std: std of ratio
% orientation: storm orientation
% errstd: standard deviation of the error terms of area
% orimean: mean of orientation
% oristd: standard deviation of orientation
% R: uniform deviates

errstd = 10494092; % 10.4 km2
orimean = 91.4;
oristd = 38.272;
ratio = 1.54;
ratiostd = 0.37;

% each day has a maximum of 5 storms, n*5
area = zeros(1,n*5);
orientation = zeros(1,n*5);
a = zeros(1,n*5);
b = zeros(1,n*5);
```

```
gratio = zeros(1,n*5);

% -----------------calculate the storm area-------------------------------
for i = 1:n*5
    day = ceil(i/5);

    % if it is convective rainfall, calculate the area based on depth
    if occurrence(day) == 1 && depth(i) > 0

        while area(i) <= 0
            % equation for 4hr area/max depth relationship(only convective)
            % area unit: m2
            area(i) = 10^6*exp(2.1784)*depth(i)^0.68507;

            p = rand();
            q = rand();

            if p >= 0.5
                area(i) = area(i)+0.5*q*errstd;
            else
                area(i) = area(i)-0.5*q*errstd;
            end
        end

    % if not convective rainfall, no area generated
    else
        area(i) = 0;
    end
end

% -------------------calculate the a and b axis length--------------------
% generate an elliptical shape storm
for j = 1:n*5
    if area(j) > 0
        r = rand();
        s = rand();
        if r >= 0.5
            gratio(j) = ratio + s*ratiostd;
        else
            gratio(j) = ratio - s*ratiostd;
```

```
        end

        b(j) = sqrt(area(j)/pi()/gratio(j));
        a(j) = b(j)*gratio(j);
    end
end

% generate a circular shape storm
% for j = 1:n
%     if area(j) > 0
%         gratio(j) = 1;
%         b(j) = sqrt(area(j)/pi()/gratio(j));
%         a(j) = b(j)*gratio(j);
%     end
% end

% --------------------generate the orientation---------------------------
% orientation is normal distributed with a mean = 91.4, std = 38.272
for j = 1:n*5
    while area(j) > 0 && (orientation(j) <= 0 || orientation(j)> 180)
        deviate = normrnd(0,1);
        orientation(j) = oristd*deviate + orimean;
    end
end

end
```

APPENDIX F: Subprogram location

```
%% subroutine spread(n,occurrence,maxdep,orient,c,a,b)
% This subroutines computes the location of each storm center and call the
% other function spread to distribute the rainfall depth inside each storm,
% however, if the generated storm is totally outside watershed boundary,
% then a new storm center will be generated until at least part of the
% storm is inside the watershed

% The boundary of analysis is xmin = 580241, xmax = 606141
% ymin = 3503600, ymax = 3515700

function [center,cell_biweekly,gage_biweekly] =
location(n,occurrence,maxdep,orient,c,a,b,num)

% step 1: generate the storm origin location
% there are 265*125=33125 cells. The storm center distribution is normal
% distribution on WG so the random number generator is used to generate the
% storm centers
% The subroutine assigns the depth to pre-determined cells with
% pre-determined cell locations along with the calculated depths
% We also want to have the rainfall depth from generated events at each
% individual gages in order to compare the simulated results with the
% long-term observations.

% read the rain gage coordinates
% variable name: gage
% column 1: x coordinates; 2: y coordinates; 3: depth, 4: gage ID
load('gage.mat');
% load index matrix, 1 indicating inside watershed, 0 out of
load('watershed_index.mat');

center = zeros(2,n*5,'single'); % store x and y coordinates of center locations
cell = zeros(265,125,3,'single'); % xc,yc,depth
gage_initial = gage; % zero rainfall days
cell_biweekly = zeros(265,125,3,16,'single');
gage_biweekly = zeros(88,4,16,'single');

% cell size = 100m*100m
% ---------assign UTM coordinates to the center of each cell---------------
```

```
yc = 3503650; % ymin+50m, the center of the first cell
for jy = 1:125
    xc = 580291; % xmin+50m, the center of first cell
    for jx = 1:265
        cell(jx,jy,1) = xc;
        cell(jx,jy,2) = yc;
        xc = 100 + xc;
    end
    yc = 100 + yc;
end
cell_initial = cell; % zero rainfall days

% ---------loop for each day in the generation period(biweekly)------------
for i = 1:n

    % total depth in the watershed
    total_depth = 0;

    % assign the storm center coordinates to ix and iy
    % case 1: non-rainy days
    if occurrence(i) == 0
        cell_biweekly(:,:,:,i) = cell_initial; % have coordinates,but no
rainfall
        gage_biweekly(:,:,i) = gage_initial;

    % case 2: frontal/tropical depression rainfall
    elseif occurrence(i) == 3 || occurrence(i) == 2
        cell_accum = cell_initial;
        for j = 1:num(i)
            cell_new = cell_initial;
            % spread the volume evenly to the whole area 148km2
            % unit: in*km2 -> in -> mm
            cell_new(:,:,3) = maxdep(5*(i-1)+j)/148*25.4;

            % add some randomness to the rainfall field
            for jj = 1:125
                for ii = 1:265
                    flag = 0;
                    p = 1;
                    while flag <= 0 && p > 0.5
```

```
                        p = rand();
                        q = rand();
                        % notes on 11/1/2017
                        % regression between avg_dep and std_dep
                        std_dep = 0.42487*cell_new(ii,jj,3)+0.57261;
                        initial = cell_new(ii,jj,3);
                        flag = initial - q*2*std_dep;

                        if p <= 0.5
                            cell_new(ii,jj,3) = cell_new(ii,jj,3) +
q*2*std_dep;
                        else
                            cell_new(ii,jj,3) = cell_new(ii,jj,3) -
q*2*std_dep;
                        end
                    end
                end
            end

            % calculate the accumulated rainfall of multiple storms in
            % a day
            cell_accum(:,:,3) = cell_accum(:,:,3) + cell_new(:,:,3);
        end

        % ---------------loop for each gage, calculate depth--------------
        for k = 1:88
            row = floor((gage(k,1) - 580241)/100) + 1;
            col = floor((gage(k,2) - 3503600)/100) + 1;
            % in case some gages outside watershed
            if row > 0 && col > 0
                gage(k,3) = cell_accum(row,col,3);
            end
        end

        % assign value of a certain day to the final biweekly matrix
        cell_biweekly(:,:,:,i) = cell_accum(:,:,:);
        gage_biweekly(:,:,i) = gage(:,:);

    % case 3: convective rainfall
    elseif occurrence(i) == 1
```

```
        while total_depth == 0 % flag to check if storm inside watershed
            cell_accum = cell_initial;
            % loop for each storm in day i
            for j = 1:num(i)
                location = 0;
                while location == 0
                    p = rand();
                    location = fix(33125*p);
                end

                % assign the cell row and column number to cell center
                % ix, iy are the coordinates index for center
                if mod(location,265) ~= 0
                    ix = mod(location,265);
                    iy = floor(location/265)+1;
                else
                    ix = 265;
                    iy = floor(location/265);
                end

                % assign cell coordinates and 0-depth values
                % loop over each cell and decide if the cell is covered by the
storm
                % if cell covered by storm, compute the storm depth on the cell
                % To compute the depth, first compute the distance between the
cell and
                % the storm center, then compute the z value
                % break ellipse into potion and compute storm depth at each
cell
                % location
                % ----------------call spread function for each storm in a day-
-----------
                % calculate rainfall depth for each cell
                q = 5*(i-1)+j;
                [cell_new] = spread(ix,iy,maxdep(q),orient(q),c(q),a(q),b(q));
                % calculate the accumulated rainfall of multiple storms in
                % a day
                cell_accum(:,:,3) = cell_accum(:,:,3) + cell_new(:,:,3);
                % once a storm is decided, record its center location
                center(1,q) = ix;
```

```
                center(2,q) = iy;
            end
            % ------------check if the whole storm is outside watershed--------
            cell_inside = squeeze(cell_accum(:,:,3)).*watershed_index;
            total_depth = sum(cell_inside(:));
        end

        % ---------------loop for each gage, calculate depth--------------
        for k = 1:88
            row = floor((gage(k,1) - 580241)/100) + 1;
            col = floor((gage(k,2) - 3503600)/100) + 1;
            % in case some gages outside watershed
            if row > 0 && col > 0
                gage(k,3) = cell_accum(row,col,3);
            end
        end

        % assign value of a certain day to the final biweekly matrix
        cell_biweekly(:,:,:,i) = cell_accum(:,:,:);
        gage_biweekly(:,:,i) = gage(:,:);
    end

end

end
```

REFERENCES

Andiego, G., Waseem, M., Usman, M., Mani, N., 2017. The Influence of Rain Gauge Network Density on the Performance of a Hydrological Model. Comput. Water, Energy, Environ. Eng. 08, 27–50. https://doi.org/10.4236/cweee.2018.81002

Arnold, J.G., Srinivasan, R., Muttiah, R.S., Williams, J.R., 1998. Large area hydrologic modeling and assesment Part I: Model development. JAWRA J. Am. Water Resour. Assoc. 34, 73–89. https://doi.org/10.1111/j.1752-1688.1998.tb05961.x

Arnold, J.G., Williams, J.R., 1989. Stochastic Generation of Internal Storm Structure at a Point. Trans. ASAE 32, 161–167.

Asong, Z.E., Khaliq, M.N., Wheater, H.S., 2016. Multisite multivariate modeling of daily precipitation and temperature in the Canadian Prairie Provinces using generalized linear models. Clim. Dyn. 47, 1–21. https://doi.org/10.1007/s00382-016-3004-z

Bárdossy, a., Das, T., 2006. Influence of rainfall observation network on model calibration and application. Hydrol. Earth Syst. Sci. Discuss. 3, 3691–3726. https://doi.org/10.5194/hessd-3-3691-2006

Bardossy, A., Plate, E.J., 1992. Space-time model for daily rainfall using atmospheric circula.pdf.

Barnolas, M., Rigo, T., Llasat, M.C., 2010. Characteristics of 2-D convective structures in Catalonia (NE Spain): an analysis using radar data and GIS. Hydrol. Earth Syst. Sci. 14, 129–139. https://doi.org/10.1016/j.atmosres.2005.08.014

Bell, V.A., Moore, R.J., 2000. The sensitivity of catchment runoff models to rainfall data at different spatial scales. Hydrol. Earth Syst. Sci. https://doi.org/10.5194/hess-4-653-2000

Beven, K., Hornberger, G., 1982. Assesing the effect of spatial pattern of precipitation in modeling stream flow hydrographs. Water Resour. Bullettin 18, 823–829. https://doi.org/10.1111/j.1752-1688.1982.tb00078.x

Bonnifait, L., Delrieu, G., Lay, M. Le, Boudevillain, B., Masson, A., Belleudy, P., Gaume, E., Saulnier, G.M., 2009. Distributed hydrologic and hydraulic modelling with radar rainfall input: Reconstruction of the 8-9 September 2002 catastrophic flood event in the Gard region, France. Adv. Water Resour. 32, 1077–1089. https://doi.org/10.1016/j.advwatres.2009.03.007

Bonta, J. V., Shahalam, a., 2003. Cumulative storm rainfall distributions: Comparison of Huff curves. J. Hydrol. New Zeal.

Bonta, J. V, 2004a. Stochastic simulation of storm occurrence,depth,duration and within-storm intensities. Trans. ASAE 47, 1573–1584.

Bonta, J. V, 2004b. Development and utility of huff curves for disaggregating precipitation amounts. Trans. ASAE 20, 641–654.

Breinl, K., 2016. Driving a lumped hydrological model with precipitation output from weather generators of different complexity. Hydrol. Sci. J. 61, 1–20. https://doi.org/10.1080/02626667.2015.1036755

Breinl, K., Di Baldassarre, G., Girons Lopez, M., Hagenlocher, M., Vico, G., Rutgersson, A., 2017. Can weather generation capture precipitation patterns across different climates, spatial scales and under data scarcity? Sci. Rep. 7, 3–7. https://doi.org/10.1038/s41598-017-05822-y

Breinl, K., Turkington, T., Stowasser, M., 2015. Simulating daily precipitation and temperature: A weather generation framework for assessing hydrometeorological hazards. Meteorol. Appl. 22, 334–347. https://doi.org/10.1002/met.1459

Breinl, K., Turkington, T., Stowasser, M., 2013. Stochastic generation of multi-site daily precipitation for applications in risk management. J. Hydrol. 498, 23–35. https://doi.org/10.1016/j.jhydrol.2013.06.015

Brissette, F.P., Khalili, M., Leconte, R., 2007. Efficient stochastic generation of multi-site synthetic precipitation data. J. Hydrol. 345, 121–133. https://doi.org/10.1016/j.jhydrol.2007.06.035

Buishand, T. a., Brandsma, T., 2001. Multisite simulation of daily precipitation and temperature in the Rhine basin by nearest-neighbor resampling. Water Resour. Res. 37, 2761–2776. https://doi.org/10.1029/2001WR000291

Calenda, G., Napolitano, F., 1999. Parameter estimation of Neyman-Scott processes for temporal point rainfall simulation. J. Hydrol. 225, 45–66. https://doi.org/10.1016/S0022-1694(99)00133-X

Caracciolo, D., Arnone, E., Noto, L., 2014. Influence of Spatial Precipitation Sampling

on Hydrological Response at the Catchment Scale. J. Hydrol. Eng. 19, 544–553. https://doi.org/10.1061/(ASCE)HE.1943-5584.0000829

Cowpertwait, P.S.P., O'Connell, P.E., Metcalfe, A.V., Mawdsley, J.A., 1996. Stochastic point process modelling of rainfall. II. Regionalisation and disaggregation. J. Hydrol. 175, 47–65. https://doi.org/10.1016/S0022-1694(96)80005-9

Doherty, J., 2015. Calibration and uncertainty analysis for complex environmental models, Brisbane, Australia: Watermark Numerical Computing. U.S. Department of Agriculture, Fort Collins,CO.

Emmanuel, I., Andrieu, H., Leblois, E., Janey, N., Payrastre, O., 2015. Influence of rainfall spatial variability on rainfall-runoff modelling: Benefit of a simulation approach? J. Hydrol. 531, 337–348. https://doi.org/10.1016/j.jhydrol.2015.04.058

Evin, G., Favre, A.C., Hingray, B., 2018. Stochastic generation of multi-site daily precipitation focusing on extreme events. Hydrol. Earth Syst. Sci. 22, 655–672. https://doi.org/10.5194/hess-22-655-2018

Faurès, J.-M., Goodrich, D.C., Woolhiser, D. a., Sorooshian, S., 1995. Impact of small-scale spatial rainfall variability on runoff modeling. J. Hydrol. 173, 309–326. https://doi.org/10.1016/0022-1694(95)02704-S

Féral, L., Sauvageot, H., Castanet, L., Lemorton, J., 2003. HYCELL - A new hybrid model of the rain horizontal distribution for propagation studies: 1. Modeling of the rain cell. Radio Sci. 38, 1–20. https://doi.org/10.1029/2002RS002802

Ferraris, L., Gabellani, S., Rebora, N., Provenzale, A., 2003. A comparison of stochastic models for spatial rainfall downscaling. Water Resour. Res. 39, 1–8. https://doi.org/10.1029/2003WR002504

Fogel, M.M., Duckstein, L., 1969. Point Rainfall Frequencies in Convective Storms. Water Resour. Res. 5, 1229–1237. https://doi.org/10.1029/WR005i006p01229

Fu, S., Sonnenborg, T.O., Jensen, K.H., He, X., 2011. Impact of Precipitation Spatial Resolution on the Hydrological Response of an Integrated Distributed Water Resources Model. Vadose Zo. J. 10, 25. https://doi.org/10.2136/vzj2009.0186

Gochis, D.J., Brito-Castillo, L., Shuttleworth, W.J., 2006. Hydroclimatology of the North American Monsoon region in northwest Mexico. J. Hydrol. 316, 53–70. https://doi.org/10.1016/j.jhydrol.2005.04.021

Goodrich, D.C., Keefer, T.O., Unkrich, C.L., Nichols, M.H., Osborn, H.B., Stone, J.J., Smith, J.R., 2008. Long-term precipitation database, Walnut Gulch Experimental Watershed, Arizona, United States. Water Resour. Res. 44, W05S04. https://doi.org/10.1029/2006WR005782

Goodrich, D.C., Lane, L.J., Shillito, R.M., Miller, S.N., Syed, K.H., Woolhiser, A., 1997. Linearity of basin response as a function of scale in a semiarid watershed. Water Resour. Res. 33, 2951–2965.

Goodrich, D.C., Unkrich, C.L., Keefer, T.O., Nichols, M.H., Stone, J.J., Levick, L.R., Scott, R.L., 2008. Event to multidecadal persistence in rainfall and runoff in

southeast Arizona. Water Resour. Res. 44, W05S14. https://doi.org/10.1029/2007WR006222

Gupta, H.V., Sorooshian, S., Yapo, P.O., 1999. Status of Automatic Calibration for Hydrologic Models: Comparison with Multilevel Expert Calibration. J. Hydrol. Eng. 4, 135–143. https://doi.org/10.1061/(ASCE)1084-0699(1999)4:2(135)

Gupta, V.K., Waymire, E.C., 1993. A Statistical Analysis of Mesoscale Rainfall as a Random Cascade. J. Appl. Meteorol. 32, 251–267. https://doi.org/10.1175/1520-0450(1993)032<0251:ASAOMR>2.0.CO;2

Hellassa, S., Souag-Gamane, D., 2019. Improving a stochastic multi-site generation model of daily rainfall using discrete wavelet de-noising: a case study to a semi-arid region. Arab. J. Geosci. 12, 1–19. https://doi.org/10.1007/s12517-018-4168-0

Hernandez, M., Miller, S.N., Goodrich, D.C., Goff, B.F., Kepner, W.G., Edmonds, C.M., Jones, K.B., 2000. Modeling runoff response to land cover and rainfall spatial variability in semi-arid watersheds. Environ. Monit. Assess. 64, 285–298. https://doi.org/10.1023/A:1006445811859

Hsieh, H.-H., 2002. Stochastic daily thunderstorm generation in southeast Arizona. Univ. Arizona. https://doi.org/10.16953/deusbed.74839

Karklinsky, M., Morin, E., 2006. Spatial characteristics of radar-derived convective rain cells over southern Israel. Meteorol. Zeitschrift 15, 513–520. https://doi.org/10.1127/0941-2948/2006/0153

Kavvas, L., Delleur, J.W., 1981. Cluster Model of Daily Rainfall Sequences. Water Resour. Res. 17, 1151–1160. https://doi.org/10.1029/WR017i004p01151

Khalili, M., Brissette, F., Leconte, R., 2011. Effectiveness of Multi-Site Weather Generator for Hydrological Modeling. J. Am. Water Resour. Assoc. 47, 303–314. https://doi.org/10.1111/j.1752-1688.2010.00514.x

Khalili, M., Brissette, F., Leconte, R., 2009. Stochastic multi-site generation of daily weather data. Stoch. Environ. Res. Risk Assess. 23, 837–849. https://doi.org/10.1007/s00477-008-0275-x

Khalili, M., Leconte, R., Brissette, F., 2006. Efficient watershed modeling using a multi-site weather generator for meteorological data. WIT Trans. Ecol. Environ. 89, 273–281. https://doi.org/10.2495/GEO060281

Kidd, C., Becker, A., Huffman, G.J., Muller, C.L., Joe, P., Skofronick-Jackson, G., Kirschbaum, D.B., 2017. So, how much of the Earth's surface is covered by rain gauges? Bull. Am. Meteorol. Soc. 98, 69–78. https://doi.org/10.1175/BAMS-D-14-00283.1

Koren, V.I., Finnerty, B.D., Schaake, J.C., Smith, M.B., Seo, D.J., Duan, Q.Y., 1999. Scale dependencies of hydrologic models to spatial variability of precipitation. J. Hydrol. 217, 285–302. https://doi.org/10.1016/S0022-1694(98)00231-5

Krajewski, W.F., Lakshmi, V., Georgakakos, K.P., Jain, S.C., 1991. A Monte Carlo Study of rainfall sampling effect on a distributed catchment model. Water Resour.

Res. 27, 119–128. https://doi.org/10.1029/90WR01977

Lanza, L.G., 2000. A conditional simulation model of intermittent rain fields. Hydrol. Earth Syst. Sci. https://doi.org/10.5194/hess-4-173-2000

Leander, R., Buishand, T.A., 2009. A daily weather generator based on a two-stage resampling algorithm. J. Hydrol. 374, 185–195. https://doi.org/10.1016/j.jhydrol.2009.06.010

Li, Z., 2014. A new framework for multi-site weather generator: A two-stage model combining a parametric method with a distribution-free shuffle procedure. Clim. Dyn. 43, 657–669. https://doi.org/10.1007/s00382-013-1979-2

Li, Z., Brissette, F., Chen, J., 2013. Finding the most appropriate precipitation probability distribution for stochastic weather generation and hydrological modelling in Nordic watersheds. Hydrol. Process. 27, 3718–3729. https://doi.org/10.1002/hyp.9499

Li, Z., Lü, Z., Li, J., Shi, X., 2017. Links between the spatial structure of weather generator and hydrological modeling. Theor. Appl. Climatol. 128, 103–111. https://doi.org/10.1007/s00704-015-1691-8

Lopes, V.L., 1996. On the effect of uncertainty in spatial distribution of rainfall on catchment modelling. Catena 28, 107–119. https://doi.org/10.1016/S0341-8162(96)00030-6

Mehrotra, R., Sharma, A., 2007. A semi-parametric model for stochastic generation of multi-site daily rainfall exhibiting low-frequency variability. J. Hydrol. 335, 180–

193. https://doi.org/10.1016/j.jhydrol.2006.11.011

Mehrotra, R., Srikanthan, R., Sharma, A., 2006. A comparison of three stochastic multi-site precipitation occurrence generators. J. Hydrol. 331, 280–292. https://doi.org/10.1016/j.jhydrol.2006.05.016

Mejía, J.M., Rodríguez-Iturbe, I., 1974. On the synthesis of random field sampling from the spectrum: An application to the generation of hydrologic spatial processes. Water Resour. Res. https://doi.org/10.1029/WR010i004p00705

Miller, S.N., Semmens, D.J., Goodrich, D.C., Hernandez, M., Miller, R.C., Kepner, W.G., Guertin, D.P., 2007. The Automated Geospatial Watershed Assessment tool. Environ. Model. Softw. 22, 365–377. https://doi.org/10.1016/j.envsoft.2005.12.004

Morin, E., Gabella, M., 2007. Radar-based quantitative precipitation estimation over Mediterranean and dry climate regimes. J. Geophys. Res. Atmos. 112, 1–13. https://doi.org/10.1029/2006JD008206

Morin, E., Goodrich, D., Maddox, R., Gao, X., Gupta, H., 2004. Spatial patterns in thunderstorm rainfall events : conceptual modeling and hydrological insights, in: Sixth International Symposium on Hydrological Applications of Weather Radar.

Morin, E., Goodrich, D.C., Maddox, R. a., Gao, X., Gupta, H. V., Sorooshian, S., 2006. Spatial patterns in thunderstorm rainfall events and their coupling with watershed hydrological response. Adv. Water Resour. 29, 843–860. https://doi.org/10.1016/j.advwatres.2005.07.014

Morin, E., Goodrich, D.C., Maddox, R. a., Gao, X., Gupta, H. V., Sorooshian, S., 2005. Rainfall modeling for integrating radar information into hydrological model. Atmos. Sci. Lett. 6, 23–30. https://doi.org/10.1002/asl.86

Nash, J.E., Sutcliffe, J. V, 1970. River Flow Forecasting through Cconceptual Models Part I-A Discussion of Pinciples. J. Hydrol. 10, 282–290.

Nearing, M.A., Unkrich, C.L., Goodrich, D.C., Nichols, M.H., Keefer, T.O., 2015. Temporal and elevation trends in rainfall erosivity on a 149 km2 watershed in a semi-arid region of the American Southwest. Int. Soil Water Conserv. Res. 3, 77–85. https://doi.org/10.1016/j.iswcr.2015.06.008

Nichols, M.H., Renard, K.G., Osborn, H.B., 2002. Precipitation changes from 1956 to 1996 on the Walnut Gulch Experimental Watershed. J. Am. Water Resour. Assoc. 38, 161–172. https://doi.org/10.1111/j.1752-1688.2002.tb01543.x

Nicks, a D., Lane, L.J., Gander, G. a, 1995. CLIGEN Weather generator. USDA–Water Eros. Predict. Proj. hillslope profile watershed Model Doc. 2.1–2.22.

Obled, C., Wendling, J., Beven, K., 1994. The sensitivity of hydrological models to spatial rainfall patterns: an evaluation using observed data. J. Hydrol. 159, 305–333. https://doi.org/10.1016/0022-1694(94)90263-1

Ogden, F.L., Julien, P.Y., 1993. Runoff sensitivity to temporal and spatial rainfall variability at runoff plane and small basin scales. Water Resour. Res. 29, 2589–2597. https://doi.org/10.1029/93WR00924

Osborn, H.B., 1983. Precipitation characteristics affecting hydrologic response of southwestern rangelands. Agricultural Research Service, Agricultural Reviews and Manuals, Western Series, No.34.

Osborn, H.B., 1982. Quantifiable differences between airmass and frontal-convective thunderstorm rainfall in the southwestern united states, in: Statistical Analysis of Rainfall and Runoff. pp. 21–32.

Osborn, H.B., Renard, K.G., Simanton, J.R., 1979. Dense networks to measure convective rainfall in the southwestern United States. Water Resour. Res. 15, 1701–1711. https://doi.org/10.1029/WR015i006p01701

Papalexiou, S.M., Koutsoyiannis, D., Montanari, A., 2011. Can a simple stochastic model generate rich patterns of rainfall events? J. Hydrol. 411, 279–289. https://doi.org/10.1016/j.jhydrol.2011.10.008

Paschalis, A., Molnar, P., Fatichi, S., Burlando, P., 2013. A stochastic model for high-resolution space-time precipitation simulation. Water Resour. Res. 49, 8400–8417. https://doi.org/10.1002/2013WR014437

Peleg, N., Morin, E., 2014. Stochastic convective rain-field simulation using a high-resolution synoptically conditioned weather generator (HiReS-WG). Water Resour. Res. 50, 1–16. https://doi.org/10.1002/2013WR014836

Peleg, N., Morin, E., 2012. Convective rain cells: Radar-derived spatiotemporal characteristics and synoptic patterns over the eastern Mediterranean. J. Geophys.

Res. Atmos. 117, 1–17. https://doi.org/10.1029/2011JD017353

Racsko, P., Szeidl, L., Semenov, M., 1991. A serial approach to local stochastic weather models. Ecol. Modell. 57, 27–41. https://doi.org/10.1016/0304-3800(91)90053-4

Rebora, N., Ferraris, L., von Hardenberg, J., Provenzale, A., 2006. RainFARM: Rainfall Downscaling by a Filtered Autoregressive Model. J. Hydrometeorol. 7, 724–738. https://doi.org/10.1175/JHM517.1

Renard, K.G., Lane, L.J., Simanton, J.R., Emmerich, W.E., Stone, J.J., Weltz, M. a, Goodrich, D.C., Yakowitz, D.S., 1993. Agricultural impacts in an arid environment: Walnut Gulch studies. Hydrol. Sci. Technol. 9, 145–190.

Richardson, C., Nicks, A., 1990. EPIC—Erosion/Productivity Impact Calculator.

Richardson, C.W., 1981. Stochastic simulation of daily precipitation, temperature, and solar radiation. Water Resour. Res. 17, 182–190. https://doi.org/10.1029/WR017i001p00182

Schuurmans, J.M., Bierkens, M.F.P., 2006. Effect of spatial distribution of daily rainfall on interior catchment response of a distributed hydrological model. Hydrol. Earth Syst. Sci. Discuss. 3, 2175–2208. https://doi.org/10.5194/hessd-3-2175-2006

Segond, M.L., Wheater, H.S., Onof, C., 2007. The significance of spatial rainfall representation for flood runoff estimation: A numerical evaluation based on the Lee catchment, UK. J. Hydrol. 347, 116–131. https://doi.org/10.1016/j.jhydrol.2007.09.040

Serinaldi, F., 2009. A multisite daily rainfall generator driven by bivariate copula-based mixed distributions. J. Geophys. Res. Atmos. 114, 1–13. https://doi.org/10.1029/2008JD011258

Shah, S.M.S., O'Connell, P.E., Hosking, J.R.M., 1996. Modelling the effects of spatial variability in rainfall on catchment response. 2. Experiments with distributed and lumped models. J. Hydrol. 175, 89–111. https://doi.org/10.1016/S0022-1694(96)80007-2

Sidman, G., Guertin, D.P., Goodrich, D.C., Unkrich, B.C.L., Burns, I.S., 2016. Risk assessment of post-wildfire hydrological response in semiarid basins : the effects of varying rainfall representations in the KINEROS2 / AGWA model. Int. J. Wildl. Fire 268–278.

Smith, M.B., Koren, V.I., Zhang, Z., Reed, S.M., Pan, J.J., Moreda, F., 2004. Runoff response to spatial variability in precipitation: An analysis of observed data. J. Hydrol. 298, 267–286. https://doi.org/10.1016/j.jhydrol.2004.03.039

Shuttleworth, W.J. 2012. Terrestrial Hydrometeorology, Wiley-Blackwell. ISBN-10: 0470659378

Srikanthan, R., McMahon, T. a., 2001. Stochastic generation of annual, monthly and daily climate data: A review. Hydrol. Earth Syst. Sci. 5, 653–670. https://doi.org/10.5194/hess-5-653-2001

Srikanthan, R. 2004. Stochastic generation of daily rainfall data using a nested model.

57th Canadian Water Resources Association Annual Congress, Montreal.

Srikanthan, R. 2005. Stochastic generation of daily rainfall at a number of sites. Technical Report 05/7, CRC for Catchment Hydrology.

Srinivasan, R., Ramanarayanan, T.S., Arnold, J.G., Bednarz, S.T., 1998. Large area hydrologic modeling and assessment part II: Model application. J. Am. Water Resour. Assoc. 34, 91–101. https://doi.org/10.1111/j.1752-1688.1998.tb05962.x

Stillman, S., Zeng, X., Shuttleworth, W.J., Goodrich, D.C., Unkrich, C.L., Zreda, M., 2013. Spatiotemporal Variability of Summer Precipitation in Southeastern Arizona. J. Hydrometeorol. 14, 1944–1951. https://doi.org/10.1175/JHM-D-13-017.1

Stone, J.J., Nichols, M.H., Goodrich, D.C., Buono, J., 2008. Long-term runoff database, Walnut Gulch Experimental Watershed, Arizona, United States. Water Resour. Res. 44, 1–5. https://doi.org/10.1029/2006WR005733

Syed, K.H., Goodrich, D.C., Myers, D.E., Sorooshian, S., 2003. Spatial characteristics of thunderstorm rainfall fields and their relation to runoff. J. Hydrol. 271, 1–21. https://doi.org/10.1016/S0022-1694(02)00311-6

Valdes, J.B., Rodriguez-Iturbe, I., Gupta, V.K., 1985. Approximations of Temporal Rainfall From a Multidimensional Model. Water Resour. Res. 21, 1259–1270. https://doi.org/10.1029/WR021i008p01259

Van Liew, M.W., Veith, T.L., Bosch, D.D., Arnold, J.G., 2007. Suitability of SWAT for the Conservation Effects Assessment Project: Comparison on USDA Agricultural Research Service Watersheds. J. Hydrol. Eng. 12, 173–189.

https://doi.org/10.1061/(ASCE)1084-0699(2007)12:2(173)

Verdin, A., Rajagopalan, B., Kleiber, W., Katz, R.W., 2015. Coupled stochastic weather generation using spatial and generalized linear models. Stoch. Environ. Res. Risk Assess. 29, 347–356. https://doi.org/10.1007/s00477-014-0911-6

Verdin, A., Rajagopalan, B., Kleiber, W., Podestá, G., Bert, F., 2018. A conditional stochastic weather generator for seasonal to multi-decadal simulations. J. Hydrol. 556, 835–846. https://doi.org/10.1016/j.jhydrol.2015.12.036

von Hardenberg, J., Ferraris, L., Provenzale, A., 2003. The shape of convective rain cells. Geophys. Res. Lett. 30, 1–4. https://doi.org/10.1029/2003GL018539

Watson, B.M., Srikanthan, R., Selvalingam, S., Ghafouri, M., 2005. Hydrologic Response of SWAT to Single Site and Multi- Site Daily Rainfall Generation Models, in: Proceedings of MODSIM05International Congress on Modelling and Simulation. pp. 2981–2987.

Wilks, D.S., 1999. Simultaneous stochastic simulation of daily precipitation, temperature and solar radiation at multiple sites in complex terrain. Agric. For. Meteorol. 96, 85–101. https://doi.org/10.1016/S0168-1923(99)00037-4

Wilks, D.S., 1998. Multisite generalization of a daily stochastic precipitation generation model. J. Hydrol. 210, 178–191. https://doi.org/10.1016/S0022-1694(98)00186-3

Wilks, D.S., Wilby, R.L., 1999. The weather generation game: a review of stochastic weather models. Prog. Phys. Geogr. 23, 329–357.

https://doi.org/10.1191/030913399666525256

Wilson, C.B., Valdes, J.B., Rodriguez???Iturbe, I., 1979. On the influence of the spatial distribution of rainfall on storm runoff. Water Resour. Res. 15, 321–328. https://doi.org/10.1029/WR015i002p00321

Wischmeier, W.H., Smith, D.D., 1978. Predicting Rainfall Erosion Losses: A Guide to Conservation Planning. Dept. of Agriculture, Science and Education Administration. Agriculture handbook, No.537.

Woolhiser, D.A., Goodrich, D.C., 1988. Effect of storm rainfall intensity patterns on surface runoff. J. Hydrol. 102, 335–354. https://doi.org/10.1016/0022-1694(88)90106-0

Xu, Y., Ma, C., Pan, S., Zhu, Q., Ran, Q., 2014. Evaluation of a multi-site weather generator in simulating precipitation in the Qiantang River Basin, East China. J. Zhejiang Univ. Sci. A 15, 219–230. https://doi.org/10.1631/jzus.A1300267